Engineering Devices with Functional Nanomaterials

A dissertation submitted by

Sailapu Sunil Kumar

to

Indian Institute of Technology Guwahati

For the award of the degree of

Doctor of Philosophy

Centre for Nanotechnology

Indian Institute of Technology Guwahati

Guwahati – 781039, Assam, India

September 2016

STATEMENT

"Engineering Devices with Functional Nanomaterials" comprises the dissertation work carried out by me under the supervision of Dr. Arun Chattopadhyay, Professor, Department of Chemistry, Indian Institute of Technology Guwahati. This thesis has been submitted by me to Centre for Nanotechnology, Indian Institute of Technology Guwahati for the award of the degree of Doctor of Philosophy.

I further declare that this work has not been submitted elsewhere for any degree to the best of my knowledge.

Sailapu Sunil Kumar

Centre for Nanotechnology
Indian Institute of Technology Guwahati
Guwahati – 781039
Assam, India

September, 2016
Guwahati

CERTIFICATE

It is certified that the work contained in the dissertation entitled **"Engineering Devices with Functional Nanomaterials"** by Sailapu Sunil Kumar, a student of Centre for Nanotechnology Indian Institute of Technology Guwahati for the award of the degree of Doctor of Philosophy is a bonafide record of research work carried out by him. The information and data reported by him are solely the results of his original findings. He has meticulously carried out the investigations and followed the guidelines of the laboratory. This work has not been submitted elsewhere for any degree or diploma.

Arun Chattopadhyay
Professor
Department of Chemistry
Indian Institute of Technology Guwahati
Guwahati - 781039, Assam, India

September, 2016
Guwahati

To

My Parents and Sister

.... who taught me the value of education and wisdom
.... for their unconditional love and support

ACKNOWLEDGEMENT

The dissertation involves help, support of many individuals and it is with utmost happiness I extend my heartfelt gratitude.

Special thanks to my advisor Prof. Arun Chattopadhyay for giving me opportunity to carry out research under his supervision and scripting the most valuable pages of my life. He has been a tremendous motivation and fatherly figure besides being a scholarly mentor. Despite many, one that severely influenced and made me love the work immensely and strive harder is his consistent high energy levels day after day and true commitment to work. I thank him for allowing me to pursue my interests and importantly transforming, and teaching me how to mould them, into an excellent masterpiece. Woking in close quarters and being involved in many insightful discussions taught me how to communicate scientific works both professionally and on a pleasurable note. In addition, all the wonderful moments shared would be valuable memories for me to look back and cherish. This dissertation wouldn't have been possible without his guidance for which I would be grateful to him throughout my life.

I would also like to thank, Prof. Siddhartha Sankar Ghosh, Dr. Biplab Bose, Dr. Tapas Kumar Mandal and Dr. Dipak Kumar Goswami for serving as my committee members and reviewing my work. I am grateful for your brilliant comments which helped me to improve consistently, revise my goals and set higher challenges.

I would like to express my gratitude to all the previous and current lab members, technical and non-technical staff at Centre for Nanotechnology (and CENTD), Department of Chemistry, Centre for Excellence for their help and support. I thank Dr. C. V. Sastri for extending assistance in designing my experimental setup. I would like to thank my collaborators, Dr. Amaresh Kumar Sahoo, Dr. Md Palashuddin Sk, Ms. Deepanjalee Dutta and Ms. Anitha T Simon for helping in experiments and giving me the opportunity to learn from them. I would like to extend my heartful thanks to all my friends and well-wishers who lend their helping hand in need, gave their quality time and many lighter moments which kept me going positively in life. I thank Central Instrument Facility, Centre for Excellence, Centre for Environment and Mechanical workshop for allowing me to access their facilities. I thank IIT Guwahati (and MHRD) for the fellowship.

I thank and pay my respect to my teachers at Dayanand Anglo Vedic (D.A.V) public school and Raghu Institute of Technology, Andhra University who were monumental in shaping my abilities and in inculcating the habit to think independently and differently towards problem solving.

A special thanks to my family. Words cannot express the gratitude to my mother and father for all of the sacrifices that you've made for me and sister. Your teachings about life, knowledge and wisdom reverberates at all stages of our life and our efforts will always be directed to make you proud and be a good human being. I thank my sister for all her love and support. I appreciate you all for your understanding, patience and encouragement throughout my life.

I may have missed mentioning few for which I apologize and extend my wholehearted acknowledgement to all of them. The roller coaster ride of PhD has been so dearest to me and it's the journey which I enjoyed the most and always tried to do the best I could.

Sunil

ABSTRACT

It is a commendable journey of human race to the 'age of super computers' from calculators, which were once regarded as 'big thing'. One cannot debate over 'integration of novel materials and techniques' being a significant factor in achieving such a giant technological leap. In the contemporary age, sublime developments in science and technology are contributing to the staggering growth of innovations. There are great endeavours for generating novel materials and methods to construct devices of potential use. Prudent interest is judiciously invested towards 'small' dimension materials to achieve 'the next big thing' in the world of devices. This may well be said as materials at the nanoscale dimensions are promising due to their versatile at the same time unique physical and chemical properties. The essence of nanotechnology is to utilize the fundamental knowledge associated with the intriguing properties prevailing at these dimensions. Hence, through effective design strategies properties at these 'small' dimensions prove to be vital in development and transformation of next generation devices and systems.

The current dissertation has been directed towards engineering devices through effective integration of nanomaterials and thereby, use of their physico-chemical attributes. In particular, salient features like catalytic, magnetic, plasmonic and luminescence nature of nanoscale materials developed through bottom-up approach of chemical synthetic routes were availed to accomplish devices with on-board intelligence and clinical importance. A device with the ability to generate electrical energy from autonomous motion of microbots was engineered. Intelligent systems capable of decision making in the liquid media were developed. For disease diagnostics, a bench top device was constructed to perform polymerase chain reaction and array based gene and protein analyses. Another device for photodynamic therapy and optical based detection was achieved. These nanotechnology oriented devices indicate greater prospects and encourage further investigations to achieve other major technological leaps.

Sailapu Sunil Kumar

September 2016

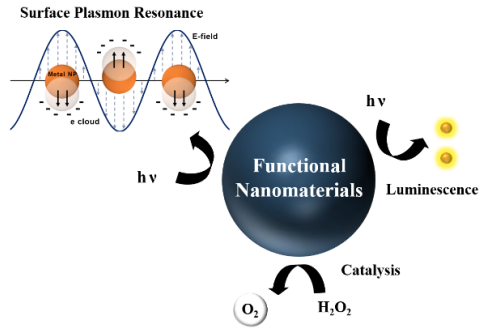

Developing devices using properties of nanoscale materials....

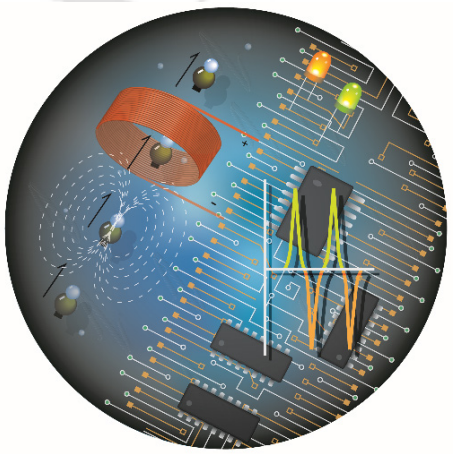

Generation of emf from autonomous motion of microbot in liquid media....

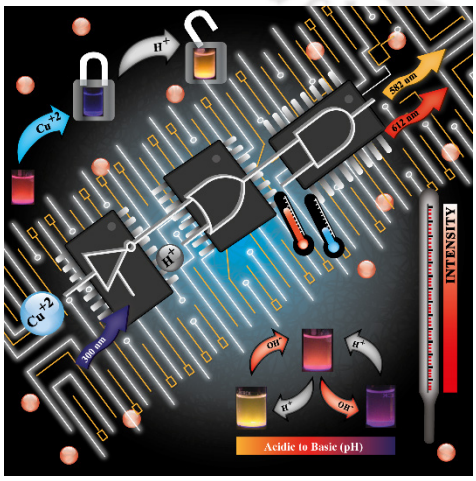

Logical implementation and sensing with nanoscale materials....

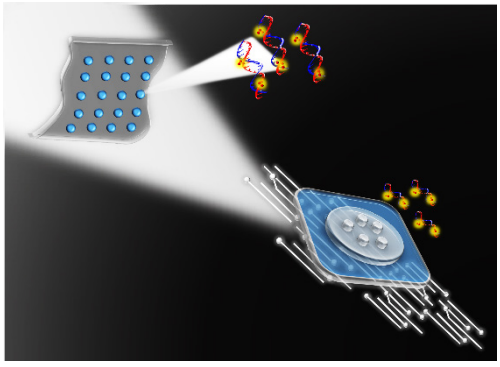

Device and methods to carry out RT-PCR and array based analysis....

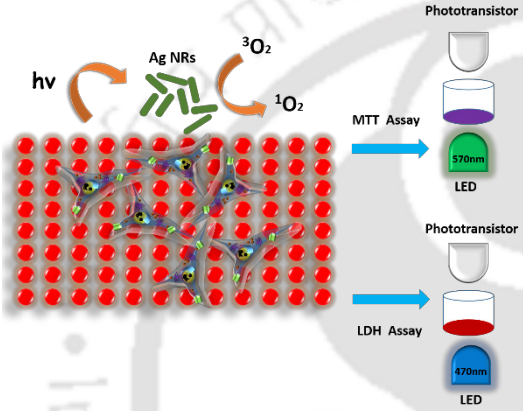

Device for PDT and colorimetric assays like MTT and LDH....

Abbreviations

ATP: Adenosine triphosphate

AAS: Atomic absorption spectroscopy

BSA: Bovine serum albumin

CNT: Carbon nanotube

CTAB: Cetyl trimethylammonium bromide

DMSO: Dimethyl sulfoxide

DOX: Doxorubicin

DPBF: 1, 3 – diphenylizobenzofuran

EMF: Electromotive force

EDX: Energy dispersive X-ray

EtBr: Ethidium bromide

FET: Field-effect transistor

FESEM: Field emission scanning electron microscope

F1-ATPase: F1-adenosine triphosphate synthase

GMR: Giant magnetoresistance

GUI: Graphical user interface

HRTEM: High resolution transmission electron microscope

LDH: Lactate dehydrogenase

LED: Light emitting diode

LSPR: Localized surface plasmon resonance

MEMS: Micro electro mechanical systems

MPA: Mercaptopropionic acid

MRI: Magnetic resonance imaging

MTT: [3-(4,5-dimethylthiazol-2-yl)-2,5-diphenyltetrazolium bromide]

NEMS: Nano-electro-mechanical systems

NPs: Nanoparticles

NCs: Nanoclusters

PDT: Photodynamic therapy

PEG: Polyethylene glycol

PWM: Pulse width modulation

PID: Proportional-integral-derivative

ROI: Region of interest

SAED: Selected area electron diffraction

SAW: Surface acoustic wave

SDS: Sodium dodecyl sulphate

SPR: Surface plasmon resonance

SSC: Saline sodium citrate

SWG: Standard wire gauge

TEM: Transmission electron microscope

XRD: X-ray diffraction

Chapter 1

Introduction

ABSTRACT

Nanotechnology offers tools and materials (with unique and diverse physicochemical properties) which are of immense importance for technological advancement. The initial developments in fields like intelligent systems and healthcare devices exhibit their potential to design and develop next generation devices.

Technological advancement is largely driven through device miniaturization, cost reduction, less energy and material consumptions, increased sensitivity and selectivity. The fusion of diverse methodologies and novel materials are essential to develop innovative devices and hence, stays as the main focus of rapidly progressing multidisciplinary research. In this regard, materials at the nanoscale dimensions are promising due to their versatile at the same time unique physical and chemical properties.[1] These sublime features which differ considerably from the atoms as well as bulk materials could be favourably exploited for construction of efficient devices targeted for various applications. Though, mankind had prior knowledge of these nanoscale materials, only with the growth in instrumentation and synthetic approaches, the underlying realm was better unravelled and identified with potential utilization in constructing devices. Also, with many biological process occurring in this size realm, pursuing further research is beneficial in understanding various natural happenings and thus presents an opportunity to either transcribe or coordinate in architecting novel systems. Hence, through effective design strategies, the attainment of desired properties from these tailored nanomaterials could well prove to be vital in the development and transformation of next generation devices with significant real-world impacts.

1.1 | Fabrication of Nanomaterials

The eventual functionality of the developed device is dependent on the physical and chemical properties of the involved nanostructures. Properties of nanoscale materials are heavily reliant on their composition, dimension and morphology.[1-2] The ability to tailor these attributes in a way to obtain desired properties is what makes research at these scales fascinating with ample opportunities to engineer novel systems. Hence, fabrication of these nanomaterials is a crucial step which ultimately dictates the overall performance of the device and its further applications.

Although nanostructures can be developed in several ways, the fabrication methods are broadly classified into either ‘top down’ or ‘bottom up’ approaches.[3-4] In top down approach of fabrication, the bulk material is reduced/reformed to desired nanostructures as shown in **Figure 1.1** with the help of precisely controlled nanofabrication tools.[4] Lithography techniques, mechanical attrition (ball milling), etching etc., are some of the major tools that result in nanostructures through top down approach.[3] By far, top down approaches had been the core ingredient in electronic industry as well

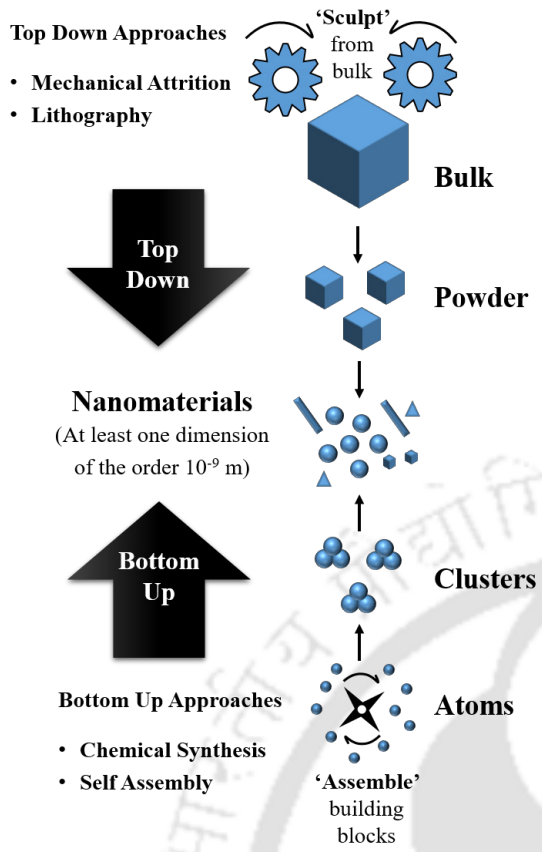

Figure 1.1. Fabrication of nanomaterials. Scheme illustrates the bottom up and top down approaches in formulating nanostructures.

as in development of MEMS (micro electro mechanical systems) technology. However, with the feature size in silicon industry reaching physical limits, the road ahead seems daunting.[5] Factors like high cost, limited access, resolution issues and exposure of substrates to high temperature, high-energy radiations and corrosive etchants; are notable limitations in this approach.[4]

The other approach, i.e., bottom up method of fabrication develops nanostructures through systemic organization and assembly of atoms, molecules and even nanomaterials. Highly controlled chemical synthetic routes, deposition techniques, self-assembly etc., are often used in bottom up fabrication of complex architectures. This style of using building blocks to achieve desired configurations is highly promising as it offers benefits like less defects, no crystallographic damage, homogenous chemical composition, achieve small dimension structures close to atoms and no waste or unused materials.[3, 5] Bottom up approaches are still at a nascent stage of development and the objects are not mass producible like in the silicon technology. However, considering each of their significances, a strategic combination of both these approaches i.e., 'hybrid methods' could result in desired outputs.[4]

1.2 | Functional Attributes of Nanomaterials

The tenacious curiosity in these materials with size regime of 1-100 nm (in atleast one dimension) is primarily due to their diverse physical and chemical properties **(Figure 1.2)** tuneable with parameters like shape, size, composition etc., As mentioned earlier, these properties are different from those of atoms or bulk materials and occur as a result of factors like new quantum effects, high surface energy, large surface to volume ratio etc.,

For example, metal particles at the nanoscale domain become very much chemically reactive due to high percentage of interfacial atoms resulting in dominant surface dependent properties.[1, 6] Novel properties like SPR,[7] luminescence[8] appear in metal nanoparticles (NPs) tuneable to size and shape; a behaviour that isn't observed in their bulk counterparts.[9] The modulations that arise in electronic structures and charge carrier densities of semiconductor nanomaterials like quantum dots result in superior optical properties. Electrically important materials like carbon nanotubes (CNTs) and

graphene possess conductive properties subject to orientation, area of cross-section, shear force etc.,[10] Nanomaterials also result in superior mechanical properties like tensile strength, hardness, elasticity, etc., Further, effects like giant magnetoresistance (GMR), superparamagnetism are very much noticeable features of magnetic NPs.[11] It is also important to understand that these properties are further affected by and can be altered using external agents like chemical molecules, electromagnetic fields, mechanical and other physical forces. Hence, as it goes with the famous visionary saying of Richard P. Feynman, "There is plenty of room at the bottom" and one needs to exploit this true potential of these fundamental properties to build efficient systems.

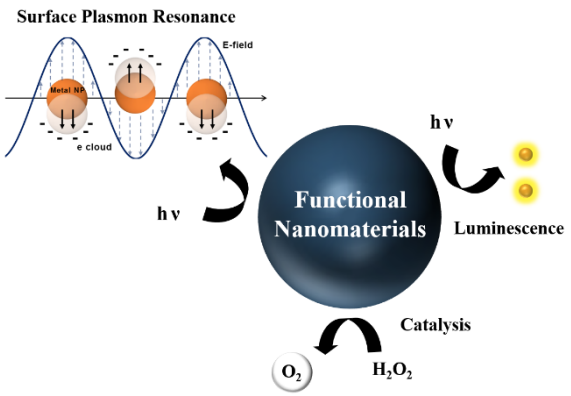

Figure 1.2. Properties of nanomaterials. Scheme illustrates some salient properties of materials at nanoscale dimensions.

1.3 | Technological Advancement

Being a highly multidisciplinary field of research, nanotechnology marked its impact in almost every arena of science and technology. To identify, some areas of potential importance for device development include robotics, intelligent systems and clinical devices where significant results obtained in the past few decades promises transformation into technology.

Ever since the challenge by Richard P. Feynman[12] in his Caltech speech to create a motor "smaller than one-sixty fourth of an inch", the interest in researchers to develop autonomous nanopropellers with on-board intelligence grew substantially.[13] Also, fabrication of intelligent systems like logic devices at lengths close to tens of atoms push the limits of feature size in devices.[14] To achieve such a feat, chemically assembled (or bottom-up) configurations offer bright prospects in the fabrication of electronic devices and circuits. Further, the powerful "tuneable" attributes of nanomaterials (as a result of quantum effects) and their ability to function in tandem with biomolecules expands the scope of application in bio-related areas[15] and could well result in devices of clinical importance.

1.4 | Autonomous Motion of Micro/Nano bots

The fascinating journey of nano-bots started with the intuition to perform astonishing tasks as they were portrayed in science fiction. However, in reality, the ability to precisely control the motion of micro- and nano structures is very much challenging due to issues arising from scaling laws, fluid dynamics, stability etc., In contrary to traditional approach in MEMS/NEMS (nano-electro-mechanical systems) to deform and move structures over defined small distances, researchers need to attain the task of fabricating synthetic propellers capable of self-propelling over long distances and must possess on board intelligence to react and carry out complex tasks when commanded

externally or internally. Such an achievement would result in ability to build complex systems and devices for real-time reconfiguration of electronics, optimization of computing power, delivering medicine, destroying toxic materials, targeted therapy, repairing of biological components, harvesting energy, operating over body parts, delivering payload etc.,[13, 16]

1.4.1 | Biological Motors

Research in motion of nanoscale structures is largely inspired by a wide variety of natural prevailing biological machines perfected over centuries of evolution. They carry complex tasks like cell division, intercellular transport, signal transmission, contraction of muscles etc., at high degrees of efficiencies.

Biological motors are capable of achieving rotational and linear motion through harnessing energy available in their vicinities cyclically as shown in **Figure 1.3**. For example, the conformational change in F_1 motor induced through the rotation of F_o ring and the central stalk as a result of flow of protons results in catalytic formation of ATP (adenosine triphosphate) by rotary engine F_oF_1-ATP.[17] Also, through the hydrolysis of ATP, the motor can perform reverse action by pumping back the protons.

The family of linear-motion biomotors constitutes kinesin, dynein, and myosin proteins. These exhibit motion in discrete steps along paths made of protein polymers by expending ATP molecules.[18]

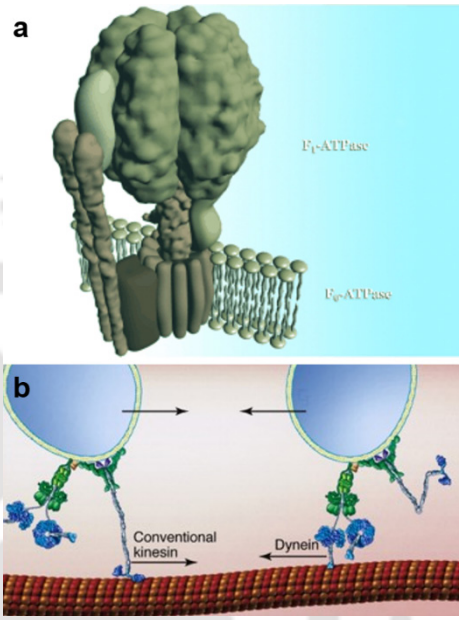

Figure 1.3. Biomotors. **(a)** Rotatory motion of F_OF_1-ATPase motor.[17] **(b)** Linear motion of kinesin and dynein motor proteins.[18] (Reprinted with permission from John Wiley and Sons [17]; Reprinted from [18], copyright 2003, with permission from Elsevier)

1.4.2 | Hybrid nanomotors – Bionanomachines

Highly evolved motor proteins like kinesin operate with efficiencies beyond 50 % which makes biomotors extremely efficient and are regarded as model systems.[19] Inorder to exploit these biomotors in technological context, conjugation of artificial and biological structures had been made. Motor proteins like, F1-adenosine triphosphate synthase (F1-ATPase) has been engineered to rotate micron-sized nickel propellers when fuelled by ATP.[20] Motor protein like kinesin had been used to transport chemical payloads along microtubules in the cell (**Figure 1.4**).[21]

Here, it is important to understand that these motors still rely on specific biological fuels and conditions. However, it may not be a viable option to create such an environment every single time to construct devices for different applications. Also, the composition of the biological environment created artificially should be almost identical with naturally existing situations which otherwise

would not result in desired motion of the motors. The dominant physical forces arising due to design constraints in devices also affect the functionality of biological motors and may in turn result in reduced or loss of activity.[13, 16]

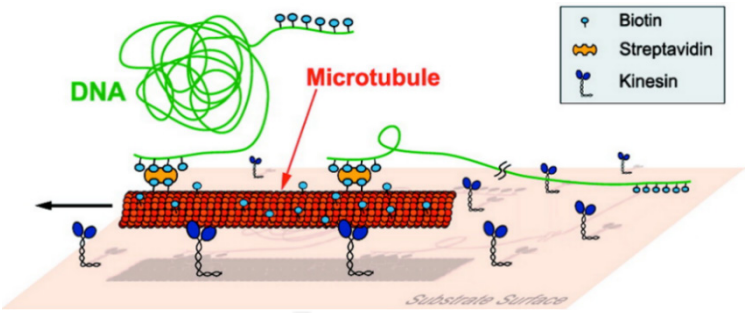

Figure 1.4. Hybrid motors. Kinesin motor propelling microtubules with DNA as cargo.[21] (Reprinted with permission from [21]. Copyright 2003, American Chemical Society)

1.4.3 | Synthetic Motors

Due to enormous complexities involved in employing biomotors (discussed earlier), researchers started to explore ways to create synthetic motors capable of achieving autonomous motion from simple liquid or surface based reactions. However, there lies certain hurdles[16] in developing these artificial nano/micro motors which are to be dealt with. Motors at such small dimensions would possess larger exposed surface area leading to asymmetric reactions causing random trajectories. High viscous drag compared to their inertial forces (at extremely low Reynolds numbers) cause hindrances to the motion. Also, stability issues arise due to dominant van der Waals forces of attraction at smaller Debye lengths and close particle distances. Hence, the above issues must be taken into consideration while formulating the design strategies inorder to achieve efficient synthetic motors.

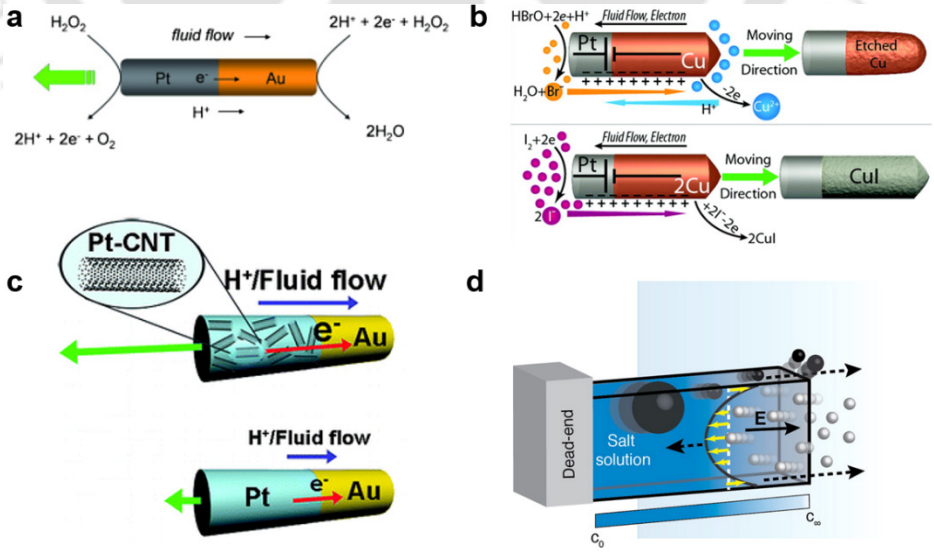

Figure 1.5. Phoretic Propulsion. (a) Electrophoretic Propulsion of bimetallic nanorod in H_2O_2.[16] **(b)** Enhanced propulsion achieved with CNTs incorporated in Pt-Au bimetallic motor.[24] **(c)** Propulsion of bimetallic motor in Br_2, I_2 solution.[25] **(d)** Charged particles motion in and out of dead end pores.[28] (Reprinted with permission from John Wiley and Sons [16]; Reprinted with permission from [24], [25] and [28]. Copyright 2011, 2008 and 2015, American Chemical Society)

The early achievement of motors had resulted from self-assembly of inorganic structures.[22] Asymmetrically shaped macroscale plates of polydimethylsiloxane coated with platinum on a small area and endowed with hydrophilic and hydrophobic regions were propelled in aqueous solution of H_2O_2 through the surface-catalysed evolution of O_2 by platinum. Since then, nanomotors of various kinds were demonstrated through different propulsion mechanisms. Self-electrophoretic motors, driven by an electric field generated across the motor in a fluid was demonstrated by Mallouk and Sen in 2004 **(Figure 1.5a)**.[23] Their motor was made of bimetallic nanorod (Pt at one end, Au at other end). These motors self-propelled at 5-10 μm s^{-1} in aqueous H_2O_2, through asymmetric decomposition, where the platinum oxidized H_2O_2 and the gold reduced it. Thereby, a proton gradient along the axis of the microrod in solution was achieved resulting in the negatively charged microrod moving towards the proton-rich region of the solution. Later, Sen's group developed another highly efficient, bubble-free, bimetallic Cu-Pt nanomotor that can self-propel in Br_2 or I_2 solution **(Figure 1.5b)**.[24] Wang's group improved the speed and power of the bimetallic motor (Pt-Au) by incorporating CNTs into the Pt segment of catalytic nanowire motors **(Figure 1.5c)**.[25] Further, their group even achieved speeds over 100 μm s^{-1} with Ag - Au alloy bimetallic nanomotors.[26] Rotational autonomous motion in aqueous H_2O_2 was demonstrated by Ozin and co-workers with bimetallic nanorods (Ni-Au).[27] Recently, motion of charged particles in and out of dead end pores had been demonstrated in the presence of an electrolyte concentration gradient involving diffusiophoretic/osmotic mechanism **(Figure 1.5d)**.[28]

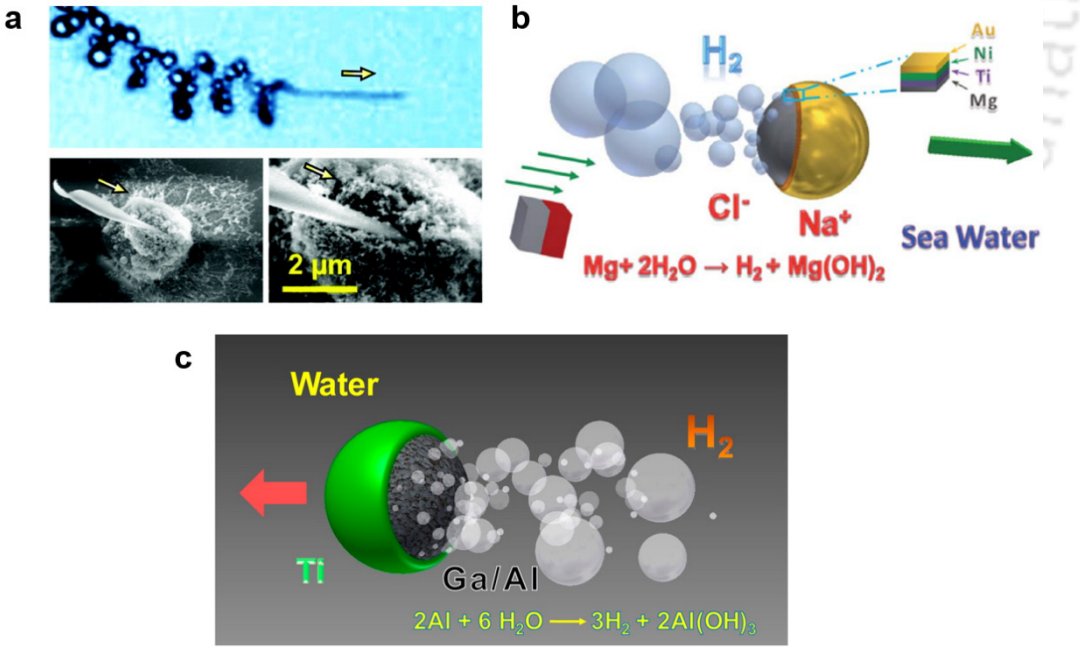

Figure 1.6. Bubble Propulsion. (a) Propulsion of nanotools capable of drilling applications.[31] **(b)** Janus motors propulsion in sea water.[33] **(c)** Janus motors capable of propelling in water.[34] (Reproduced from [33] with permission of The Royal Society of Chemistry; Reprinted with permission from [31], [34]. Copyright 2012, 2012, American Chemical Society)

Another common propulsion mechanism in micro/nano motors is bubble propulsion through the recoil thrust caused by the gas bubble. Tubular micromotors based on rolled up structures and

lithographically patterned with Au and Pt were shown to propel through oxygen bubbles generated from the decomposition of H_2O_2.[29] Self-propulsion of Ti/Fe/Pt rolled-up microtubes was also demonstrated with capabilities of being controlled by magnetic field to perform selective loading, transportation, and delivery of microscale objects.[30] Also, InGaAs/GaAs/(Cr)Pt tubes were autonomously propelled using bubble propulsion mechanism and were remotely guided to drill and embed into biomaterials (**Figure 1.6a**).[31] Tubular micromotors composed of rolled-up functional nanomembranes consisting of Fe/Pt bilayers were self-propelled in H_2O_2 for degrading organic pollutants in water.[32] Fuels other than H_2O_2 were also used to achieve bubble propulsion based micro/nano motors. Janus micromotors based on Mg NPs were shown to be propelled through hydrogen bubbles in sea water.[33] These motors were also magnetically controlled by incorporation of Ni and promises application in environmental oil remediation (**Figure 1.6b**). Water (ultrapure) - driven Janus micromotor (Al - Ga/Ti binary alloy) through ejection of hydrogen bubbles was demonstrated to move efficiently in different biological media (e.g., human serum) as shown in **Figure 1.6c**.[34]

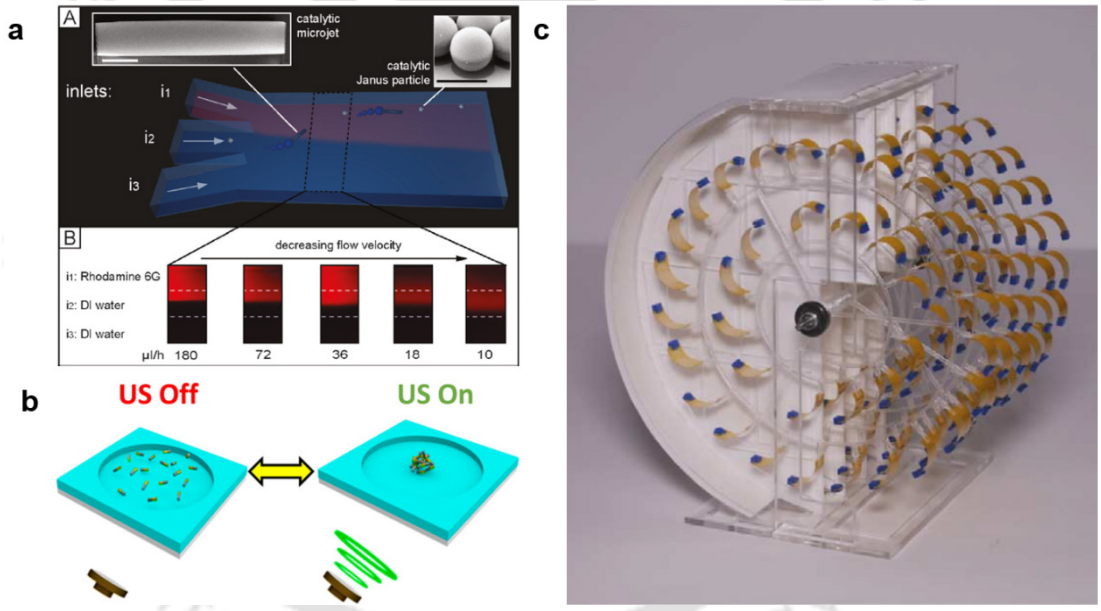

Figure 1.7. (a) Chemotaxis of microjets and janus micromotors in microfluidic device.[35] **(b)** Schooling behaviour of nanorods using ultrasound.[38] **(c)** Autonomous engine driven by evaporation with bacterial spores.[39] (Reprinted with permission from John Wiley and Sons [35]; Reprinted with permission from [38]. Copyright 2015, American Chemical Society; Reprinted with permission from Nature Publishing Group [39])

Chemotaxis is a phenomenon where the motion of the motor is driven towards (or away from) the source of signalling chemical gradients or molecules or particles. Catalytic Ti/Pt microjets and janus micromotors were shown to exhibit this behaviour by propelling towards high concentrations of H_2O_2 in a microfluidic device **(Figure 1.7a)**.[35] Pt-Au rods (2 µm long) were also shown to exhibit directed movement toward higher H_2O_2 concentrations.[36] Autonomous motors in addition to showcasing chemotactic behaviour, exhibit collective dynamic patterns (chemotactic migration) in response to chemical and physical signals by nearby active swimmers. Micrometer-sized AgCl particles were shown to secrete chemicals (ions) as it propels in water through self-diffusiophoresis under UV

illumination. Other particles in the vicinity responded by 'schooling' thus resulting in higher particle concentrations.[37] Also, similar effect through acoustic field application was achieved where self-propelling Pt-Au nanowire motors (diameter: 200 nm, length: 2 μm) in H_2O_2 migration towards pressure nodes **(Figure 1.7b)**.[38] Further, recent works on autonomously driven macroscale evaporation-driven engines with bacterial spores strongly suggest device construction possibilities employing micro/nano motors **(Figure 1.7c)**.[39]

1.5 | Decisive Logic Systems and Sensors

Intelligent systems are capable of prompt decision making by responding to various forms of stimuli. These are very common in silicon based electronics in the form of logical devices and sensors. However, with feature size of microchips decreasing drastically to physical limits and also issues in other physical parameters led to pursue alternative paths.[40] Most of these attempts were targeted to fabricate devices on the nanometer-length scale. Molecular logic device and sensors are such promising objects, where molecules function as the key elements in decision making and computational devices. The core idea in the molecular logic systems is to process input data given in the form physical and chemical signals through molecules and their inherent chemical transformations to result the output through means of physical (like in terms of light) and chemical signals.[41] This approach gives a possibility to achieve small feature size, deal with quantum effects, specific organization and integrated functionality. Molecular logic devices offer advantages like no physical connections (if communication is carried in terms of light) and flexible variation of the input and/or output reading. Currently, the focus has been directed to fabricate molecular building blocks to emulate functions of semiconductor based computing and also to project their applications in areas such as medical diagnostics, smart materials, sensing etc.,

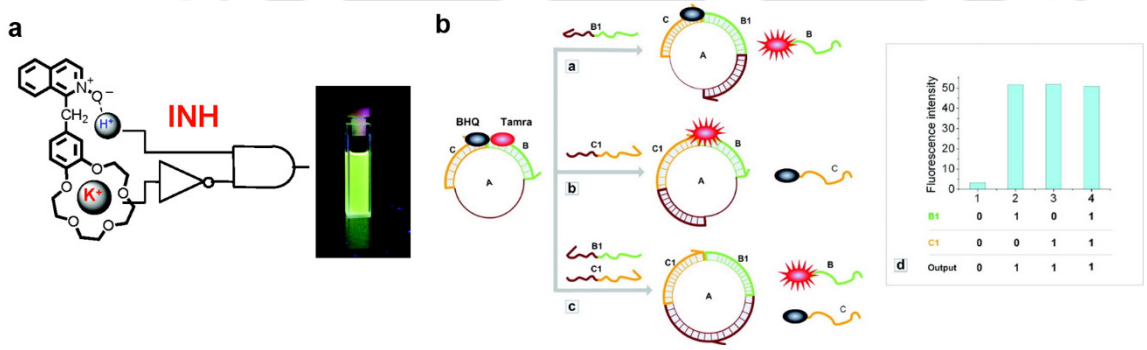

Figure 1.8. (a) INHIBIT logic achieved with organic molecule and ions as inputs.[50] **(b)** OR logic implementation with circular DNA.[53] (Reprinted with permission from [50], [53]. Copyright 2004, 2010, American Chemical Society)

The idea of using molecules for achieving logic gate operation was initiated by A. P. de Silva et. al.,[42] By using organic molecules, they developed AND logic operation with protons and sodium ions as chemical inputs with output signal as fluorescence. Since then, several organic molecules were employed to achieve basic gates, half adder, half subtractor, multiplexer, demultiplexer, encoder, decoder, keypad, reversible lock, boolean and fuzzy logic, sequential logic, parity checker

with varieties of inputs such as ions, chemicals, light and output measured in terms of luminescence, absorbance, singlet oxygen generation etc.,[43-51] Also, several decision making systems were developed by exploiting the activity of several biological moieties.[52-55] A couple of logic implementation mention above were shown in **Figure 1.8**.

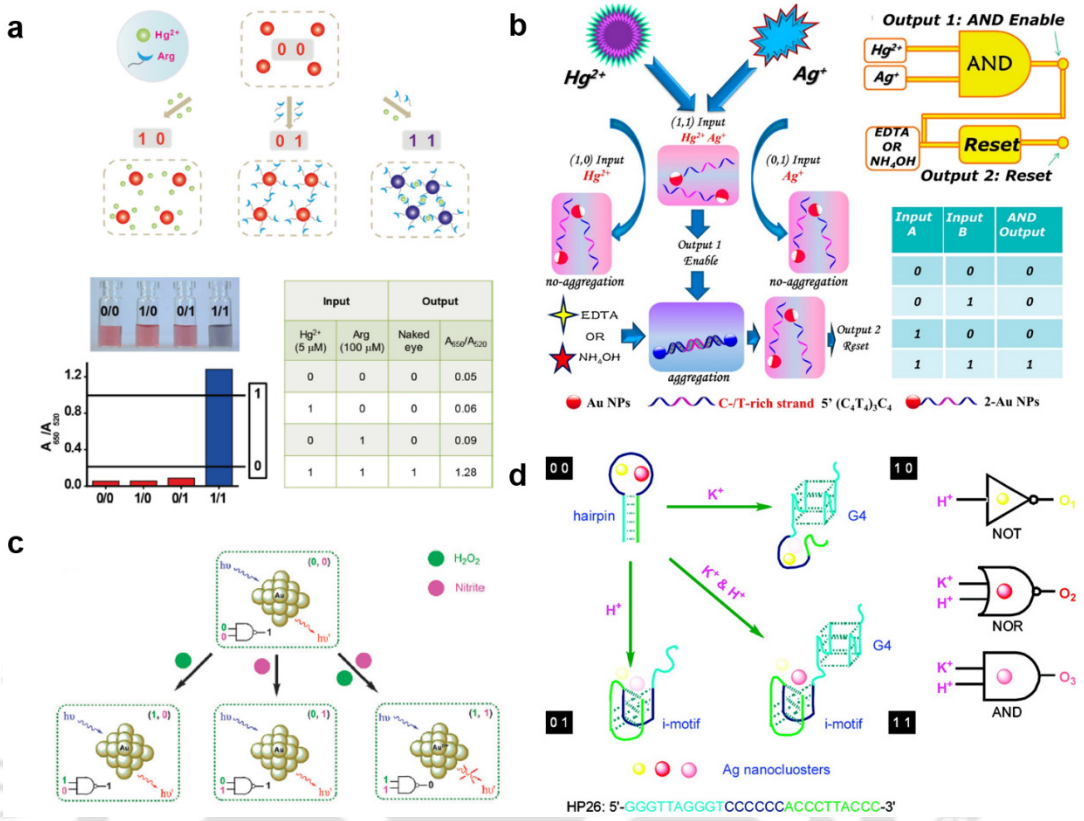

Figure 1.9. (a, b) Colorimetric implementation of AND logic based on Au NPs with ions as inputs.[57-58] (c) NAND logic for nitrite detection using luminescent Au NCs.[61] (d) Multiple logic gates using fluorescent Ag NCs.[62] (Reprinted with permission from John Wiley and Sons [57]; Reproduced from [61] with permission of The Royal Society of Chemistry; Reprinted with permission from [58], [62]. Copyright 2013, 2011, American Chemical Society)

Optical based reading in terms of luminescence and absorbance had been widely employed in molecular logic systems as they offer the fastest mode of communication along with no physical connections. Nanomaterials exhibit "tuneable" optical properties like luminescence and SPR with various physicochemical perturbations. These materials offer advantages like high absorption extinction coefficients, high sensitivity, good solubility, high luminescence, low photoblinking, less photobleaching, wide ranges of absorbance and emissions, large stoke shift compared to organic counterparts. Due to the above mentioned advantages, nanomaterials had been used widely in developing decision making systems. A colorimetric non-implication logic gate with gold NPs was developed with inputs as melamine and Hg^{2+}.[56] Also, alongside elementary (AND, OR and INHIBIT), integrative (AND + OR) logic operations based on specific coordination effect between amino acids and metal ions were demonstrated using functionalized Au NPs (**Figure 1.9a**).[57] Nanomaterials were also conjugated with various biomolecules for development of these logic systems. Based on aggregation of the DNA modified Au NPs, a set of logic gates (YES, AND,

INHIBIT and XOR) were successfully demonstrated (**Figure 1.9b**).[58] Further, AND, INHIBIT and IMPLICATION logic was achieved with the coordination chemistry of cytosine-Ag^{+}-cytosine (C–Ag+–C) and disparate adsorption properties of ssDNA and dsDNA modified AuNPs.[59] Luminescence based logic gates (OR and XOR) based on dual aptamer strategy was achieved by employing high photoluminescence quality of QDs.[60] Bovine serum albumin (BSA) functionalized luminescent Au NCs were employed in nitrite ions detection through construction of NAND logic gate (**Figure 1.9c**).[61] Multiple logic structures were also developed using ion-tuned DNA/Ag fluorescent nanoclusters (NCs), with K^{+} and H^{+} as two inputs (**Figure 1.9d**).[62]

1.6 | Medical Devices

With the existence of functional components of living systems (cellular components) at the nanoscale dimensions, the possible applications of nanomaterials in life sciences is arguably predominant.[63-64] The exciting features of nanomaterials, their ability to integrate with biological components and the high-end technological tools present great prospects to develop devices for healthcare. Significant features like surface to volume ratio, surface modifications, good solubility, specificity, multifunctionality along with characteristic physical and chemical properties of nanomaterials are worth investigating for various biological applications. There is a huge amount of work being carried out in diverse areas related to those of life sciences. Particularly, bulk amount of efforts had been targeted towards disease diagnostics and therapy. Also, with today's advancement in technology and communication, devices of clinical importance are expected to become integral parts of life making diagnosis and therapy must rapid and simple.

1.6.1 | Diagnostics

The growing database and knowledge of genomics and proteomics are creating opportunities to make disease diagnostics possible at early stages or even before the symptoms arise. The tools of nanotechnology and the attributes of nanomaterials are being employed in various approaches and techniques to devise novel diagnostics systems and devices.

***In-vitro* systems:** The applications of nanomaterials in the field of genomics and proteomics[65] were featured in several methods developed to enhance the efficacy of the existing techniques in PCR and array based methods. NPs, QDs, CNTs, carbon nano-powder, graphene etc., are some of the materials which are shown to improve the efficacy of PCR process.[66-69] Plasmonic property of the Au NPs have been exploited in the colorimetric detection of PCR products and for biomarker samples in microarray devices.[70] Owing to several advantages over conventional organic dyes/probes, QDs have been used as fluorometric probes in analyses involving gene and protein expression studies.[71] As a result of miniaturization in technology several types of biochips, biosensors and analytical systems based on optical (luminescence, absorbance, SPR etc.,), electrochemical (potentiometric, amperometric, capacitive, impedimetric etc.,) and mass sensitive (SAW (surface acoustic wave), microcantilever etc.,) principles have been developed (**Figure 1.10**).[72-76] With unique spectral

barcodes, an analytical method for DNA detection using quantum dots has been achieved.[77] The development of microfluidics have resulted in nanopore technologies through electrophoresis or chromatographic principles.[78] Also, with 'Lab on a Chip', the idea to integrate basic diagnostic facilities on a single platform with minimal quantities of substance promises great applications of nanomaterials and nanotechnology.[79]

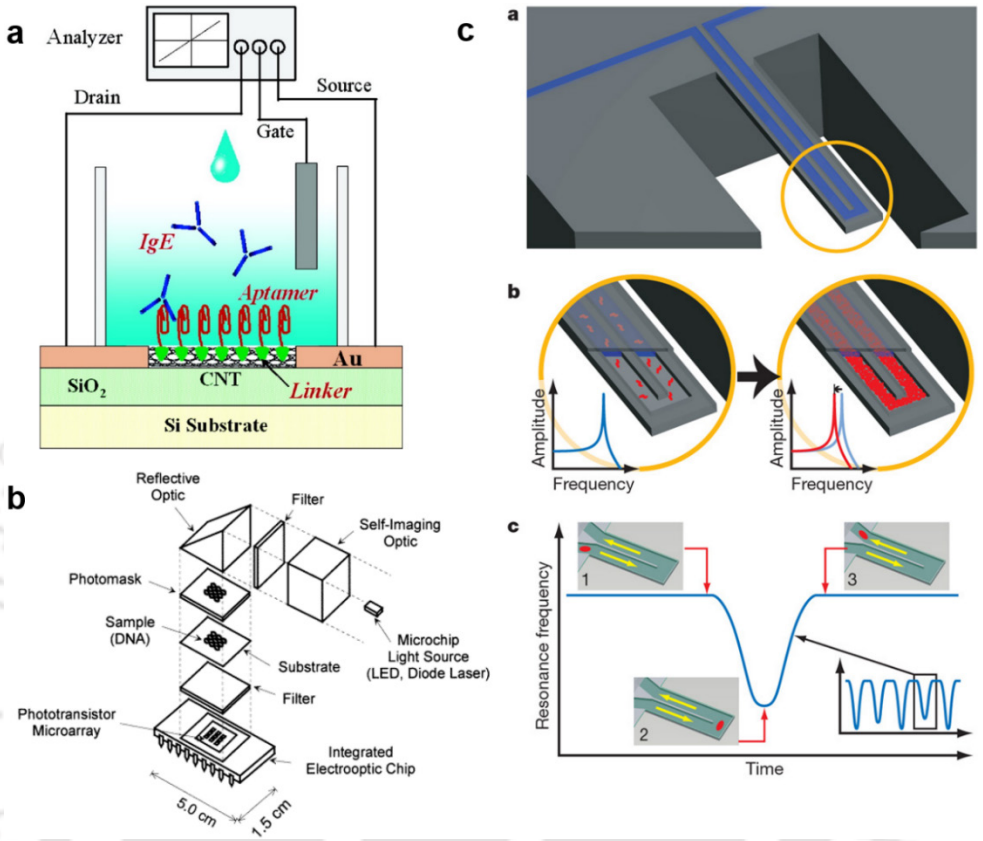

Figure 1.10. **(a)** Field-effect transistor (FET) based biosensor.[72] **(b)** Block diagram of DNA Chip.[73] **(c)** Micro cantilever based biosensors.[75] (Reprinted with permission from [72], [73]. Copyright 2007,1999, American Chemical Society; Reprinted by permission from Macmillan Publishers Ltd: Nature [75], copyright (2007)

***In-vivo* systems:** Nanomaterials are playing important roles in enhancing the efficiency and reliability in diagnosis and imaging of *in-vivo* systems. Specific contrast agents and radiopharmaceuticals given to the patient to perform molecular imaging of biomarkers responsible for disease occurrence had been made with nanomaterials.[80]

Also specialized techniques like ultrasonic vibrations, nuclear imaging, MRI (magnetic resonance imaging), X-ray imaging have been developed with their specific imaging modules and contrast agents. These imaging techniques not only help in diagnosing the disease but also in continuous monitoring, evaluation and progress of the given therapy. Perfluorohydrocarbons based NPs were used as ultrasonic contrast agents.[81] Magnetic nanomaterials based on Fe_2O_3, Fe_3O_4 have been put to use extensively as MRI contrast agents.[82] QDs and atomic clusters had been applied for fluorescence based imaging of cellular components.[83-84] Importantly, medical appliances for rapid, simple and relatively cheap diagnostics of diseases and pathogenic infections have been developed using nanomaterials and tools of nanotechnology.[85] Recent progress in soft and stretchable

electronics using CNTs and graphene indicates the possibility for implantable devices for health care.[86]

1.6.2 | Therapy

Different classes of nanomaterials had been put into action to combat diseases.[87] With small dimensions, good solubility, surface modifiability for encapsulation and coating, these can be transported in media like blood to function either as 'carriers' of drugs/genes and/or to act as therapeutic modules by themselves. Further, conjugation of these materials with 'targeted molecules' helps to achieve delivery to regions of particular interest. Through incorporation of suitable nanomaterials, targeting of the delivery vehicle and/or the release of the active substance at desired locations can be done externally by means of magnetic fields,[88] near-infrared radiation,[89] ultrasonic vibrations,[90] heat[91] etc., Au NPs, Ag NPs, nanoshells, DNA NPs, fullerenes, Fe_2O_3, Fe_3O_4 NPs, liposomes; peptides based NPs, CNT, QDs, nanogels, dendrimers, micelles, polymer NPs have been used for therapeutic purposes.[92]

As mentioned above, in addition to the role as delivery vehicles, these nanomaterials showed capabilities of therapeutic effect. Ag NPs were reported to cause cancer cell death through ROS mediated apoptosis.[93] Also, external agents like near-infrared radiation or rapid oscillating magnetic field have been employed to heat metal-containing nanomaterials in order to kill cancer cells.[94-95] Treatments like PDT with photosensitizers have been shown to be augmented in the presence of nanomaterials. Also, on a much promising note, several nanomaterials are shown to act as photosensitizers for PDT treatment with the capability of singlet oxygen generation under suitable excitation.[96] Delivery vehicles are often conjugated with contrast agents for the purpose of tracking their progress. In some cases, these contrast agents act as a therapeutic agent, thus enabling simultaneous diagnosis and therapy coupled with active substances.[97]

1.7 | Opportunities and Challenges

The tremendous progress achieved in research at these small scales envisages heavy prospects for technological transformation. The developments in self-propelled micro/nano motors indicate their potential in carrying out complex tasks. With expertise gained in fabricating these motors and knowledge about their dynamics, it presents a wonderful opportunity to engineer devices utilizing their autonomous motion. The initial success of logic systems developed through bottom up fabrication of nanomaterials encourages to design application oriented devices and sensors based on these responsive characteristics. Also, there lies ample opportunities to construct novel systems to operate in diverse environmental platforms and be simultaneously influential to various forms of chemical and physical stimuli. The promising implications of nanotechnology in life science could very well lead to medical devices with increased efficiencies in both diagnosis and therapy. It also opens up new possibilities to simply existing techniques and modify the device functionality without comprising on efficiency. Further, by identifying the close intimacy between the fields of intelligent

systems and medical devices, it would be highly promising to aspire for devices with on-board intelligence capable of addressing clinical needs.

However, to achieve substantial growth in development of devices utilizing these nanomaterials, there are certain areas which seek improvement. It is of immense importance to achieve functional nanomaterials with nearly uniform physical and chemical characteristic in every batch of production. The synthetic approaches adopted should be simple, rapid and capable of mass production. The various methods adopted should easy, quick, bio and environmentally friendly. Importantly, the challenges also arise in maintaining the functionality of the nanomaterials while amalgamating to device environment. Hence, the device must be flexible in nature built with provision for hierarchical design. The current dissertation is an attempt to address the above mentioned issues and design devices utilizing the properties of nanomaterials.

1.8 | References

1) C. Burda, X. Chen, R. Narayanan, et al., *Chem. Rev.* **2005**, *105*, 1025.
2) E. Roduner, *Chem. Soc. Rev.* **2006**, *35*, 583.
3) A. Biswas, I. S. Bayer, A. S. Biris, et al., *Adv. Colloid Interface Sci.* **2012**, *170*, 2.
4) B. D. Gates, Q. Xu, M. Stewart, et al., *Chem. Rev.* **2005**, *105*, 1171.
5) V. Balzani, A. Credi, M. Venturi, *Chem. Eur. J.* **2002**, *8*, 5524.
6) R. Narayanan, M. A. El-Sayed, *J. Phys. Chem. B* **2005**, *109*, 12663.
7) M. A. Garcia, *J. Phys. D: Appl. Phys.* **2012**, *45*, 389501.
8) C. Feldmann, *Nanoscale* **2011**, *3*, 1947.
9) Y. Yin, A. P. Alivisatos, *Nature* **2005**, *437*, 664.
10) T. Ando, *NPG Asia Mater.* **2009**, *1*, 17.
11) A. H. Lu, E. L. Salabas, F. Schuth, *Angew. Chem. Int. Ed. Engl.* **2007**, *46*, 1222.
12) R. Michael, *PhyW* **2001**, *14*, 25.
13) G. A. Ozin, I. Manners, S. Fournier-Bidoz, et al., *Adv. Mater.* **2005**, *17*, 3011.
14) V. Bojinov, N. Georgiev, *Journal of the University of Chemical Technology and Metallurgy* **2011**, *46*, 3.
15) S. Shrivastava, D. Dash, *Journal of Nanotechnology* **2009**, *2009*, 1.
16) S. Sengupta, M. E. Ibele, A. Sen, *Angew. Chem. Int. Ed. Engl.* **2012**, *51*, 8434.
17) D. W. Wendell, J. Patti, C. D. Montemagno, *Small* **2006**, *2*, 1324.
18) R. D. Vale, *Cell* **2003**, *112*, 467.
19) S. M. Block, *Trends Cell Biol.* **1995**, *5*, 169.
20) R. K. Soong, G. D. Bachand, H. P. Neves, et al., *Science* **2000**, *290*, 1555.
21) S. Diez, C. Reuther, C. Dinu, et al., *Nano Lett.* **2003**, *3*, 1251.
22) R. F. Ismagilov, A. Schwartz, N. Bowden, et al., *Angew. Chem. Int. Ed.* **2002**, *41*, 652.
23) W. F. Paxton, K. C. Kistler, C. C. Olmeda, et al., *J. Am. Chem. Soc.* **2004**, *126*, 13424.
24) R. Liu, A. Sen, *J. Am. Chem. Soc.* **2011**, *133*, 20064.

25) R. Laocharoensuk, J. Burdick, J. Wang, *ACS Nano* **2008**, *2*, 1069.
26) U. K. Demirok, R. Laocharoensuk, K. M. Manesh, et al., *Angew. Chem. Int. Ed. Engl.* **2008**, *47*, 9349.
27) S. Fournier-Bidoz, A. C. Arsenault, I. Manners, et al., *Chem. Commun. (Camb.)* **2005**, 441.
28) A. Kar, T.-Y. Chiang, I. Ortiz Rivera, et al., *ACS Nano* **2015**, *9*, 746.
29) K. M. Manesh, M. Cardona, R. Yuan, et al., *ACS Nano* **2010**, *4*, 1799.
30) A. A. Solovev, S. Sanchez, M. Pumera, et al., *Adv. Funct. Mater.* **2010**, *20*, 2430.
31) A. A. Solovev, W. Xi, D. H. Gracias, et al., *ACS Nano* **2012**, *6*, 1751.
32) L. Soler, V. Magdanz, V. M. Fomin, et al., *ACS Nano* **2013**, *7*, 9611.
33) W. Gao, X. Feng, A. Pei, et al., *Nanoscale* **2013**, *5*, 4696.
34) W. Gao, A. Pei, J. Wang, *ACS Nano* **2012**, *6*, 8432.
35) L. Baraban, S. M. Harazim, S. Sanchez, et al., *Angew. Chem. Int. Ed. Engl.* **2013**, *52*, 5552.
36) Y. Hong, N. M. Blackman, N. D. Kopp, et al., *Phys. Rev. Lett.* **2007**, *99*, 178103.
37) M. Ibele, T. E. Mallouk, A. Sen, *Angew. Chem. Int. Ed. Engl.* **2009**, *48*, 3308.
38) T. Xu, F. Soto, W. Gao, et al., *J. Am. Chem. Soc.* **2015**, *137*, 2163.
39) X. Chen, D. Goodnight, Z. Gao, et al., *Nat. Commun.* **2015**, *6*, 7346.
40) J. M. Tour, M. Kozaki, J. M. Seminario, *J. Am. Chem. Soc.* **1998**, *120*, 8486.
41) J. Andreasson, U. Pischel, *Chem. Soc. Rev.* **2015**, *44*, 1053.
42) P. A. de Silva, N. H. Q. Gunaratne, C. P. McCoy, *Nature* **1993**, *364*, 42.
43) J. Andreasson, U. Pischel, S. D. Straight, et al., *J. Am. Chem. Soc.* **2011**, *133*, 11641.
44) P. L. Gentili, *Chem. Phys.* **2007**, *336*, 64.
45) S. Erbas-Cakmak, E. U. Akkaya, *Angew. Chem. Int. Ed. Engl.* **2013**, *52*, 11364.
46) P. Remon, M. Balter, S. Li, et al., *J. Am. Chem. Soc.* **2011**, *133*, 20742.
47) H. Tian, *Angew. Chem. Int. Ed. Engl.* **2010**, *49*, 4710.
48) J. Andréasson, S. D. Straight, T. A. Moore, et al., *J. Am. Chem. Soc.* **2008**, *130*, 11122.
49) R. Guliyev, S. Ozturk, Z. Kostereli, et al., *Angew. Chem. Int. Ed.* **2011**, *50*, 9826.
50) J.-M. Montenegro, E. Perez-Inestrosa, D. Collado, et al., *Org. Lett.* **2004**, *6*, 2353.
51) M. Balter, S. Li, J. R. Nilsson, et al., *J. Am. Chem. Soc.* **2013**, *135*, 10230.
52) M. Hoffman-Sommer, A. Supady, E. Klipp, *Front. Physiol.* **2012**, *3*, 287.
53) C. Zhang, J. Yang, J. Xu, *Langmuir* **2010**, *26*, 1416.
54) T. S. Moon, C. Lou, A. Tamsir, et al., *Nature* **2012**, *491*, 249.
55) A. S. Deonarine, S. M. Clark, L. Konermann, *Future Generation Computer Systems* **2003**, *19*, 87.
56) J. Du, S. Yin, L. Jiang, et al., *Chem. Commun. (Camb.)* **2013**, *49*, 4196.
57) Y. Xianyu, Z. Wang, J. Sun, et al., *Small* **2014**, *10*, 4833.
58) L. Zhang, Z. X. Wang, R. P. Liang, et al., *Langmuir* **2013**, *29*, 8929.
59) Y. Zhang, M. Li, H. Liu, et al., *New J. Chem.* **2016**, *40*, 5516.
60) S. J. Xiao, P. P. Hu, L. Q. Chen, et al., *PLoS One* **2013**, *8*, e53935.

61) J. Zhang, C. Chen, X. Xu, et al., *Chem. Commun. (Camb.)* **2013**, *49*, 2691.
62) T. Li, L. Zhang, J. Ai, et al., *ACS Nano* **2011**, *5*, 6334.
63) O. Salata, *J. Nanobiotechnology* **2004**, *2*, 1.
64) J. Gao, B. Xu, *Nano Today* **2009**, *4*, 37.
65) M. R. Mohamadi, L. Mahmoudian, N. Kaji, et al., *Nano Today* **2006**, *1*, 38.
66) X. Lou, Y. Zhang, *ACS Appl. Mater. Interfaces* **2013**, *5*, 6276.
67) H. Li, J. Huang, J. Lv, et al., *Angew. Chem. Int. Ed. Engl.* **2005**, *44*, 5100.
68) Y. Bai, Y. Cui, G. C. Paoli, et al., *ACS Appl. Mater. Interfaces* **2015**, *7*, 13142.
69) F. Sang, Y. Yang, H. Wang, et al., *J. Biomed. Sci. Eng.* **2012**, *05*, 295.
70) D. Kim, W. L. Daniel, C. A. Mirkin, *Anal. Chem.* **2009**, *81*, 9183.
71) R. Q. Liang, W. Li, Y. Li, et al., *Nucleic Acids Res.* **2005**, *33*, e17.
72) K. Maehashi, T. Katsura, K. Kerman, et al., *AnaCh* **2007**, *79*, 782.
73) T. Vo-Dinh, J. P. Alarie, N. Isola, et al., *AnaCh* **1999**, *71*, 358.
74) H. Shi, F. Yang, W. Li, et al., *Biosens. Bioelectron.* **2015**, *66*, 481.
75) T. P. Burg, M. Godin, S. M. Knudsen, et al., *Nature* **2007**, *446*, 1066.
76) R. Raiteri, M. Grattarola, H.-J. Butt, et al., *Sensors Actuators B: Chem.* **2001**, *79*, 115.
77) M. Han, X. Gao, J. Z. Su, et al., *Nat Biotech* **2001**, *19*, 631.
78) T. Sano, N. Iguchi, K. Iida, et al., *ApPhL* **2003**, *83*, 4438.
79) J. G. Gardeniers, A. van den Berg, *Anal. Bioanal. Chem.* **2004**, *378*, 1700.
80) W. Lin, *Chem. Rev.* **2015**, *115*, 10407.
81) S. Son, H. S. Min, D. G. You, et al., *Nano Today* **2014**, *9*, 525.
82) J. Estelrich, M. J. Sanchez-Martin, M. A. Busquets, *Int J Nanomedicine* **2015**, *10*, 1727.
83) S. Zhu, J. Zhang, S. Tang, et al., *Adv. Funct. Mater.* **2012**, *22*, 4732.
84) S. Palmal, N. R. Jana, *Wiley Interdiscip Rev Nanomed Nanobiotechnol* **2014**, *6*, 102.
85) V. R. Singh, *Irbm* **2008**, *29*, 326.
86) C. Choi, M. K. Choi, T. Hyeon, et al., *ChemNanoMat* **2016**.
87) L. Zhang, F. X. Gu, J. M. Chan, et al., *Clin. Pharmacol. Ther.* **2008**, *83*, 761.
88) V. V. Mody, A. Cox, S. Shah, et al., *Appl. Nanosci.* **2013**, *4*, 385.
89) B. Radt, T. A. Smith, F. Caruso, *Adv. Mater.* **2004**, *16*, 2184.
90) S. Mitragotri, *Nat. Rev. Drug Discov.* **2005**, *4*, 255.
91) A. Gandhi, A. Paul, S. O. Sen, et al., *Asian J. Pharmacol.* **2015**, *10*, 99.
92) R. Lehner, X. Wang, S. Marsch, et al., *Nanomedicine* **2013**, *9*, 742.
93) P. P. Fu, Q. Xia, H. M. Hwang, et al., *J. Food Drug Anal.* **2014**, *22*, 64.
94) L. R. Hirsch, R. J. Stafford, J. A. Bankson, et al., *Proc. Natl. Acad. Sci. U. S. A.* **2003**, *100*, 13549.
95) A. Hervault, N. T. Thanh, *Nanoscale* **2014**, *6*, 11553.
96) S. S. Lucky, K. C. Soo, Y. Zhang, *Chem. Rev.* **2015**, *115*, 1990.
97) K. H. Bae, H. J. Chung, T. G. Park, *Mol. Cells* **2011**, *31*, 295.

Chapter 2

Induction of Electromotive Force by Autonomously Moving Magnetic Bot

ABSTRACT

Induction of electromotive force (emf) into a Faraday coil by an autonomously moving composite magnetic particle in aqueous medium is achieved. The particle consisted of a micron-sized polymer sphere, which was decorated with catalytic palladium nanoparticles (Pd NPs) and attached to a micron-scale magnet. The Pd NPs catalytically decomposed H_2O_2 to generate O_2, resulting in buoyancy-driven vertical motion of the particle, while the micro magnet induced emf during the flight. The signal was sufficiently strong to illuminate light-emitting diodes following appropriate amplification. This distinctive approach is expected to pave the way to developing synthetic bots which are autonomously propelled, generating their own signal for running complex circuitry.

The advent of nanoscale science and technology has kindled vigorous interest in the systematic development in the field of autonomous motion of microscopic objects in liquid media.[1-2] Significant developments had been based on the use of the catalytic decomposition of H_2O_2 and nanoscale manipulation of biomolecules in moving objects of micronscale and nanoscale dimensions. Bubble propulsion,[3-5] electrophoresis,[6] thermophoresis,[7] diffusophoresis,[8] magnetophoresis[9] and motion due to interfacial gradients[10] are the primary mechanisms forming the basis of motion of these objects. Control over the motion has been achieved by external magnetic fields,[11] thermal modulations,[12-14] light,[15] ultrasonic wave,[16] internal pH[17] and chemical gradients,[18] viscosity of the medium[19] and surface tension[20] of the liquid. Further, nanoscale motors based on organic molecules[21] and DNA[22] offer the option of specific functionalization and thereby molecular control over their properties and motion. Essentially, the efforts have been to emulate the function of naturally occurring biological nanoscale motors[23-24] - at least partially - using chemical energy as the driving force for the motion. The generated motion of these nanoscale objects could well be useful as a source of secondary energy. For example, it is conceivable that the production of electrical energy in situ would make it possible for the nanobots not only to display controlled motion but also to perform higher level functions for which the required additional energy may not be available or achievable using conventional bots. Thus an autonomously moving magnetic device could generate electrical energy induced by its motion through a metallic or otherwise electrically conducting coil. This could also pave the way for communicative bots. However, the possibility of such a transduction needs to be demonstrated first.

This chapter reports the induction of electromotive force (emf) into a Faraday coil by an autonomously moving magnetic microparticle which was attached to a polymer resin containing catalytic Pd NPs. The catalytic decomposition of aqueous H_2O_2 generated O_2 bubbles which were

adsorbed on the microbot resulting in buoyancy driven vertical motion of the attached magnet. Alternating electrical signals were generated about 20 times per minute for the vertical flights up and down a glass tube. The signal strength could also be improved to be sufficiently strong for amplification to light an LED (light emitting diode), when a larger magnet was used. The experimental design also allowed for periodic vertical motion of the bot until the fuel was exhausted.

2.1 | Autonomous Signal Generator

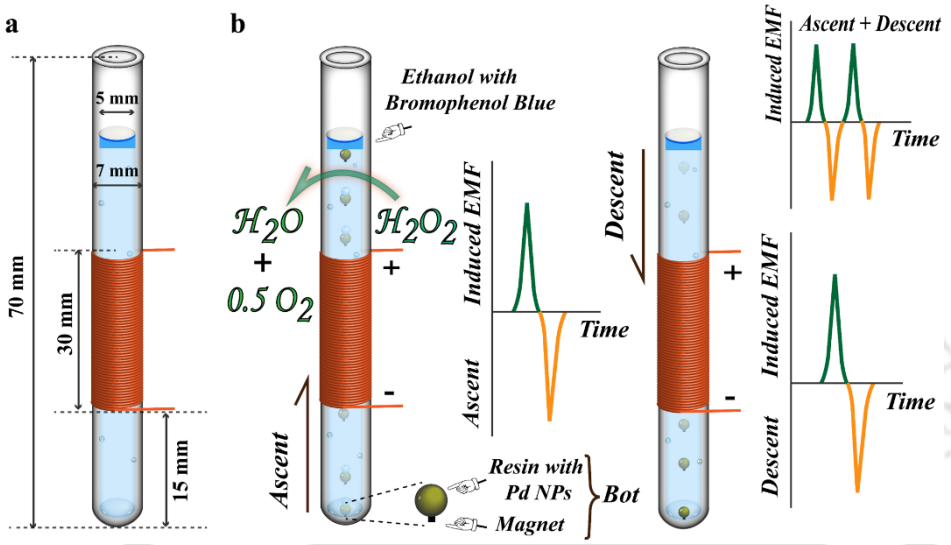

Figure 2.1. Experimental design. (a) In the experiment a glass tube contains 1 mL of 5 % aqueous H_2O_2, along with 60 µL of ethanol (mixed with bromophenol blue) layered on the top. A part of the tube was wrapped with a copper coil (red) for emf induction. **(b)** The bot, which is a resin bead containing embedded Pd NPs with an attached rare-earth magnet, was placed at the bottom of the tube. Left tube: Pd-catalyzed decomposition of H_2O_2 generates O_2, which forms bubbles providing buoyancy for the upward motion of the bot. Right tube: The bubbles burst when the bot comes in contact with ethanol, making the bot descend. Each flight (ascent and descent) generates an emf signal as shown in the plots beside the tubes. The overall signal for one cycle is shown on top right.

Figure 2.1 shows the overall experimental setup and the resultant emf generated by the vertical motion of the microbot. The microbot was made of two components: Pd NPs embedded in a micron-sized polymer resin sphere and a micron-sized (N-42 grade) rare-earth magnet which was affixed to the polymer. The overall diameter of the object was 1.4 mm (**Figure 2.1b**). The fabrication of the bot is detailed in **Appendix A** (Design and Characterization of the Bot). The bot was placed in a Borosil glass tube which was wrapped with copper wire (34 SWG (standard wire gauge), 1000 windings) as shown in **Figure 2.1a**. The glass tube was filled with 1 mL of 5% (w/v) aqueous H_2O_2. The Pd NPs catalysed the decomposition of H_2O_2 into O_2; the so-produced oxygen bubbles adhered to the polymer bead and eventually a single larger bubble formed by coalescence of several smaller bubbles.[11, 19] When the number of bubbles or the total volume of the bubble was sufficiently high, then the buoyancy force balanced the gravitational and viscous forces on the bot and the bead moved upward with terminal velocity[11] (ascent phase in **Figure 2.1b**). Driven by the catalytic decomposition of H_2O_2 (fuel), the bot marked a thermodynamic efficiency of 8.7 x 10^{-5} % (Reaction

Kinetics and Efficiency Calculations in **Appendix A**), which is generally higher than the efficiencies calculated for fuel-driven propulsion.[25]

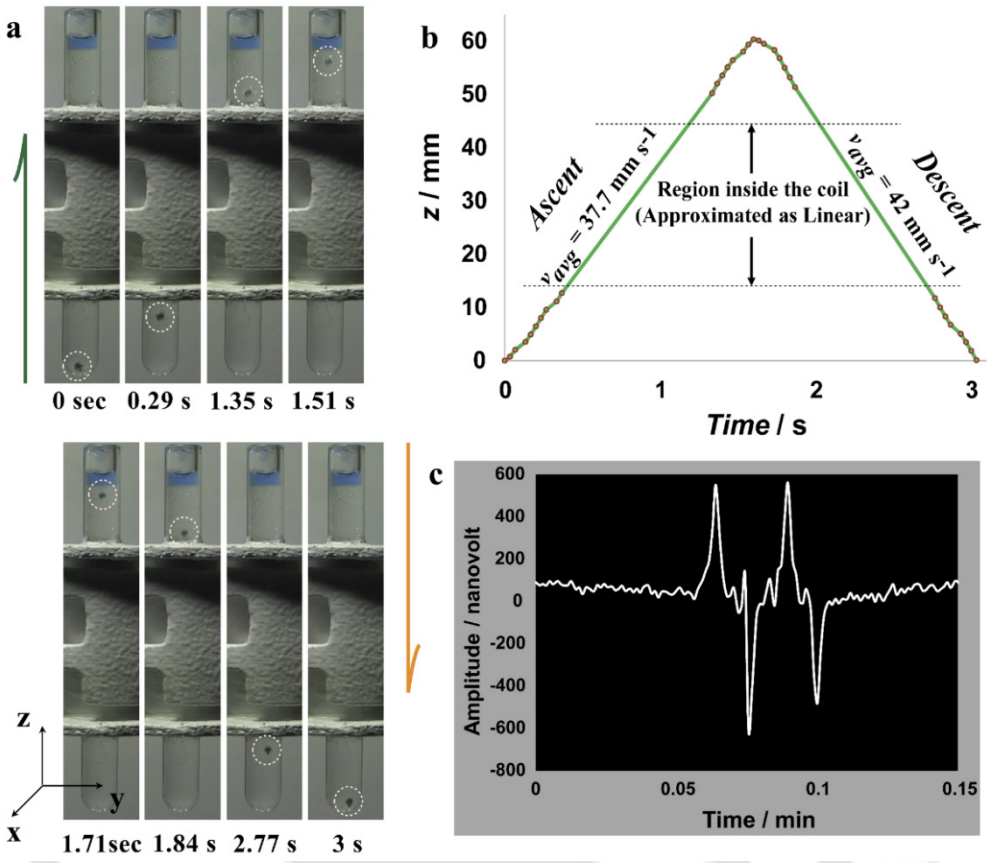

Figure 2.2 Motion profile of the bot and induced voltage. (a) Frame-by frame images showing the ascending (top) and descending (bottom) phases of the bot. (b) Position versus time plot of the ascent and the descent phases with average velocity in each phase. (c) Plot illustrates the induced voltage resulting from one cycle of the autonomous motion of the bot.

It may be mentioned here that when the bot was made of only the magnet, then the H_2O_2 decomposition rate was significantly small and thus the rate of bubble growth was very slow (**Appendix A, movie A2.1, Figure A2.1**). Incorporation of Pd NPs embedded polymer sphere led to faster bubble formation and hence this construction was preferred. Further, it was observed that the bot remained stationary at the meniscus for a sufficiently long time or moved to the wall of the tube, due to the attached bubbles and a rapid downward movement was prevented (descent phase in **Figure 2.1b**). This was addressed by layering 60 mL of ethyl alcohol (95% v/v) - a known bubble breaker[26] - mixed with bromophenol blue on the top of the reaction liquid (**Figure 2.1**). Here, bromophenol blue was used to observe and record the stability of the alcohol layer and it did not participate in any reaction. Thus the experimental arrangement allowed the repeated vertical motion of the microbot with a frequency of about five cycles per minute.

Figure 2.2a shows images of the microbot at different vertical positions during its motion for a complete cycle. As is clear from the images, the bot stayed away from the wall and moved through nearly the center of the liquid column during its flight. It is important to mention here that the average velocity of the bot during its upward movement was 37.7 mm s^{-1} and for the downward movement it

was 42 mm s^{-1}; this corresponds to 27 and 30 times its body length per second as inferred from the motion profile in **Figure 2.2b**.

Further, as the magnetic chemical locomotor moved up and down, its magnetic flux induced emf into the surrounding copper coil. The terminals of the copper coil from the experimental setup were connected to the nanovoltmeter (2182A, Keithley) to measure the generated signal. The nanovoltmeter is interfaced to the computer using NI PCI-GPIB, NI-488.2. The programming intended for communicating with the instrument, extracting the signal and further processing to display in analog form (designed according the experiment) was done in NI LabVIEW, Version 11. The front panel of the user interface is shown in **Appendix A, Figure A2.2**. Data samples were extracted every 100th ms with simultaneous capturing of motion and voltage generation. The electrical signal appeared in the form of spikes with a magnitude on the order of nanovolts for each direction of motion. A typical voltage output profile for one cycle of motion is shown in **Figure 2.2c**.

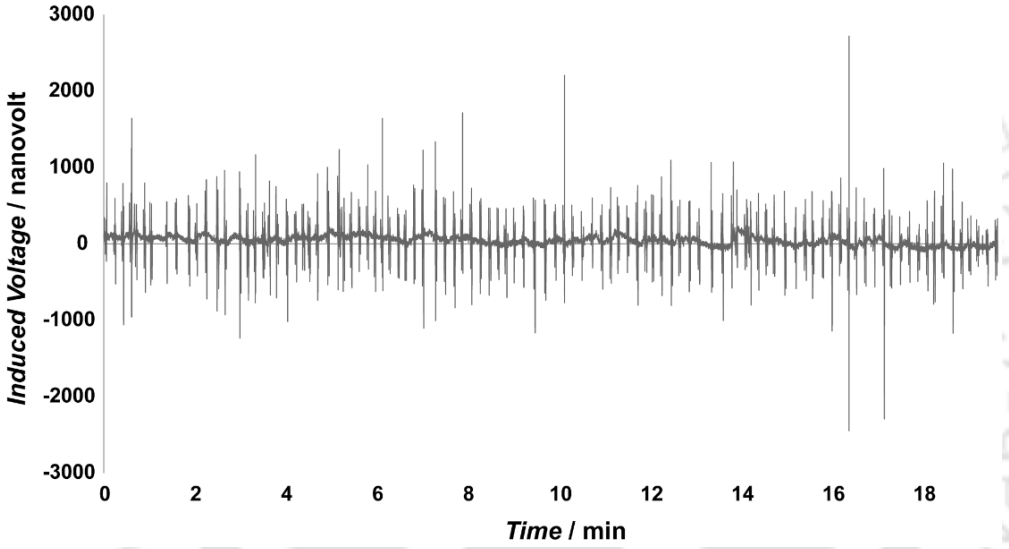

Figure 2.3. Signal generated from autonomous motion. Induced voltage generated from the motion of the bot for a period of about 20 min. The spike denote the signal observed during the flight of the bot.

Thus when the magnetic bot approaches the coil from one end of the tube, an induced signal is generated in response to the change in magnetic flux. Also, when the bot comes out of the coil from the other end, the flux alters again, inducing another signal but with opposite polarity (also shown schematically in **Figure 2.1b**). For one cycle of motion (**Appendix A, movie A2.2**) four signal spikes could be observed, two corresponding to the ascent phase and other two corresponding to the descent phase (**Figure 2.2c**). For an observation period of 20 min (**Figure 2.3**), the bot cycled with an average frequency of five times per min (**Appendix A, Figure A2.3**). As the number of windings in the copper coil was fixed, the variation in the amplitudes of the voltages can only be attributed to the rate of change of flux through the coil as the bot is propelled. The periodicity, reproducibility of motion of the bot, and corresponding electrical signal generation are clearly supported by the observed results (**Figures 2.2 and 2.3**). It is worth mentioning here that the signal was much higher than the noise and significant spikes were generated only when the bot was in motion. Further, when

the concentration of H_2O_2 was changed there was no discernible effect on the velocity, since the bot achieved terminal velocity when the buoyant force was balanced by the gravitational and viscous forces.[11] However, the number of times the bot moved up and down changed. At low H_2O_2 concentration (2%) the rate was low (1-2 cycles per min), while it was high (5 cycles per min) at higher concentration (5%).

2.2 | Autonomous Triggering Device

It is interesting to gauge the quality of the electrical signal generated by the motion of the bot. In order to illustrate this, another device was developed. The construction of the bot for this device included a slightly larger dimension of magnet as cargo (900 micron sided cube) and the affixed crushed microspheres as catalytic elements. A commercially available test tube (12 cm x 75 cm, Borosil) was coiled with the same gauge wire as mentioned above (10000 windings). Other dimensions of the setup were as mentioned in **Figure 2.1**. The output from this setup was connected simultaneously to the nanovoltmeter and the custom designed circuit.

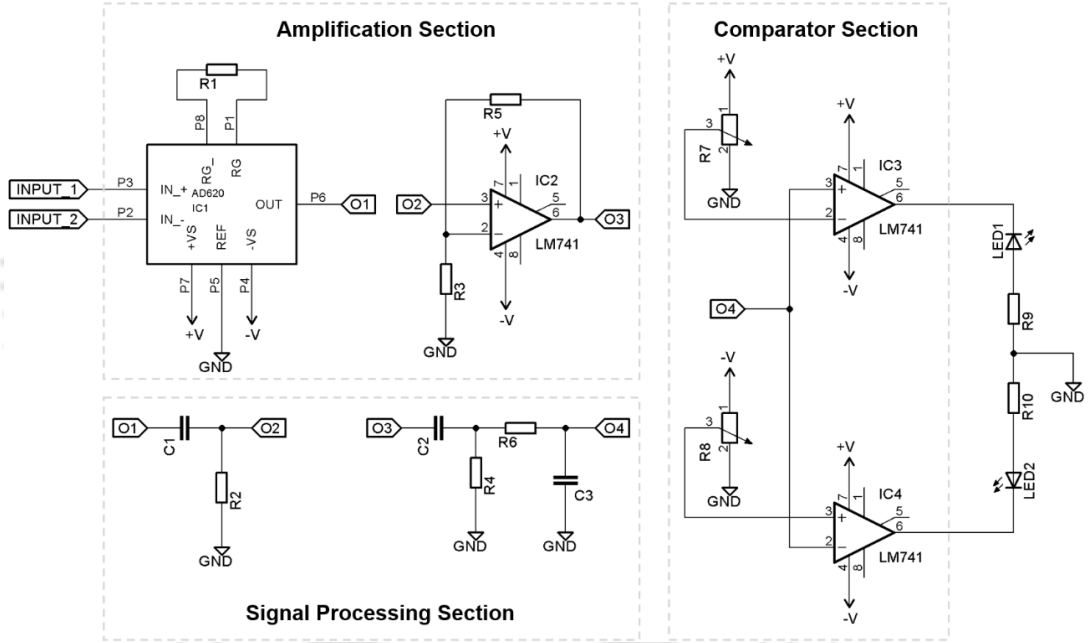

Figure 2.4. Schematic of the circuit used in construction of autonomous triggering device.

Electronic Circuit: The electronic circuit was developed to trigger LEDs from the signal generated through the autonomous motion of bot. Circuit design was done using the commercially available integrated circuits as shown in **Figure 2.4**. Briefly, the first section of the circuit includes the amplification stage, where the signal obtained directly from the experimental setup was amplified in two stages to millivolt range. Processing of the signal was carried out by incorporation of filters to eliminate out the unwanted frequency zones. A comparator is succeeded with adjustable reference levels as suited to the input signal. The whole circuit can be operated with a two 5V power supply, i.e. can be operated with a battery. The circuit is expected to trigger the LEDs when the signal level from the setup crosses the pre-set reference levels. If one LED glows for one polarity, the other illuminates for the opposite polarity.

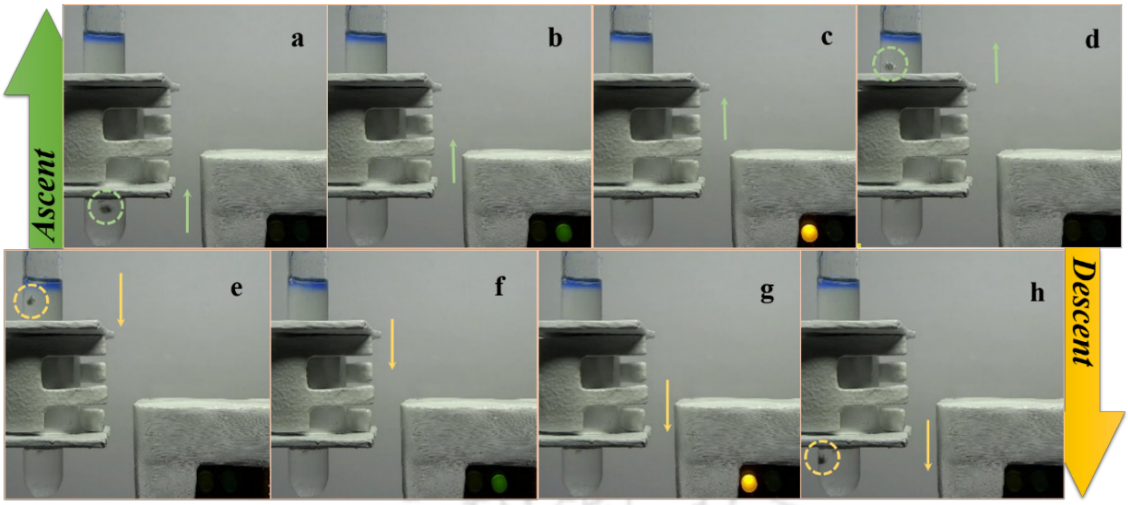

Figure 2.5. Autonomous Triggering Device. The device was constructed by connecting the output of the autonomous signal generator to the circuit. (a - d) Ascent Period: The bot, driven by buoyancy, generated a trigger with opposite polarities, glowing up the green and then the yellow LEDs respectively. (e - h) Descent Period: The bot journeys downwards (after the bubble bursts) due to gravity again triggering the LEDs likewise.

A stronger signal was generated triggering the LEDs in each spike. Both the LEDs were illuminated in each phase of ascent and descent systematically. The motion and simultaneous voltage generation could be captured alongside the lighting of the LEDs (green and orange) on the upward and downward flights of the bot (**Figure 2.5; Appendix A, movie A2.3**). This depicts not only the quality of the signal generated but also the adaptability of the system in constructing smaller and larger bots. This also shows that the bot can perform secondary actions as a result of its motion and thus it may be possible to introduce versatility in a more complex system.

2.3 | Theoretical Deductions

In order to account for the shape and magnitude of the observed emf, first of all it is important to have a clear picture of the average velocity and path of the bot. An analysis of the motion of the bot (**Figure 2.2b**) indicates that the locomotor moves with nearly constant velocity. Also, the path of the bot is nearly vertical in both its upward and downward journeys. The motion profile linked with the induced voltage is theoretically modelled (**Figure 2.6**) under certain assumptions. These assumptions include that the force resulting from the capillary pressure inside the bubble ($\mathbf{F_p}$) balances the capillary force ($\mathbf{F_c}$).[19] The magnet is assumed to be a perfect dipole. The fluid is considered incompressible and the drag forces to be governed by Stokes law. The buoyancy force $\mathbf{F_b}$, the gravitational force $\mathbf{F_g}$ and the drag force $\mathbf{F_d}$ together largely account for the dynamics of the bot as depicted in the **Figure 2.6a**. Hence, from the Newton's laws, it can then be written as $\mathbf{F_b} \cong \mathbf{F_d} + \mathbf{F_g}$. If the mass of the of the bot is considered to be m_{bot}, then,

$$6\pi\eta r v = F_b - m_{bot}\, g$$

$$v = \frac{F_b - m_{bot}\, g}{6\pi\eta r} \qquad (1)$$

where r is the radius of the equivalent sphere with the highest dimension of the system (bot and bubble) as the diameter, η being viscosity and g is the acceleration due to gravity.

The autonomous motion of the magnet only is also governed by **equation 1**, the changes being r, here will be the equivalent sphere with the highest dimension of the system (magnet and bubble) as diameter and m_{bot} being the mass of the magnet. Clearly, from above the velocity of the bot depends upon the buoyancy force, with the rest remaining constant.

To simplify the calculation, the coil is assumed to be moving and the bot is kept in a fixed position; this does not alter the problem to be addressed. Here, $\mathbf{v_a} = -\mathbf{v}$, the expression of which is given from **equation 1**. Considering the magnet as an ideal dipole crossing the centre of the coil of radius s, with the velocity v_a and moment m, the magnetic flux through the coil can be calculated at distance z is by $\phi_{dip} = \int B_{dip} \cdot dS$, where B_{dip} being the magnetic field produced by dipole is given by,[27]

$$\mathbf{B_{dip}} = \frac{\mu_o m}{4\pi (s^2+z^2)^{5/2}} \times (3 s z Cos\varphi \hat{\mathbf{i}} + 3 s z Sin\varphi \hat{\mathbf{j}} + (2z^2 - s^2)\hat{\mathbf{k}}) \;,\quad d\mathbf{S} = s\, ds\, d\varphi \hat{\mathbf{k}}$$

Upon integration with proper limits, i.e., $\phi \to 0$ to 2π, $s \to 0$ to s, the expression for flux can be written as,

$$\varphi_{dip} = \frac{\mu_o m s^2}{2(s^2+z^2)^{3/2}}$$

For n turns of coil, the induced emf equation as given by Faraday's law is $\varepsilon_{dip} = -n\frac{d\varphi_{dip}}{dt}$. So the final relation can be generated (by substituting the magnitude of v_a from equation 1) as,

$$\varepsilon_{dip,\,spatial} = \frac{3n\mu_o m z s^2}{2(s^2+z^2)^{5/2}} \cdot \frac{dz}{dt} = \frac{-3n\mu_o m z s^2}{2(s^2+z^2)^{5/2}} \cdot v_a = \frac{-3n\mu_o m z s^2}{2(s^2+z^2)^{5/2}} \cdot \left(\frac{F_b - m_{bot} g}{6\pi\eta r} \right) \tag{2}$$

The temporal dependence of the equation can also be obtained by substituting $\pm v_a t$ in place of z in above equation,[27] giving rise to

$$\varepsilon_{dip,\,temporal} = \frac{-3n\mu_o m v_a^2 t s^2}{2(s^2+v_a^2 t^2)^{5/2}} \tag{3}$$

Rest remaining constant, **equations 2, 3** can be rewritten as

$$\varepsilon_{dip,\,spatial} = k \cdot \frac{z}{2(s^2+z^2)^{5/2}} \tag{4}$$

$$\varepsilon_{dip,\,temporal} = c \cdot \frac{{v_a}^2 t}{2(s^2+{v_a}^2 t^2)^{5/2}} \tag{5}$$

where $k = -3n\mu_o m s^2 v_a$ and $c = -3n\mu_o m s^2$.

The above two equations are plotted in spatial (as a function of *z*, in terms of coil radius) and temporal co-ordinates (**Figure 2.6**). The data points are obtained from suitable programming in Wolfram Mathematica, Version 9.

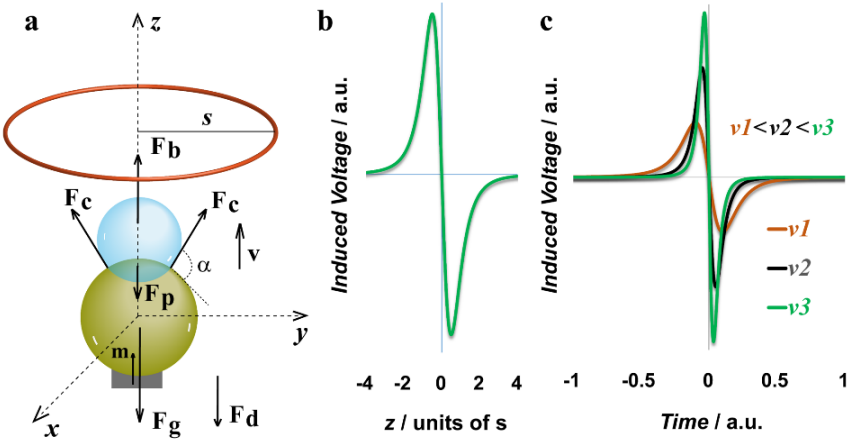

Figure 2.6. **(a)** Theoretical model showing the various forces acting on the system. Here F_b, F_g, and F_d represent the buoyancy, gravitational, and drag forces, respectively. F_c is the capillary force and F_p is the force resulting due to capillary pressure inside the bubble. Magnetic moment and the radius of the coil are denoted by **m** and *s*, respectively. **(b)** Spatial plot: Induced voltage generated as function of position, when the bot moves in and out of the static coil. Here, 'z' is taken in units of 's', where 's' is the radius of the coil. **(c)** Temporal plot: Induced voltage plotted with the variations in velocity clearly indicates that as the velocity increases, the amplitude rises with the decrease in time span. Here, origin is taken as the time when the polarity of the signal alters.

The spatial (**Figure 2.6b**) and temporal patterns (**Figure 2.6c**) of the signal as it crosses the origin are of alternating type. The theoretical model predicts the same type of signal as that observed in the experiments. Moreover, the signal shape, being associated with the coil radius, also depends upon the distance the bot travels after crossing the coil (**Figure 2.6b**). Needless to mention, only changes in fluxes through the coil would result in the generation of signal, that is, when the bot is in motion. Also, the faster the motion of the bot in linear direction with no change in orientation, the shorter the time period and the stronger the signal (**Figure 2.6c**). Further, if the orientation of the bot changes during the flight, it affects the rate of change of flux through the coil accordingly, resulting in the generation of a signal with corresponding strength and polarity. The model depicted here clearly shows possible variations with alterations in the basic parameters. It was not possible to obtain quantitative results since the variations in fluxes were too small to be measured.

2.4 | Concluding Remarks

In the quest for developing an autonomously moving bot with secondary function, a new function, namely production of electrical energy was achieved using a composite system. Thus, while the catalytic Pd NPs present in the polymer microsphere generated oxygen needed for the motion of the bot, the magnetic component induced emf into a coil connected to an electrical circuit. The periodicity and reproducibility of the vertical motion and generation of electrical current of sufficient magnitude for lighting LEDs during the course of the motion indicate favorable prospects for the design of multifunctional autonomous microscopic bots. The generation of an electrical signal could

be accounted for using a conventional Faradaic model and this promotes the possible incorporation of low-voltage operating devices in autonomously moving electrically operative microbots.

2.5 | References

1) G. A. Ozin, I. Manners, S. Fournier-Bidoz, et al., *Adv. Mater.* **2005**, *17*, 3011.
2) C. R. Lowe, *Curr. Opin. Struct. Biol.* **2000**, *10*, 428.
3) Y. Wu, Z. Wu, X. Lin, et al., *ACS Nano* **2012**, *6*, 10910.
4) S. Sanchez, A. A. Solovev, S. M. Harazim, et al., *J. Am. Chem. Soc.* **2011**, *133*, 701.
5) J. G. Gibbs, Y.-P. Zhao, *Appl. Phys. Lett.* **2009**, *94*, 163104.
6) R. Liu, A. Sen, *J. Am. Chem. Soc.* **2011**, *133*, 20064.
7) L. Ionov, M. Stamm, S. Diez, *Nano Lett.* **2006**, *6*, 1982.
8) M. E. Ibele, P. E. Lammert, V. H. Crespi, et al., *ACS Nano* **2010**, *4*, 4845.
9) L. Baraban, D. Makarov, O. G. Schmidt, et al., *Nanoscale* **2013**, *5*, 1332.
10) W. F. Paxton, K. C. Kistler, C. C. Olmeda, et al., *J. Am. Chem. Soc.* **2004**, *126*, 13424.
11) K. K. Dey, D. Sharma, S. Basu, et al., *J. Chem. Phys.* **2008**, *129*, 121101.
12) S. Balasubramanian, D. Kagan, K. M. Manesh, et al., *Small* **2009**, *5*, 1569.
13) S. Sanchez, A. N. Ananth, V. M. Fomin, et al., *J. Am. Chem. Soc.* **2011**, *133*, 14860.
14) L. Soler, C. Martinez-Cisneros, A. Swiersy, et al., *LChip* **2013**, *13*, 4299.
15) V. Balzani, M. Clemente-León, A. Credi, et al., *Proc. Natl. Acad. Sci. U. S. A.* **2006**, *103*, 1178.
16) W. Wang, L. A. Castro, M. Hoyos, et al., *ACS Nano* **2012**, *6*, 6122.
17) K. K. Dey, S. Bhandari, D. Bandyopadhyay, et al., *Small* **2013**, *9*, 1916.
18) L. Baraban, S. M. Harazim, S. Sanchez, et al., *Angew. Chem. Int. Ed.* **2013**, *52*, 5552.
19) A. Agrawal, K. K. Dey, A. Paul, et al., *J. Phys. Chem. C* **2008**, *112*, 2797.
20) L. Courbin, F. Artzner, *Nature Mater.* **2012**, *11*, 1008.
21) D. A. Wilson, R. J. M. Nolte, J. C. M. van Hest, *Nature Chem.* **2012**, *4*, 268.
22) Y. Chen, M. Wang, C. Mao, *Angew. Chem. Int. Ed.* **2004**, *43*, 3554.
23) E. S. Russell, *Nature* **1941**, *147*, 190.
24) H. C. Berg, *Nature* **1975**, *254*, 389.
25) W. Wang, T.-Y. Chiang, D. Velegol, et al., *J. Am. Chem. Soc.* **2013**, *135*, 10557.
26) K. Cho, S. Chida, M. Sasaki, et al., *Acta Paediatr. Jpn.* **1996**, *38*, 322.
27) P. Carpena, *Am. J. Phys.* **1997**, *65*, 135.

Appendix A

A.1 | Movies

Comments on movie A2.1: This video illustrates the catalytic ability of the NdFeB magnet fragment. Though its catalytic ability was slow, it showed autonomous motion in 5% (w/v) H_2O_2 and 1% (w/v) sodium dodecyl sulphate (SDS). The details regarding its motion is mentioned in **Appendix A, Figure A2.1** below. In this case also, 60 µL of ethyl alcohol with bromophenol blue was added to halt the magnet being pulled towards the corners of the tube and help to burst the bubble attached to the magnet on reaching the top of the liquid.

Comments on movie A2.2: This video demonstrates the buoyancy driven bot generating an electrical signal. The bot moves in 5% H_2O_2. To measure the induced voltage, and present in analog form, a suitable set of programs were written to communicate with nanovoltmeter, acquire and process the signal. The inset shows the signal obtained from this programmed application. The signal is very evident as the flux through the coil changes during the flight of the bot.

Comments on movie A2.3: This video demonstrates the quality of the signal and its effective implementation in illumination. A circuit was constructed with the bot remodelled. Its construction included a slightly larger dimension of magnet as cargo (900 micron sided cube) and the affixed crushed microspheres (with embedded Pd NPs) as catalytic elements. In constructing this device, a commercially available test tube (12 cm X 75 cm, Borosil) was coiled with the same gauge wire (10000 windings). A stronger signal was generated triggering the LEDs in each spike. Both the LEDs were illuminated in each phase of ascent and descent systematically. This depicts not only the quality of the signal generated but also the adaptability of the system in constructing smaller and larger bots.

A.2 | Figures

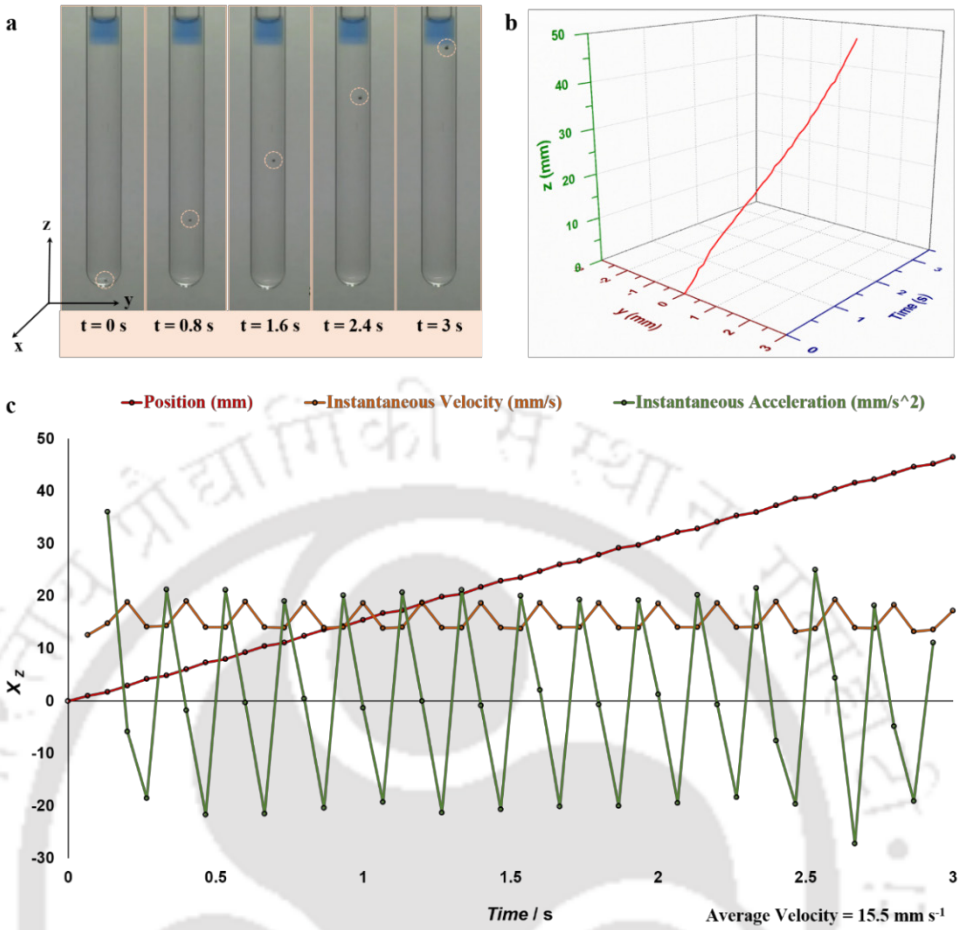

Figure A2.1. Magnet's Motion Profile. (a) Snapshots of the magnet moving vertically upward due to buoyancy. (b) Spatiotemporal trajectory of the magnet. (c) Plot descripting the various motion parameters. Here in X_z, X denotes either the position or instantaneous velocity or instantaneous acceleration of the magnet.

Comments on Figure A2.1: Further observations include the catalytic ability of the magnet itself. Interestingly, when the magnet filling was placed in 800 µL of 5% (w/v) H_2O_2 and 1% (w/v) SDS, bubbles were observed on the surface, followed by its movement (**Figure A2.1a**) due to buoyancy. This behaviour can be accounted due to presence of catalytic elements in the rare earth magnet aiding decomposition for production of oxygen bubbles. The max average velocity of the magnet was around 15.5 mm s^{-1}. Further the frequency of movement (to and fro inside the tube) was significantly less (once in five minutes) compared to the bot (five times a minute). Nevertheless, with certain improvements, these micron size magnets can be a good candidate as synthetic bots due to their added advantage of being inherently magnetic. Motion analysis of its journey is shown in **Figure A2.1b, A2.1c**.

Calculation of motion parameters: The position coordinates were obtained with the origin taken as the starting position of the motion of the bot. Setting the reference scale with the calibrated ruler, all the other calculations were performed accordingly with frame by frame analysis. Instantaneous velocity and acceleration calculations were performed using finite difference methods. On the other hand, the average velocity is given by considering the initial and final positions.

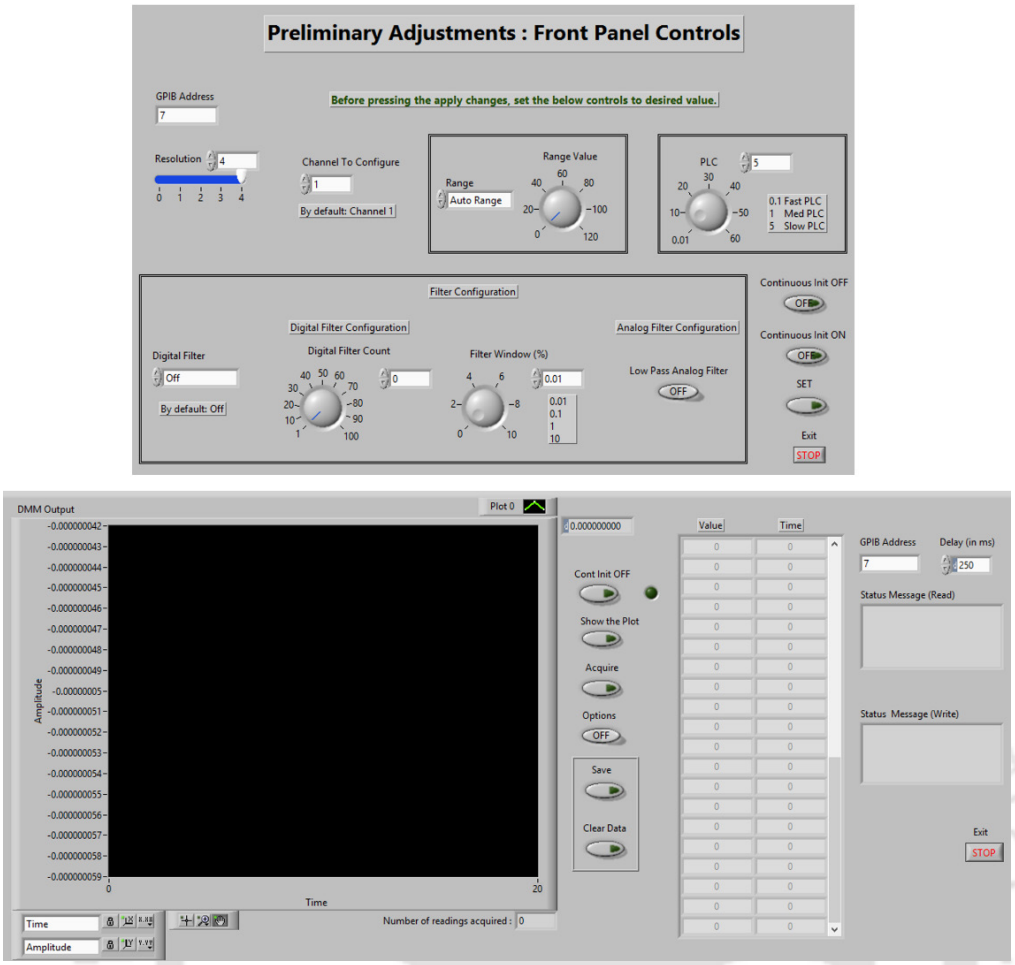

Figure A2.2. User interface. Figure shows the front panels of the user interface developed for communicating with nanovoltmeter, acquiring and processing the measured signal.

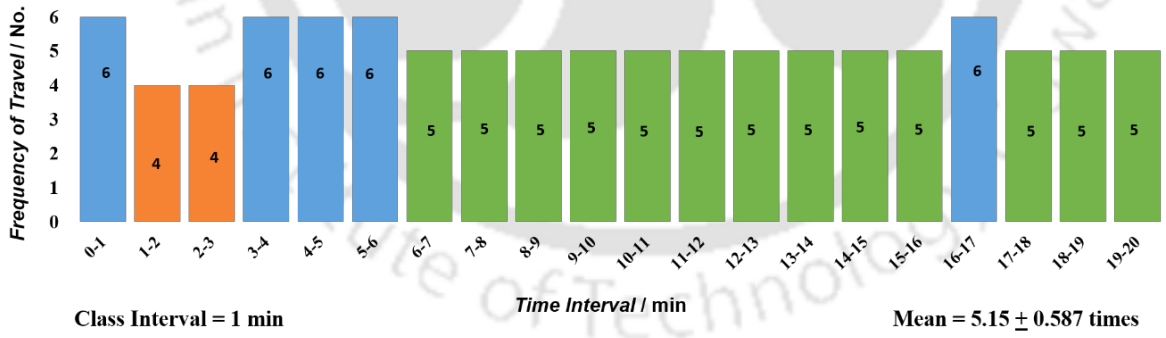

Figure A2.3. Motion Profile of the bot. Plot depicts number of the times bot ascended and descended with in a time interval of 1 min for an analysis carried out for the duration of 20 min.

Comments on Figure A2.3: Oxygen bubble, being formed on the polymer, aids the bot in travelling vertically upwards, due to buoyancy. On reaching the top, bursting of the bubble results in downward fall on account of gravity. This cycle of roving up and down continues until the complete decomposition of the fuel, i.e., H_2O_2. This cycling of the ascent and descent phases (counted as one) per minute was calculated and plotted. It was observed that the bot cycled up and down at an average of over 5 times a minute.

A.3 | Design and Characterization of the Bot

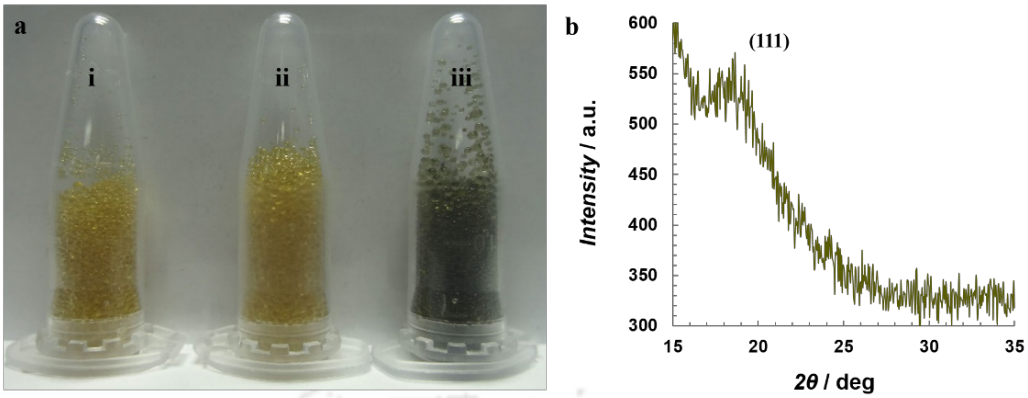

Figure A2.4. Visual Observation and X-ray diffraction (XRD) pattern of product formation. (a) Photographs of resins. (i) Activated resin beads. (ii) Pd^{2+} exchanged resin beads. (iii) Pd NP embedded resin beads. **(b)** XRD analysis of the Pd NP coated beads.

Preparation of Pd NPs on micron-sized beads involved, firstly, activation of highly stable polymer spheres (3 g, polystyrene divinylbenzene copolymer, Amberlite-IR 120, Merck) by placing them in HCl (10 mL, 3 M, Merck) for an hour. After thorough washing with Milli Q grade water, the cation exchange beads were transferred to a solution containing H_2PdCl_4 (5 mL, 0.2 M, Sigma-Aldrich) and they were then left for three hours in order to exchange Pd^{2+}. The beads were washed with water and then treated with $NaBH_4$ (5 mL, 10 mM, Merck), which was added slowly with stirring for 2 h. They were washed with water again and then air dried.

Visual examination (**Figure A2.4a**) of the control and the coated particles gave the first signs of the formation of Pd NPs on the polymer. A distinct grey colour change can be observed on the Pd NP coated beads in contrast to the yellow colour of the original beads providing a visible indication of the transformation of Pd NPs on the beads. X-ray diffraction (XRD) measurements of the Pd NP coated beads were carried out by Seifert 3003-TT with Mo anode of X-ray wavelength 0.70930Å. A distinct hump can be observed at around 18.5º corresponding to [111] plane of Pd (JCPDS 02-1439) (**Figure A2.4b**).

The formation of particles was confirmed using electron microscopic analysis (**Figure A2.5**). For TEM analysis, the beads were first crushed and then the synthesis of Pd NPs was carried out on the crushed ones following the same synthesis procedure. These tiny crushed fragments were dispersed in water and then dried on the grid. Thereafter, inspection was done using a transmission electron microscope (TEM, JEOL 2100 UHR-TEM), operating at a maximum accelerating voltage of 200 kV. As shown in the **Figure A2.5a**, the Pd NPs formed on the bead were clear. High resolution transmission electron microscope (HRTEM) analysis (**Figure A2.5b**) further provided a lattice spacing of 0.224 nm for one such NP, corresponding to the [111] plane in FCC packing of Pd.[1] The average particle size was calculated to be 9.4 nm ± 5.9 nm (**Figure A2.5c**). The presence of Pd was further confirmed by the energy dispersive X-ray analysis (EDX) (**Figure A2.5d**).

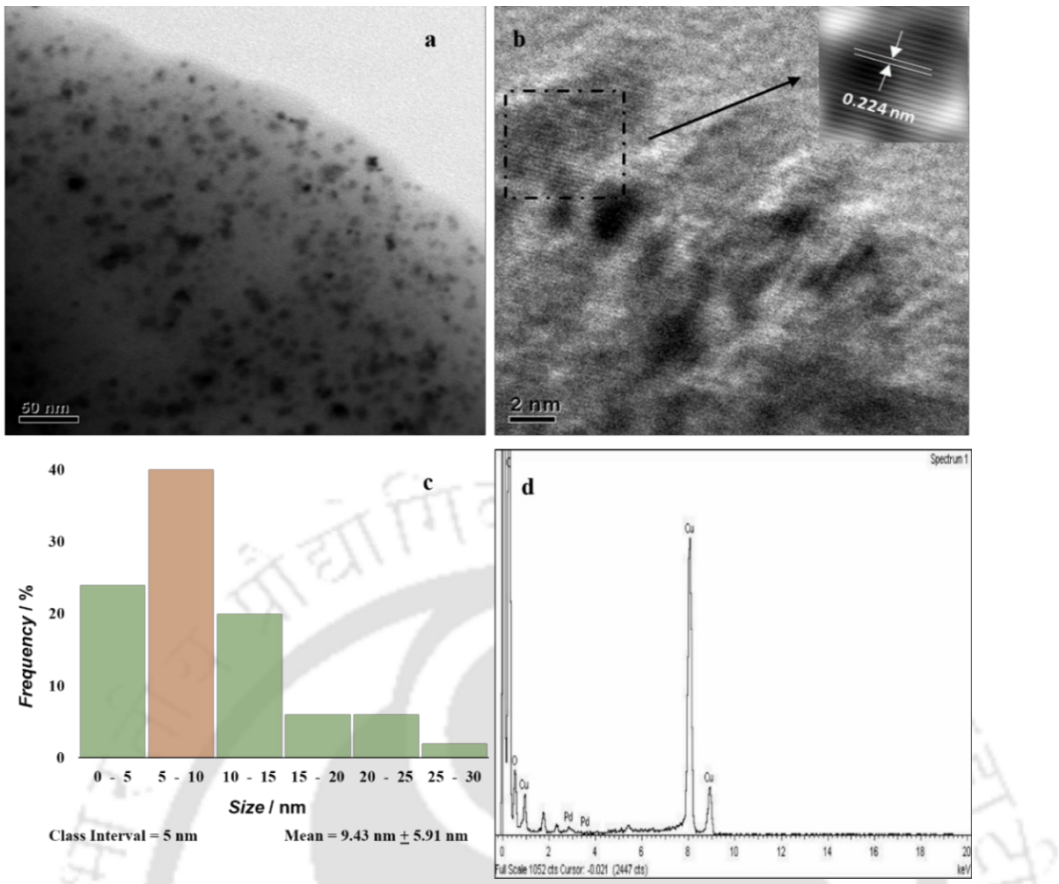

Figure A2.5. TEM Analysis of the Pd NP coated microspheres. (a) TEM image of Pd NP coated bead. **(b)** HRTEM of Pd NP coated bead. **(c)** Particle size distribution of Pd NPs as calculated from the TEM image. **(d)** EDX spectrum of the Pd NP coated Bead.

Field emission scanning electron microscope (FESEM) analysis was carried out by Zeiss Sigma Advanced Analytical Microscopy operated at 5 kV. As is clear from the **Figure A2.6**, nearly uniform particles of average size of 14.7 ± 7.7 nm were formed on the bead.

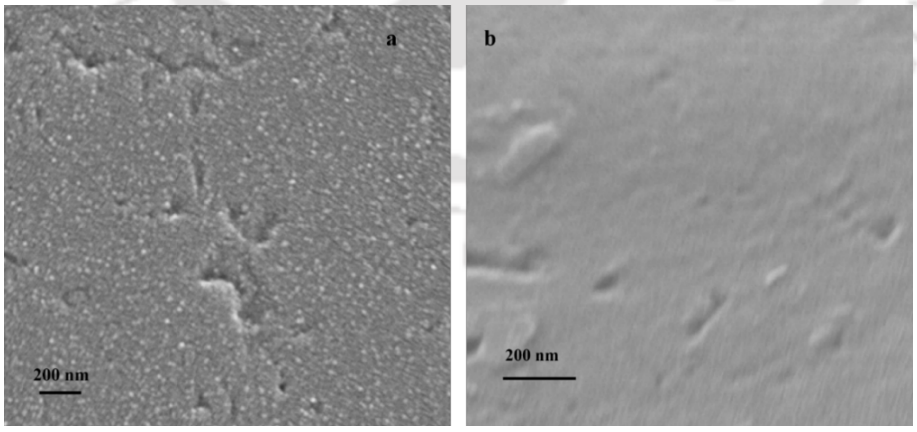

Figure A2.6. FESEM analysis of polymer microspheres. (a) FESEM image of Pd NP embedded bead. **(b)** FESEM image of an ordinary resin bead.

An extracted small fragment of a N-42 grade magnet was affixed to this NP-coated microsphere using epoxy adhesive. The fragment of the magnet (**Figure A2.7**) used for the experiment was characterized in order to confirm its salient properties.

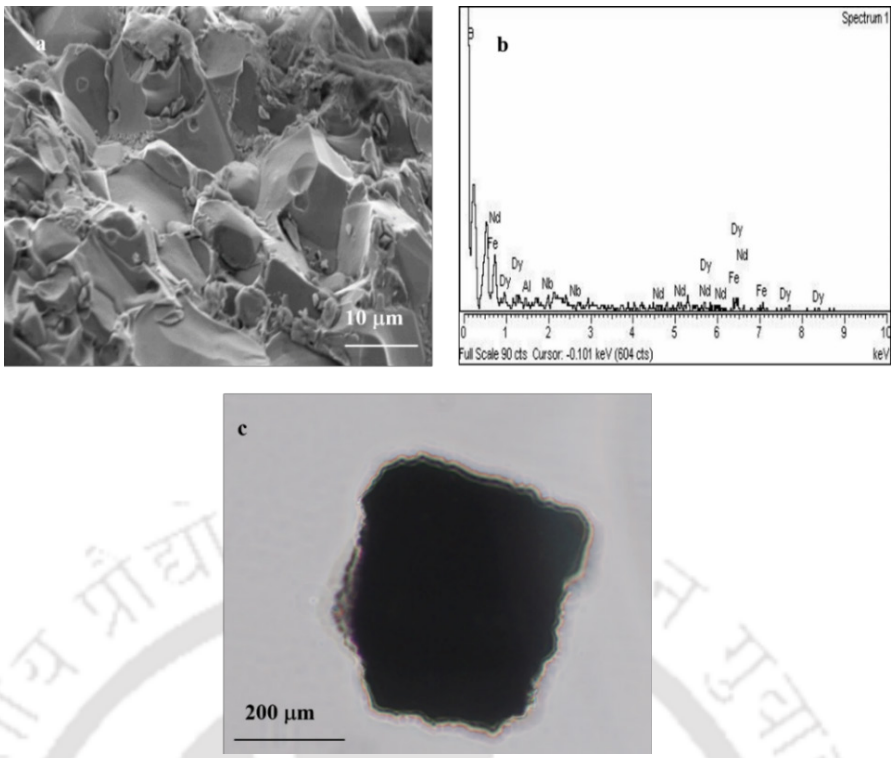

Figure A2.7. Characterization of the NdFeB rare earth magnet. (a) SEM image of a piece of crushed magnet. **(b)** EDX analysis of the piece. **(c)** Bright field microscopic image of magnet.

The topography and the chemical composition of the extracted magnet fragment for the experiment were examined by SEM (JEOL JSM 6360 scanning electron microscope), operating at a maximum voltage of 30 kV. All the prominent elements which make up the rare earth magnet (**Figure A2.7b**) were confirmed by EDX analysis. Bright field image (**Figure A2.7c**) of the used fragment was recorded using an epi-fluorescence microscope (Nikon ECLIPSE, TS100, Tokyo).

A.4 | Reaction Kinetics and Efficiency Calculations

In order to demonstrate the catalytic ability and to measure the effective rate constant of catalytic decomposition of 5% H_2O_2, the reaction kinetics of the catalytic beads was studied. The rate of decomposition of H_2O_2 in presence of catalytic (k_{cat}) and non-catalytic beads ($k_{non\text{-}cat}$) was obtained. Eventually, the effective rate constant was obtained from their difference ($k_{cat} - k_{non\text{-}cat}$). The k_{eff} in the **Figure A2.8** corresponds to 100 mg of Pd NP coated micron spheres.

Calculation of effective rate constant of single bead, k_{bead} : To obtain the effective rate constant, 100 mg each of resin and Pd NP embedded resin beads were taken separately. In each case, the rate of decomposition of 5% hydrogen peroxide was studied and rate constants for non-catalytic and catalytic beads were obtained as $k_{non\text{-}cat}$, k_{cat} respectively. Effective rate constant of 100 mg beads was obtained from their difference ($k_{cat} - k_{non\text{-}cat}$). Further effective rate constant for a single bead, k_{bead} can be obtained by dividing with the number of beads present in 100 mg.

The mass of single bead was found out to be 'x'. Hence, n, the number of beads in 100 mg can be obtained by dividing 100 mg with x. Finally, the effective rate constant of single bead is given by

calculating the expression $(k_{cat} - k_{non\text{-}cat})/n$**.** The effective rate constant of the single bead is found out to be 0.000054 min^{-1}.

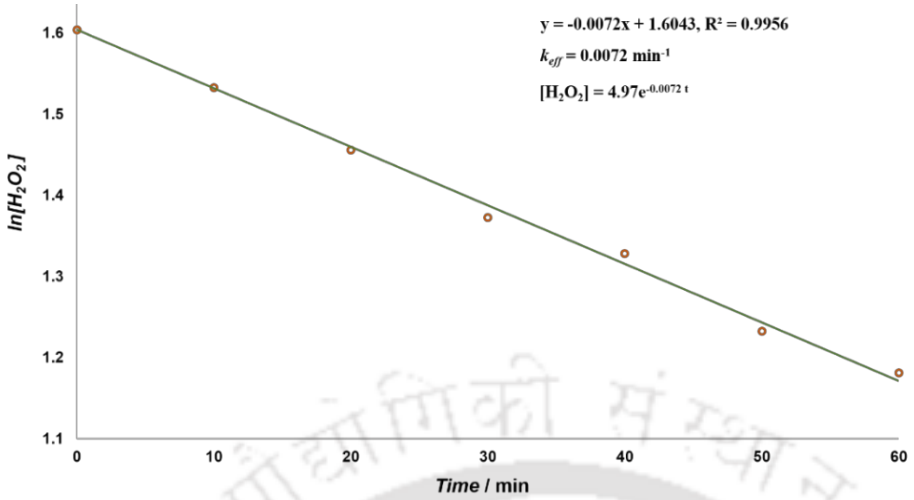

Figure A2.8. Reaction Kinetics. Effective rate constant (k_{eff}) of H_2O_2 decomposition for 100 mg of Pd NP coated micron beads.

Calculation of effective rate constant of the bot, k_{bot} : Since a part of the bead is covered by magnet, the fractional portion of the bead covered by magnet is given by the ratio of the surface areas of the face of the magnet (affixed to bead) and the bead. The fractional active portion of the bead, f_{act} (not covered by magnet) responsible for catalysis is obtained by subtracting the ratio from 1. Effective rate constant from the active portion alone can be calculated by the product of the effective rate constant due to single bead and the fractional active portion, i.e., $k_{bot} = \{(k_{cat} - k_{non-cat}) \times f_{act} / n\}$.

Calculation of efficiency of performance of the bot: The number of moles of H_2O_2 consumed in 20 min was calculated using the established rate law for the bot using effective rate constant, k_{bot}. The non-expansion work under constant pressure from decomposition of hydrogen peroxide per mole is given by the change in Gibbs free energy.[2] The chemical energy used up is hence calculated by the product of number of moles consumed and change in Gibbs free energy per mole.

Kinetic energy from the motion of the bot is calculated for ascent and the descent phases using the ascent and descent velocities. The total kinetic energy is given by the summation of the energies in both phases over the period of 20 min. Finally, the efficiency of the bot is given by the ratio of the total kinetic energy to the chemical energy.

A.5 | References

1) M. Han, S. Liu, J. Bao, et al., *Biosens. Bioelectron.* **2012**, *31*, 151.
2) P. Atkins, J. d. Paula, *Atkin's Physical Chemistry*, 8th ed., Oxford University Press, Great Britain.

Chapter 3

Hierarchical Logic Structures Based on Responsive Luminescent Gold Nanoclusters

ABSTRACT

Biocompatible gold nanoclusters (NCs) dispersed in water were used for constructing multi-level Boolean logic operations. This is based on the reversible change in luminescence of the NCs in response to changes in pH, metal ion concentration and temperature. These responsive NCs could be used for tri-state logic operation, OR logic, decoder, keypad lock and are also capable of higher order functions. These 'few-atom' clusters could be potential candidates for futuristic bionic devices, where the decision making process could involve conditions similar to physiological environment and beyond.

As computational electronics reaches its limit of speed and memory, newer technological development(s) is (are) necessary for future devices to keep up with the demand. Further, with increased miniaturization, conventional electronics - in addition to scaling problems - faces challenges involving important issues such as energy efficiency, terminal contact resistance, heat generation, leakages and dielectric breakdown.[1]

A plausible solution could originate from computation with molecular or nanoscale species in liquid medium.[2-3] This has the unique advantage of drawing knowledge and inspiration from biological cells and organelles, which perform numerous logic operations with extraordinary degrees of specificity, sensitivity and efficacy.[4] In fact, one could take advantage of external handles such as light, electric field, magnetic field and internal parameters such as concentrations of ionic or molecular species, temperature and not to mention emulating the complex and highly evolved intercellular signalling pathways, in order to make even more voluminous as well as complex decisions and calculations at faster pace. In this regard, initial success of "chemo photonic" logic gates[5-8] and other logic operations,[9-11] data transmission,[9] fuzzy logic[8] portends the brighter side of the proposition. Biomolecular logic gates[12-14] have also been shown to follow Boolean algebra. The new entrant highly luminescent and photostable noble metal atomic clusters can become candidates for fluid phase versatile logic operations, owing to the practical advantages[15] over their counterparts, i.e., the well-established systems based on plasmonics of NPs,[16-17] organic molecules,[7] biomarcomolecules[14, 18] and quantum dots.[19] However, a key challenge that needs to be addressed is the possibility of layered logic operations, which are essential for hierarchical computation. There remains significant opportunity to develop newer schemes for cascading logic

operations based on the modulation of optical properties of the nanoclusters (NCs) in response to chemical and physical perturbations in the immediate environment.

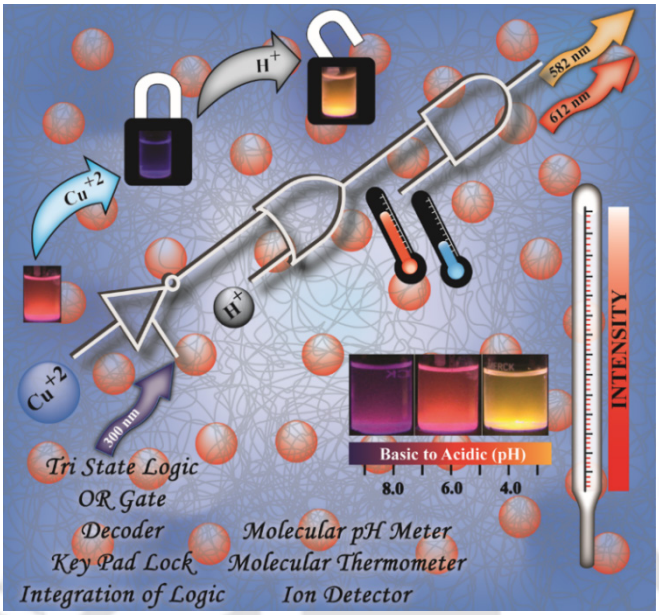

Figure 3.1. Schematic representation of the luminescent atomic cluster-based logically operative molecular devices. The scheme explains the principle of operation of various photonic molecular devices based on luminescent Au NCs in a single liquid system. Boolean logic operations such as tri-state logic, OR gate, decoder, keypad lock and integration of logic to higher levels are achieved. Further its responsive characteristics represent molecular pH meter, thermometer and ion detector.

Herein, the use of biocompatible Au NCs, dispersed in water for multi-level Boolean logic operations is demonstrated. This is based on the reversible change in luminescence of the NCs in response to changes in pH, metal ion concentration and temperature. These responsive NCs could be used for tri-state logic operation, OR logic, decoder, keypad lock and are also capable of higher order functions. The essential idea behind the principles of operation of the NCs for cascade functions under different experimental conditions is depicted schematically in **Figure 3.1**. We also conjecture that these 'few-atom' clusters could be potential candidates for futuristic bionic devices, where the decision making process could involve conditions similar to physiological environment and beyond.

3.1 | Sensing with Au NCs

3.1.1 | pH Sensor

The Au NCs were synthesized in the biopolymer chitosan using an established procedure.[20] The average particle size was measured to be 0.83 ± 0.29 nm. The as-synthesized NCs at pH 6.5 emit at 612 nm, when excited by 300 nm light. When the pH of the medium was increased to 9.0 (using alkali) the emission peak shifted to 615 nm when recorded immediately; however, after 2 h the peak shifted to 627 nm with a significant decrease in intensity.[20] On the other hand, when the pH was made acidic (3.5) then the emission peak appeared at 582 nm, accompanied by a sharp increase in intensity. The luminescence behaviour was found to be reproducible with respect to change in pH. The details of results are shown in **Figure 3.2**.

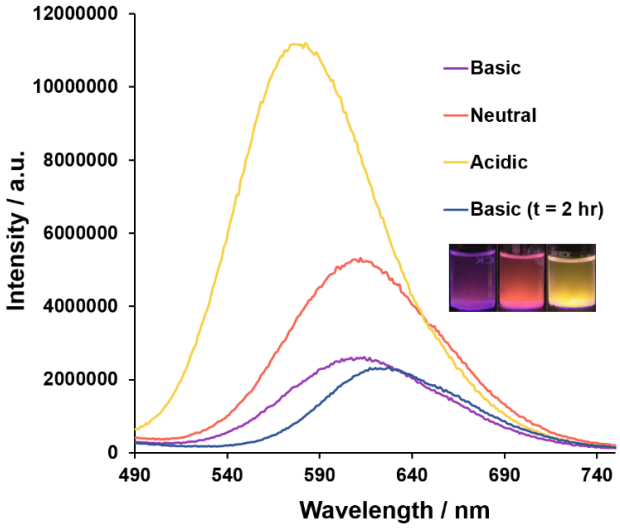

Figure 3.2. pH - dependent emission spectra. Au NCs, upon excitation at 300 nm, show emission with different wavelength and intensity, depending on the pH of the medium (as indicated in the legends).

The pH-dependent emission of the Au NCs could have its origin in the stabilizer which is primarily mercapto-propionic acid (MPA, HSC_2H_4COOH) and in addition chitosan. The overall charge on the stabilized cluster depends on the pH of the medium. It has been reported that ligand to metal charge transfer influences the emission behaviour of the NCs.[21] More electropositive ligand increases the emission quantum yield. At lower pH the acid would be protonated and at higher pH it would be deprotonated, thus changing the electron donating ability of the ligand. In addition, similar interaction with amine and carboxylic groups of chitosan would also influence the emission as a function of pH of the medium. The results indicated ease of emission control through changes in pH and thus its potential use in developing logic devices and as molecular pH meter/sensor.[22]

3.1.2 | Temperature Sensor

The emission intensity of the clusters was observed to be sensitive to the temperature of the medium, thus exhibiting the behaviour of a molecular thermometer.[23] For example, when the temperature was increased gradually from room temperature to 70 ºC the intensity went down; however, when it was decreased to 5 ºC the intensity increased significantly (**Figure 3.3**). The ratio of intensities at 70 ºC to that at 5 ºC was measured to be 0.16. The variation in intensity was found to be 2.3 ± 0.6 % per ºC during cycle of increasing temperature and 2.2 ± 0.8 per ºC during decreasing cycle, which is comparable to the earlier reported values.[23-24] The excellent reproducibility of the temperature responsive intensity variation was observed for six cycles, which is reported in **Appendix B, Figure B3.1**. The lowering of luminescence emission intensity with increase in temperature could be due to enhanced internal conversion. It is known that thermal energy aids in internal conversion, where electronic energy is converted to the vibrational energy of the clusters shifting the equilibrium towards non-radiative decay process.[23]

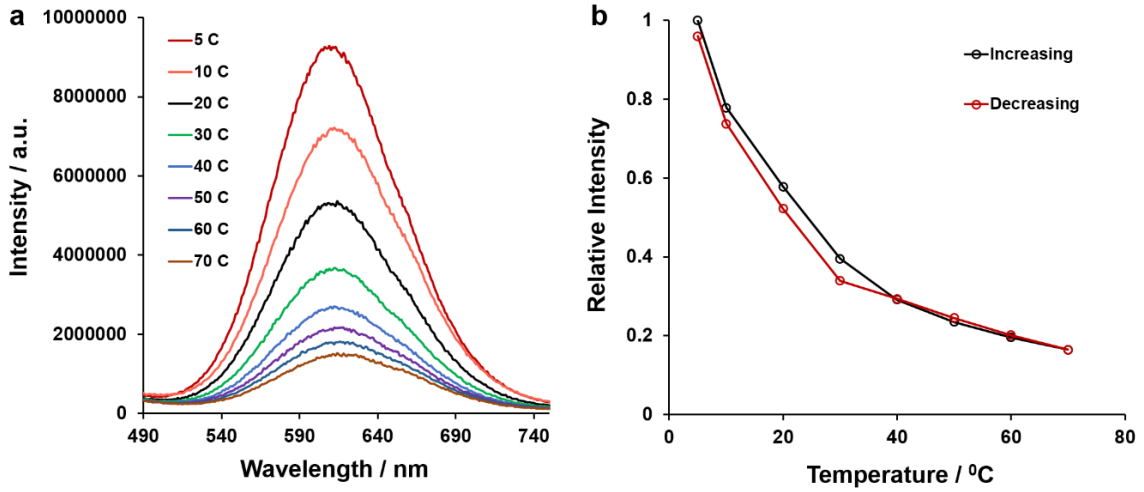

Figure 3.3. Luminescence intensity variation with temperature. (a) Figure depicts the temperature dependent emission intensity variations due to Au NCs. The clusters were highly luminescent at low temperature and the luminescence intensity decreased with increasing temperature. **(b)** The reversibility of temperature-dependent intensity variation of Au NCs.

3.1.3 | Metal Ion Sensing

Further experimental studies showed that the intensity of luminescence of Au NCs was quenched by the presence of metal ions in the medium. Among the metal ions tested (Na^+, K^+, Ca^{2+}, Mg^{2+}, Cu^{2+} and Fe^{2+}; **Figure 3.4**), the most significant decrease was due to the presence of Cu^{2+}. Cu^{2+} may reversibly bind with the –COO- group of MPA and thus quench the luminescence of the clusters following its addition in the medium.

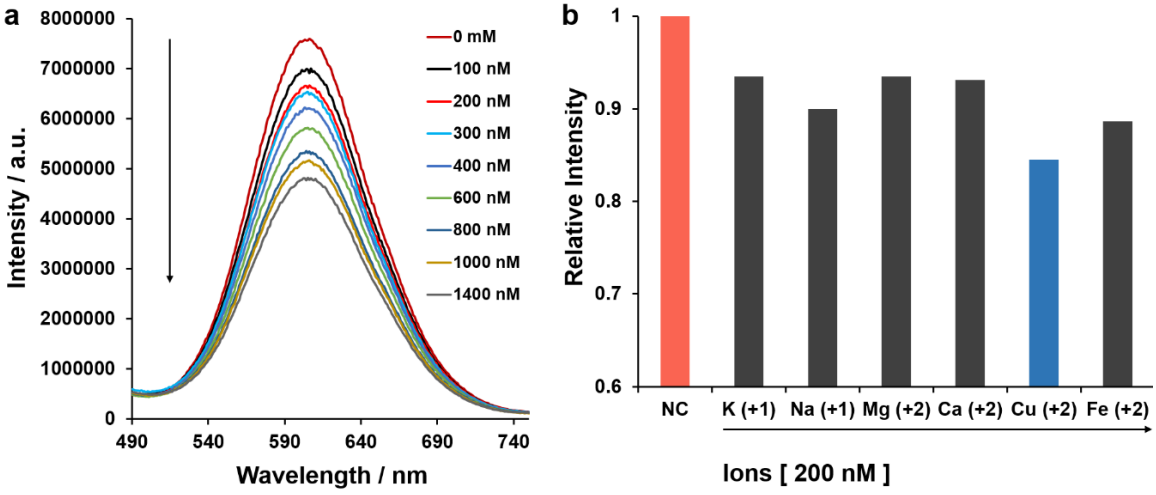

Figure 3.4. Response of luminescence of clusters to metal ions. (a) Luminescence intensity of Au NCs decreased immediately upon addition of Cu^{2+} ion in water as shown in the Figure. The concentrations of Cu^{2+} are indicated in the legends. **(b)** A comparative study of intensity changes for various ions (at 200 nM), added externally to the medium. These ions are typically present in human serum (at lower concentrations though).

On the other hand, addition of excess [H^+] i.e. lowering of pH results in shifting of equilibrium towards MPA formation. This results in the restoration of emission of the clusters. Thus, the intensity due to quenching by Cu^{2+} could be recovered by addition of [H^+] to the medium, which was accompanied by a blue-shift in emission maximum, as was observed in the case of pH dependence

emission mentioned above (**Figure 3.2**). The results additionally pointed out that human blood serum also quenched the luminescence (**Appendix B, Figure B3.2**), possibly due to presence of metal ions. Further experiments with external addition of Cu^{2+} to blood serum indicated quenching and recovery of luminescence similar to that observed in water medium (**Appendix B, Figure B3.3**). The dispersion of clusters in the human blood serum and their reversible luminescence properties similar to aqueous medium indicated possible use of them in human physiological conditions with wider implications.

3.2 | Logic Systems with Au NCs

The reversible tuning of emission of the Au NCs by changes in pH as well as temperature of the medium and in the presence of metal ions provides significant opportunity for fabrication of hierarchical structures for logic operations. In the following sections, we will present results demonstrating four basic logic operations, namely, tri-state buffer, OR gate, decoder, keypad lock and also cascading of such operations using the luminescence properties of Au NCs.

3.2.1 | Tri State Buffer

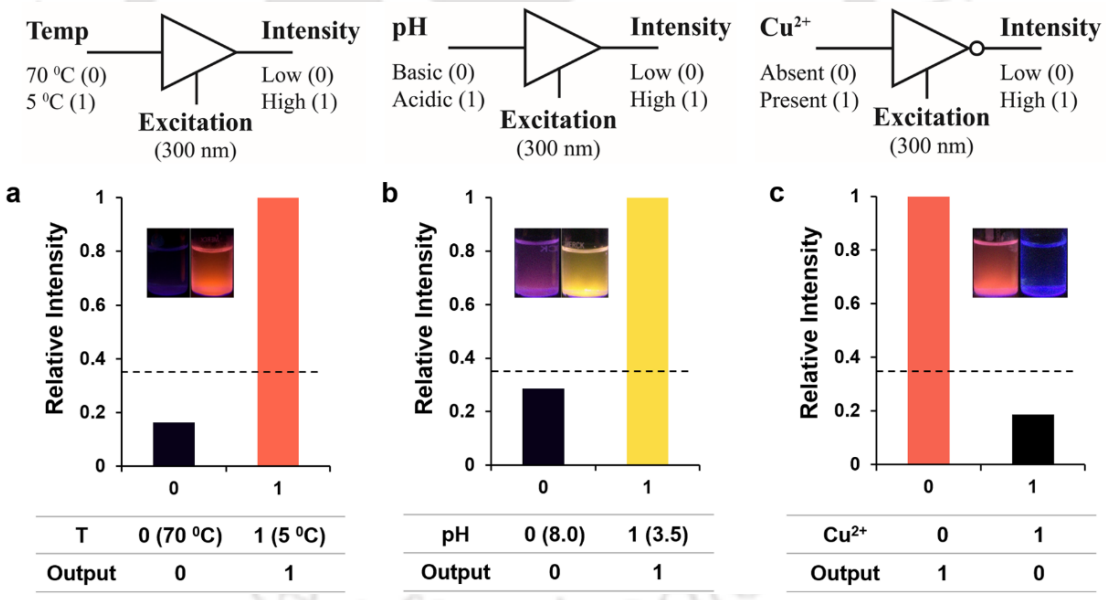

Figure 3.5. Tri-State Buffers. (a, b, c) The logic implementations through inputs of temperature, pH and ion concentration, respectively, are shown to operate as path enabling devices. To achieve the same, the control input is chosen to be the excitation wavelength (300 nm). In output, logic 1 indicates high intensity of luminescence and logic 0 represents low intensity luminescence, relative to a defined threshold value.

Tri-state buffers are efficient in controlling traffic when multiple signals are to be dealt with in a busy network, serving the ultimate purpose of molecular switches for different common inputs. Such networks for decision making are prevalent in naturally occurring biological systems. Here, we demonstrate three kinds of tri-state buffers - of which the first two send the output likewise as input when active, while the third negates the input in active state. In the tri-state buffer, the device is active only when the control input is high. The as-synthesized Au NCs act as tri-state buffers at various pH in the so proposed logic devices. While the control input to the tri-state buffer is the excitation

wavelength (300 nm) in all the cases, as shown in the **Figure 3.5**, the output is monitored in terms of luminescence intensity (at the emission maximum and irrespective of wavelength). The higher intensity levels are considered as HIGH (or logic 1) and the lower intensity levels are treated as LOW (or logic 0).

In the first of the tri-state buffers, the Au NCs can be kept initially at pH 7.0. Temperature is given as the logical input. As depicted in **Figure 3.5a**, at 70 ºC (input logic 0) with control input active, the intensity is low (output logic 0) in contrast to the response at 5 ºC (input logic 1) where the luminescence intensity is high (output logic 1). In the second configuration, the cluster initially is at pH 8.0. Then selecting basic pH (pH = 8.0) and lower pH (pH = 3.5) as inputs, resembling logic 0 and 1 respectively, the responses are obtained likewise (output) in terms of logic, as shown in the **Figure 3.5b**. Finally, in the third structure the cluster is operated at pH 7.0 with copper ion chosen to be the input as shown in **Figure 3.5c**. In the absence of copper ion (input logic 0), the cluster exhibits its inherent luminescence at 612 nm (output logic 1) providing a negation of the input signal. When the copper ion is added (input logic 1) to the system, the luminescence diminishes (output logic 0). Further, as the results of the experiments involving Cu^{2+} ions in human blood serum suggest (reported above), the tri-state logic operations could possibly be performed in physiological conditions, providing additional advantage of using the biocompatible clusters.

3.2.2 | OR Gate

Another important basic logic function is the OR operation. It was achieved by placing the Au NCs at pH 8.0 and choosing pH and temperature as inputs as shown in **Figure 3.6a**. The output is examined with the relative luminescence intensities (irrespective of wavelength) as before. Upon proper construction, the cluster exhibits luminescence for three combinations suiting the OR logic as shown in the **Figure 3.6a**.

3.2.3 | Decoder

With a scope of multi input multi output functioning, the Au NCs exhibit a unique property useful in data multiplexing for decryption and storage.[9] Dividing the zone of output in terms of emission wavelength as well as intensity, the output is divided into four levels as shown in **Figure 3.6b**.

Keeping the inputs as pH and temperature, the output is decoded in terms of the four different luminescent output levels. With each combination of inputs, only one output is active. The decoder primarily at pH 8.0, upon proper combination of inputs, each of these levels can be obtained as the output. For example, for a combination of acidic pH and low temperature (5 ºC), the output is at wavelength 582 nm with comparatively high intensity, thus triggering the D_3 output. Hence, the construct forms a 2 to 4 decoder.

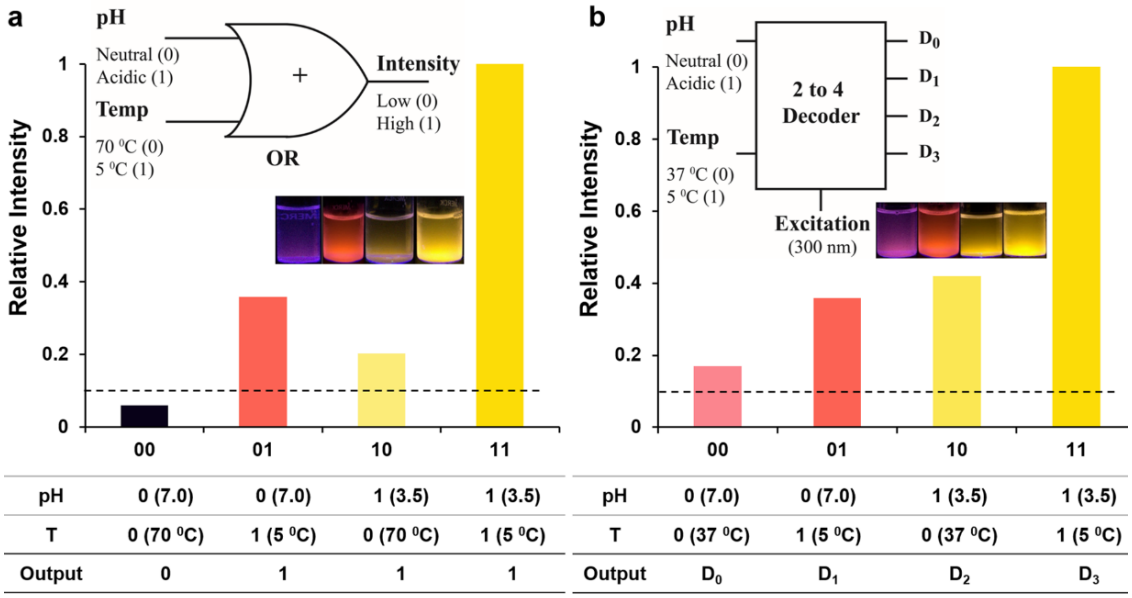

pH	0 (7.0)	0 (7.0)	1 (3.5)	1 (3.5)
T	0 (70 °C)	1 (5 °C)	0 (70 °C)	1 (5 °C)
Output	0	1	1	1

pH	0 (7.0)	0 (7.0)	1 (3.5)	1 (3.5)
T	0 (37 °C)	1 (5 °C)	0 (37 °C)	1 (5 °C)
Output	D_0	D_1	D_2	D_3

Figure 3.6. (a) OR logic operation: The clusters at pH 8, with pH and temperature as the inputs exhibits logic OR operation with their luminescence relatively high in three cases as shown. The respective operation is denoted in the logic table. **(b) 2 to 4 Decoder:** The proposed decoder exhibits four different luminescent output combinations of wavelength-intensity for appropriate input combinations of pH and temperature. The variations are clearly observable in terms of both intensity and wavelength, which represent the system as a data decoder.

3.2.4 | Lock and Key

The Au NCs at any pH (of the medium) could be used as lock and key.[10] The locking is denoted by the quenching of their inherent luminescence by the addition of Cu^{2+}. The same could be unlocked, which is signified by re-emergence of luminescence, was achieved by protonation. The protonation could accompany dissolution of the attached Cu^{2+} ions into the medium – akin to activation of ion-exchange resins - thus increasing the luminescence of the clusters. The details of reversible luminescence change, with emission switching between 612 nm (red) and 582 nm (yellow), are described in **Appendix B, Figure B3.4**. The molecular lock and key was not only demonstrated in water but also in human blood serum, expanding its potential utility.

3.2.5 | Cascading to Higher Levels

The potential of any logic operating system is exhibited by its adaptability to higher level integration.[25] Taking the versatility of response of the emission of the clusters into advantage, cascading of operations was demonstrated. In **Figure 3.7**, the first level shows the tri state buffer at pH 7.0, which allows the traffic only on activating the control input i.e. excitation at 300 nm. Following proper excitation, the first level negated the logic upon ion detection. An important observation made in our experiments is that once the luminescence is quenched upon addition of metal ion, it can be regenerated with the protonation. This property was used in cascading to second level where it functioned as OR logic. Finally, the third important parameter, i.e., temperature was used to alter the intensity levels of the output of second stage accordingly, which ultimately led to

the functionally operative AND gate. The complete logic function obtained is $(\overline{Cu^{2+}} + pH) \cdot Temp$. This three level execution of operation depicts not only the ability of the system to achieve low order functions but also can be hierarchically operated with suitable design and construction.

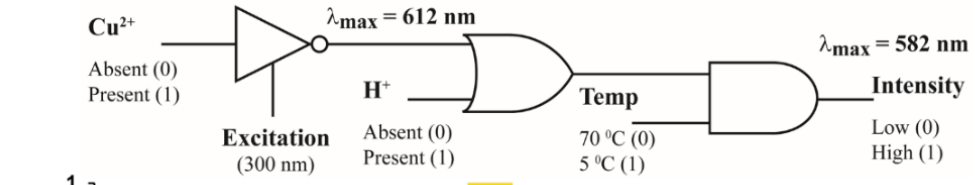

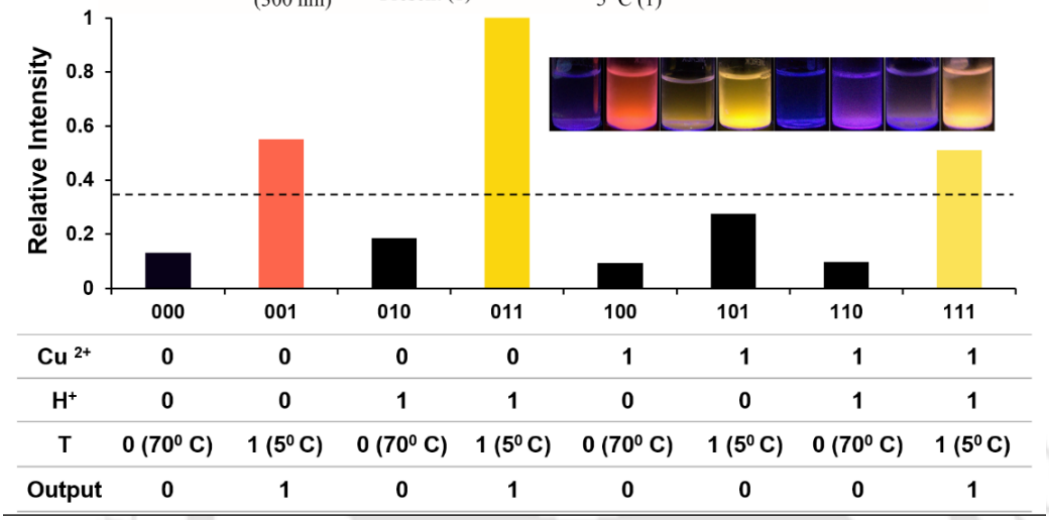

Cu 2+	0	0	0	0	1	1	1	1
H+	0	0	1	1	0	0	1	1
T	0 (70⁰ C)	1 (5⁰ C)	0 (70⁰ C)	1 (5⁰ C)	0 (70⁰ C)	1 (5⁰ C)	0 (70⁰ C)	1 (5⁰ C)
Output	0	1	0	1	0	0	0	1

Figure 3.7. Cascading to higher level operations. The system can be integrated to perform complex logical operations. One such construction using pH, temperature and Cu^{+2} ion is shown in the above figure. The logical function is implemented by integrated tri-state buffer, OR and AND gates respectively. The function that is realized using the system is $(\overline{Cu^{2+}} + pH) \cdot Temp$.

3.3 | Concluding Remarks

Overall, through a serious of experiments, we have been able demonstrate that the sensitivity of luminescence of Au NCs to pH, temperature and metal ions could be utilized for cascade logic operations in liquid medium. This can be considered as important so far as new development in alternative computing is concerned. The atomistic approach towards electronics through photonic responses avoids many complications present in existing systems and is promising for contact-less devices. Developing such versatile bio compatible systems paves way for synthetic static and mobile systems, which mimic the highly evolved biological structures in bringing to fruition a combination of natural and artificial logic based operations for futuristic bionic devices. Although a proof of concept of development of logic structures based on luminescence and responsive Au NCs has been reported, the implementation in real world would require substantial further development. One can conceive of light-induced or magnetic field induced local heating (in the presence of metal or magnetic NPs), introduction of acid/base and dissolved metal ions through microfluidic circuits for operation of logic structures. On the other hand, in bionic systems, change in temperature, pH of the medium or local ion concentration change could be reported in the form of logic output. We do hope that the current work will help bring newer ideas in molecular computation in liquid media.

3.4 | References

1) J. M. Tour, M. Kozaki, J. M. Seminario, *J. Am. Chem. Soc.* **1998**, *120*, 8486.
2) A. P. de Silva, H. Q. N. Gunaratne, C. P. McCoy, *Nature* **1993**, *364*, 42.
3) G. Seelig, D. Soloveichik, D. Y. Zhang, et al., *Science* **2006**, *314*, 1585.
4) Y. Benenson, *Science* **2013**, *340*, 554.
5) J. Andréasson, U. Pischel, S. D. Straight, et al., *J. Am. Chem. Soc.* **2011**, *133*, 11641.
6) J. Zhang, C. Chen, X. Xu, et al., *Chem. Commun.* **2013**, *49*, 2691.
7) S. Uchiyama, N. Kawai, A. P. de Silva, et al., *J. Am. Chem. Soc.* **2004**, *126*, 3032.
8) P. L. Gentili, *Chem. Phys.* **2007**, *336*, 64.
9) H. Tian, *Angew. Chem. Int. Ed.* **2010**, *49*, 4710.
10) M. Suresh, A. Ghosh, A. Das, *Chem. Commun.* **2008**, 3906.
11) M. Bälter, S. Li, J. R. Nilsson, et al., *J. Am. Chem. Soc.* **2013**, *135*, 10230.
12) T. S. Moon, C. Lou, A. Tamsir, et al., *Nature* **2012**, *491*, 249.
13) C. Zhang, J. Yang, J. Xu, *Langmuir* **2010**, *26*, 1416.
14) J. Elbaz, F. Wang, F. Remacle, et al., *Nano Lett.* **2012**, *12*, 6049.
15) X. Yuan, Z. Luo, Q. Zhang, et al., *ACS Nano* **2011**, *5*, 8800.
16) L. Zhang, Z.-X. Wang, R.-P. Liang, et al., *Langmuir* **2013**, *29*, 8929.
17) P. Zhan, J. Wang, Z.-G. Wang, et al., *Small* **2014**, *10*, 399.
18) K. S. Park, M. W. Seo, C. Jung, et al., *Small* **2012**, *8*, 2203.
19) C.-H. Lu, B. Willner, I. Willner, *ACS Nano* **2013**, *7*, 8320.
20) A. K. Sahoo, S. Banerjee, S. S. Ghosh, et al., *ACS Appl. Mater. Interfaces* **2013**, *6*, 712.
21) Z. Wu, R. Jin, *Nano Lett.* **2010**, *10*, 2568.
22) S. Uchiyama, Y. Makino, *Chem. Commun.* **2009**, 2646.
23) D. Cauzzi, R. Pattacini, M. Delferro, et al., *Angew. Chem. Int. Ed.* **2012**, *51*, 9662.
24) L. Shang, F. Stockmar, N. Azadfar, et al., *Angew. Chem. Int. Ed.* **2013**, *52*, 11154.
25) S. Erbas-Cakmak, E. U. Akkaya, *Angew. Chem. Int. Ed.* **2013**, *52*, 11364.

Content of the chapter has been reproduced with permission from John Wiley and Sons (S. K. Sailapu, A. K. Sahoo, S. S. Ghosh, et al., *Small* **2014**, *10*, 4067).

Appendix B

B.1 | Figures

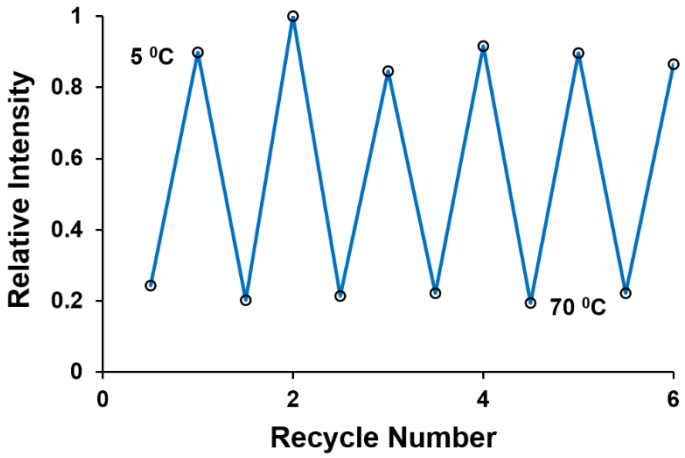

Figure B3.1. Degree of luminescence intensity variation of Au NCs with temperature. Figure shows the intensity variations upon repetitive heating and cooling of the sample. The intensities remained almost at the same level upon for a temperature, during cycling for multiple times.

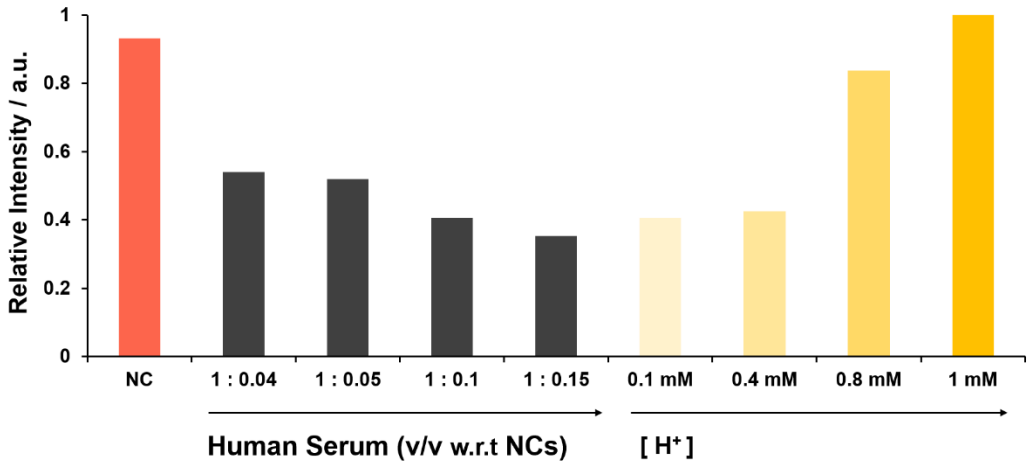

Figure B3.2. Response of Au NCs to human blood serum. The figure shows the decrease in intensity of luminescence upon increasing volumes of human blood serum added to the Au NCs. The intensity was measured at emission wavelength maximum of 612 nm, while excitation wavelength was fixed at 300 nm. The luminescence is regenerated back upon protonation with the emission maximum appearing at 582 nm eventually (in strongly acidic medium).

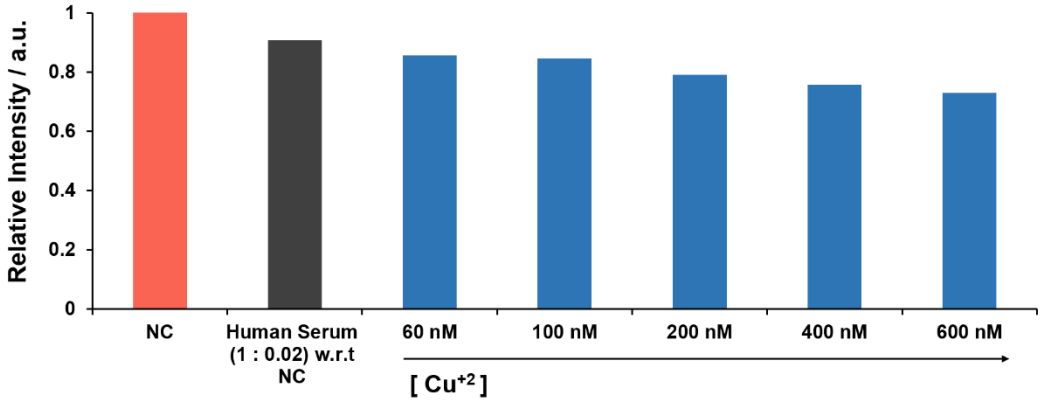

Figure B3.3. Influence of copper ions on Au NCs – human blood serum luminescence. As shown in the figure, the luminescence intensity decreased when human blood serum was introduced into Au NC containing human serum medium. Further, the luminescence continued decreasing upon external addition of copper ions into the mixture. The concentration of serum is kept low for easy probe using luminescence.

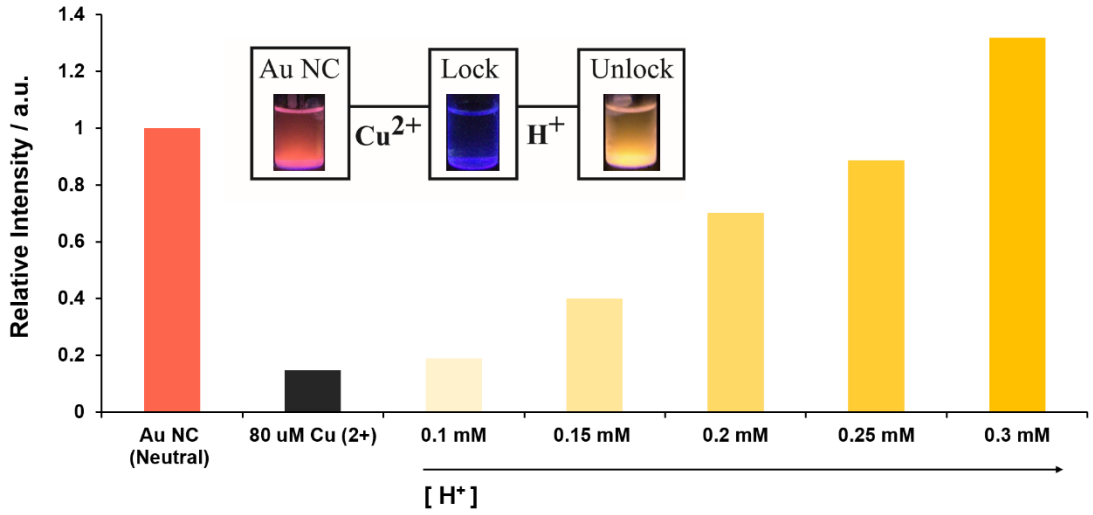

Figure B3.4. Lock and Key. The Au NCs at any pH can act as lock and release system. The system can be locked upon addition of Cu^{2+} which is evident by decline in luminescence intensity and can only be released upon protonation of optimum concentration demonstrating the lock and key system.

B.2 | Synthesis and Characterization of Au NCs

Au NCs were synthesized, with the biopolymer chitosan as template and at room temperature, based on a simple protocol described elsewhere.[1] The Au NCs were characterized and studied by TEM (JEOL 2100 UHR-TEM operating at a maximum accelerating voltage of 200 kV), UV-vis (Perkin Elmer Lambda 45) and fluorescence spectroscopy studies (Horiba fluorolog 3, **Figure B3.5, B3.6**).

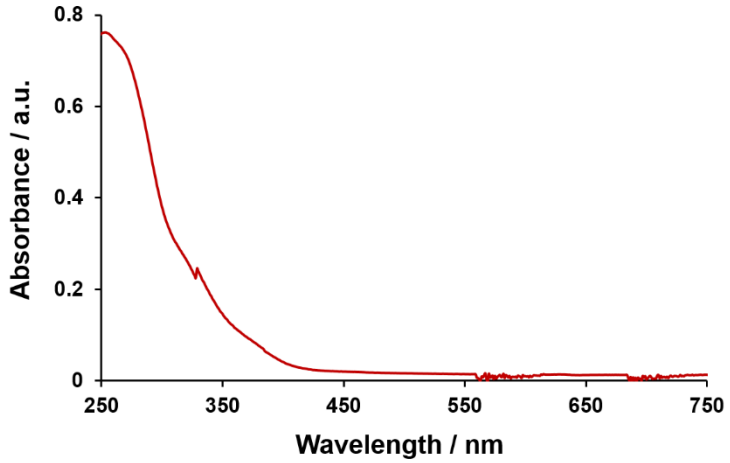

Figure B3.5. UV-Vis spectrum of the as synthesized Au NCs. As is evident from the figure, there is no SPR peak suggesting lack of formation of Au NPs in the medium.

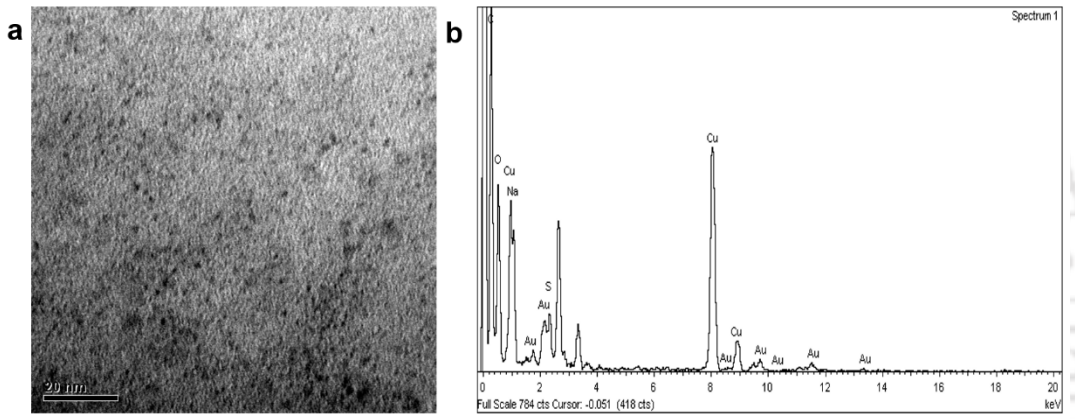

Figure B3.6. (a) TEM image of the synthesized NCs. **(b)** The presence of gold is confirmed by EDX analysis for the same sample.

B.3 | References

1) K. Sahoo, S. Banerjee, S. S. Ghosh, et al., *ACS Appl. Mater. Interfaces* **2013**, *6*, 712.

Content of Appendix B has been reproduced with permission from John Wiley and Sons (S. K. Sailapu, A. K. Sahoo, S. S. Ghosh, et al., *Small* **2014**, *10*, 4067).

Chapter 4

A Device with Integrated Methods for Gene Expression Analyses

Note: This work was carried out in collaboration with Ms. Deepanjalee Dutta and a portion of the work (protein analyses) would be part of her thesis. The basic machine and the principle of synthesis of gold nanoclusters in both the works are the same (or an alternate form of this).

ABSTRACT

A bench top device with integrated methods is proposed to carry out gene expression studies. Employing luminescent gold nanoclusters (Au NCs) as the signal generating agents, the device enables carrying out reverse transcriptase polymerase chain reaction and array-based gene analysis with switchable holders and custom designed user friendly graphical user interfaces. As proof of concept, the device and methods were applied to evaluate gene profiling related to apoptosis in HeLa cancer cells. A simple and rapid method to directly synthesize Au NCs on DNA template was developed using the device. The method of synthesis is versatile and can be applied to different classes of DNA. The portable device with user friendly methods offer potential use in disease diagnostics with a vision to extend health care facilities to remote geographical locations.

Analyses of genes and proteins can be considered as two pillars key to molecular basis of health analysis and are thus important for developing novel molecules and materials for targeted therapy. An important aspect of the field is to develop new methods and devices for the analyses so that not only faster and sensitive techniques are made available but also a broad spectrum of the global populace accrue the benefit of such developments. This can possibly be achieved by combining the best of well-established protocols and currently developing fields. We have developed a new platform technology and a bench-top device for gene analysis based on the photoluminescence of in situ synthesized gold (Au) NCs as the probe. This is based on combining conventional methods of gene analyses and nanoscale materials with extraordinary optical properties.

Recent technological developments, in fields of genomics and proteomics, have helped to provide vital information coded in DNA and proteins in order to predict potential disease targets and mutations, infer on disease susceptibility and to discover novel therapeutic agents.[1-2] The reverse transcriptase – polymerase chain reaction (RT-PCR, in case of genes) and high throughput array based methods (for analyses of genes and proteins) have been central to the achievements.[3-4] However, the advancements have been associated with sophisticated instrumentation, complex and multistep fabrication and analysis techniques, involved processes for functionalization of the probes in order to achieve high sensitivity and selectivity.[5-8] Additionally, there is concern over the largescale use of hazardous organic dyes and radioactive isotopes.[9] Thus there is a genuine need to

develop new technology that would address point-of-care diagnosis for easy access by a large population at an affordable cost.

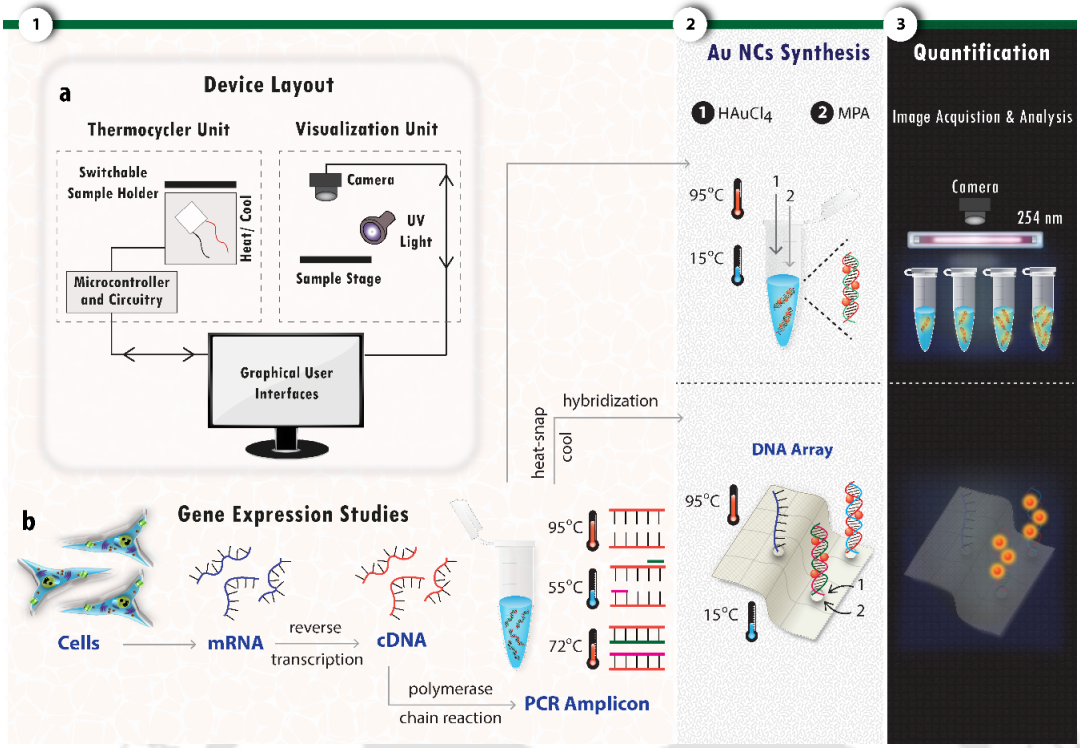

Figure 4.1: Schematic illustration of device and methods: (a) Device layout. The constituents of the bench top portable device for gene expression studies are shown in the figure. Graphical User Interfaces (GUIs) allows control of the device, acquiring of the data and analyses of the results through interfacing to a computer/laptop. **(b) Gene expression studies.** i) Amplification of DNA: Genes of interest in the cDNA (cDNA converted from isolated RNA of cells) were amplified using the device. Synthesis of Au NCs was then carried out on the PCR amplicon (in the tube) in a single temperature cycle with the thermocycler unit. The Au NCs synthesized in the PCR products were imaged in the visualization unit under UV illumination. The intensities of emissions from the Au NCs were analysed using the GUIs to generate information about amplification. ii) DNA Array: The PCR amplicons were subjected to heat-snap-cool to obtain single stranded products using the device and they were then spotted over the nitrocellulose membrane containing pre-immobilized complementary ssDNA. Au NCs were synthesized in a single temperature cycle on these spots and the membrane was imaged and analysed in a similar way as described before.

The efficiency of the PCR process has been improved through the usage of NPs, QDs, CNTs, carbon nano-powder, graphene etc.[10-13] The plasmonic[14-15] and luminescent[16] nanomaterials are useful as diagnostic probes in PCR and array based methods. However, due to high sensitivity and background related issues fluorometric techniques are preferred over colorimetric assays. Use of conventional organic fluorophores are limited due to photo-bleaching, photo-blinking and often the carcinogenic nature of the molecule. Though quantum dots have been used as fluorometric tags in gene expression studies as better materials, their toxicity is a concern.[17] It is also worth noting here that most of the diagnostic techniques (for RT-PCR and microarray) adopt initial synthesis of nanomaterial followed by specific functionalization for conjugation with biomolecules. This particular approach demands extra labour (such as isolation of the probe), processing and thus is time consuming. Also, since interaction of nanomaterial takes place after synthesis, there lies possibility

that complete conjugation with biomolecules may be difficult to achieve. Validation in every step is necessary to certify the functionality of the nanomaterial, which is vital for subsequent interactions to occur. Few atom luminescent metal NCs are an exciting option as fluorophore due to their salient features including small size, high photostability, low toxicity in respect to other fluorophores and low photo-blinking.[17] However, extensive applications of these NCs have so far been limited in rapid detection assays involving DNA, due to the requirement of large amount of precursors, longer time period of synthesis and extensive purification steps. In the current context, to employ them as signal generating agents, the synthesis should be applicable in liquid as well as solid phase. Provided such an efficient synthesis procedure is obtained integrating into the core functionality of PCR and array based studies, it could pave for the development of a device for study of genes.

Herein, a bench top device and integrated methods capable of carrying out RT-PCR and array based gene analysis were reported as shown in **Figure 4.1.** Ultra small Au NCs were used as signal generating agents in case of PCR amplicon quantification and DNA array based analysis. The synthesis of Au NCs involved a rapid single-step method being carried out directly on the PCR products in the tube itself (or) on the hybridised PCR products in nitrocellulose membrane using the device itself (with running a single temperature cycle) and is all in one platform as illustrated in **Figure 4.1**. The synthesis was carried out in a rather short time to achieve nearly homogeneous Au NCs without any need for further processing and thereby making it an excellent choice in applications as diagnostic probe. The luminescence of the Au NCs was proportional to the amount of template present, i.e., DNA concentration. Hence, study of the luminescence profile revealed the nature of reactions/interactions happened provided there was a change in the amount of the biomolecule. This principle of detection was applied for semi-quantitative analysis of PCR products and for array based analysis of DNA. In case of PCR amplicon quantification, the device facilitates direct analysis using the luminescence of the Au NCs within the PCR tube, thus avoiding the additional step of gel electrophoresis. Paper based membrane methods were adopted for array based analysis to avoid complex fabrication procedure and made the whole process less expensive, easy to handle, flexible and disposable, so that the device can easily be adopted for medical diagnostics even in remote areas.[18-19] As a proof of concept, the device and the methods proposed were applied to evaluate gene profiling for apoptotic pathway where HeLa cancer cells were treated with a commercially available drug doxorubicin (DOX) and their apoptotic gene expression profile was studied by Au NC luminescence in an array based method as illustrated in **Figure 4.1**. With increasing demands of low cost, portable, easily operable point-of-care diagnostic tools, the device promises utility in particularly remote areas.

4.1 | Description of the Device

The layout of the device and the methods used are as described in **Figure 4.1**. The image of the device is shown in **Figure 4.2a**. The device is modular in design with different modules as shown in **Figure 4.2b**. The device comprises of two major modules – thermocycler unit and visualization

unit. The device incorporates embedded circuit with both the thermocycler and visualization unit being controlled by custom designed GUIs coded in LabVIEW. The device is portable and can easily be accessed on any PC/Laptop through these GUIs. The GUIs allow the user to input various parameters (along with predefined ones), control the sequence of operations, carry out image acquisition and analysis.

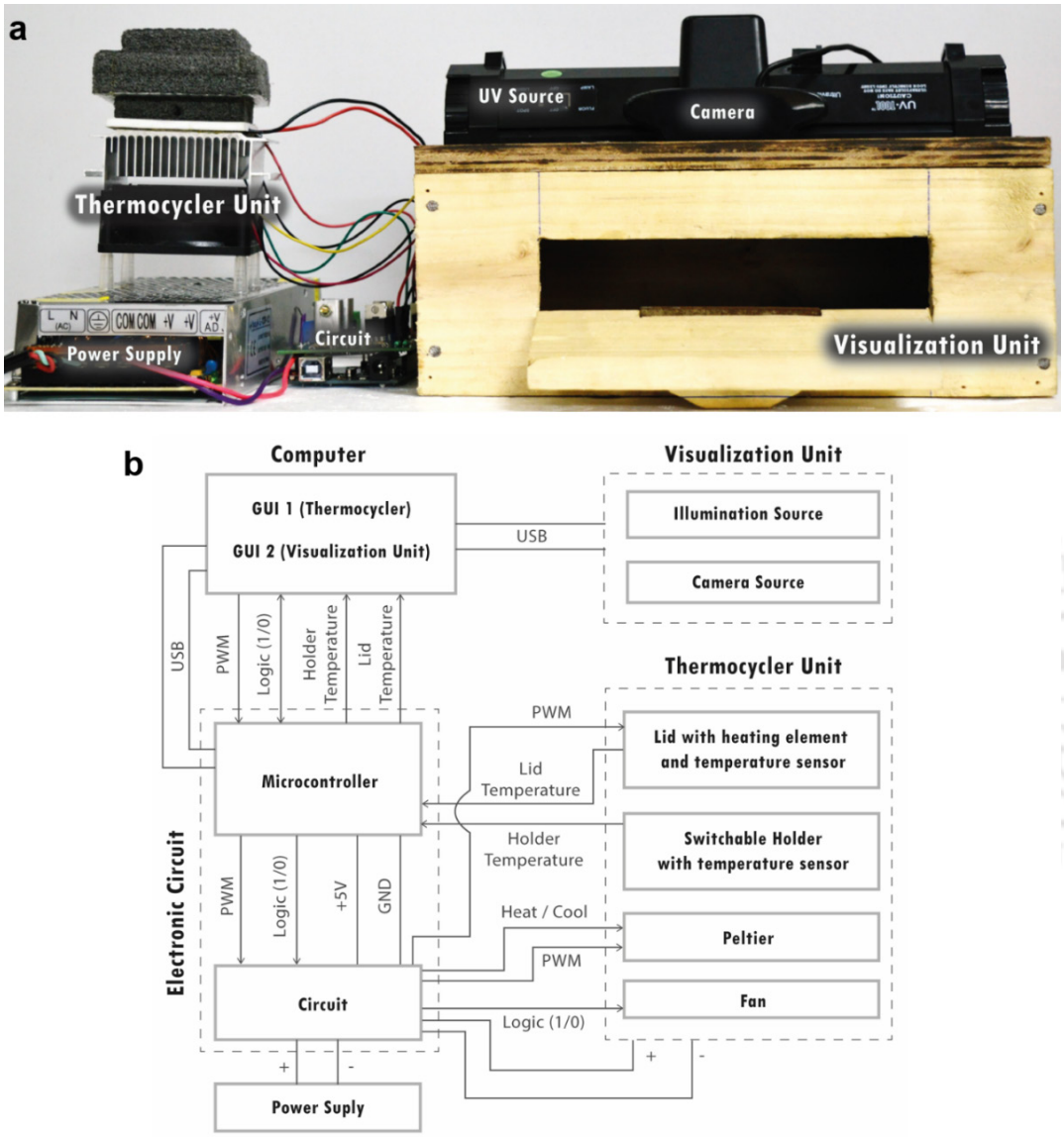

Figure 4.2. **(a)** The picture represents the physical construction of the benchtop device for carrying out reverse transcriptase polymerase chain reaction (RT-PCR) and DNA array based analyses. **(b)** Flow chart describing various elements in the device and their interconnections.

Thermocycler unit: All the temperature cycling is achieved through the thermocycler unit. Thermocycler unit is responsible for carrying out the RT-PCR process, array based experiments and synthesis of Au NCs – the signal generating agents in both liquid and on membrane. The thermocycler accommodates switchable sample holders: for 0.2 mL PCR tubes (liquid samples) and for placing membrane as shown in **Figure 4.3** facilitating easy switching between two process. These switchable holders make it feasible for carrying out PCR and array based studies on a single platform. The bottom of the holder is exposed to peltier unit (connected to heatsink and fan) which heats and

cools the sample holder. The sample holder can achieve temperature ranging from 10 ºC to 95 ºC in 150s. For the PCR process, a lid with cartridge heater as heating element is provided to avoid evaporation of the sample while PCR amplification. The temperature of the lid can quickly go up to 120 ºC. Sensors for monitoring the temperatures are equipped to both holders and the lid. A custom designed embedded circuit is the core electronic element responsible for operation of the thermocycler.

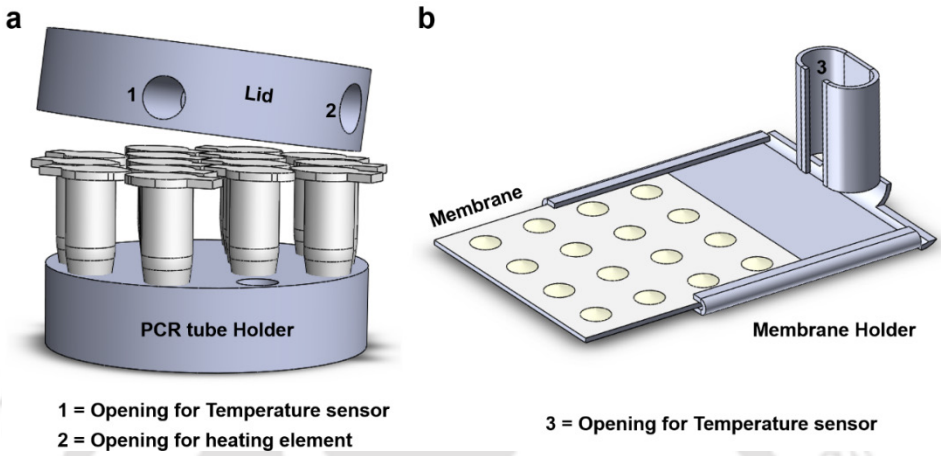

Figure 4.3. Switchable Holders and Lid. The device is incorporated with switchable holders to hold both commercially available PCR tubes and membrane (for array based analysis) facilitating easy switching between the two process. The figure shows the graphical representation of the holders and lid. **(a)** 0.2 mL PCR tube holder with lid on the top. **(b)** Membrane holder for array based studies.

The thermocycler is controlled by GUI 1 whose front panel is shown in **Figure 4.4**. The GUI is broadly classified into three segments.

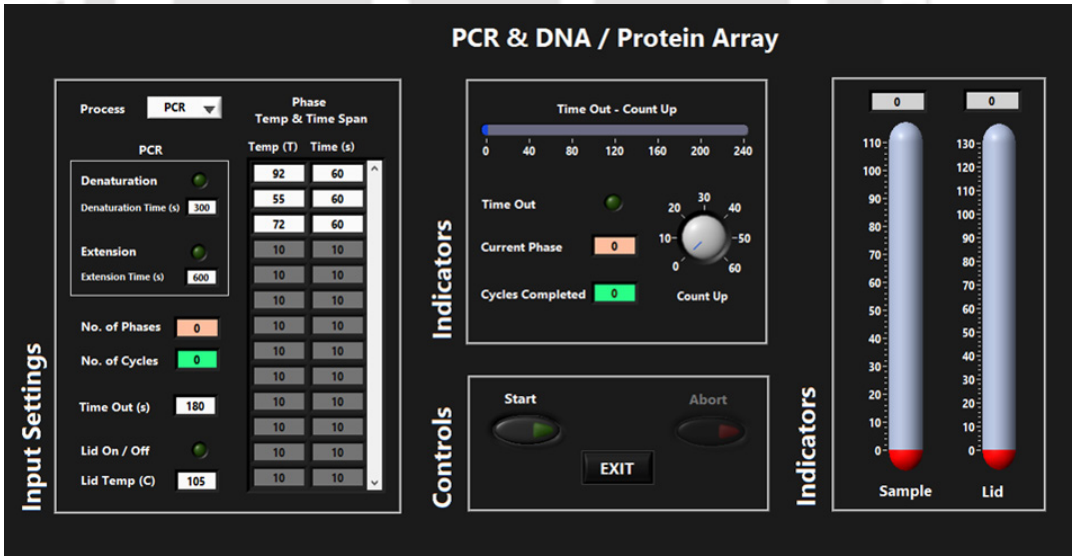

Figure 4.4. Front panel of the GUI 1 to control the thermocycler unit.

Input settings – These settings allow a particular process to be chosen i.e., PCR or array based analysis. In PCR mode, inputs related to initial denaturation (on/off) with denaturation time, final extension (on/off) with extension time, number of cycles can be given. Also, the lid (on/off) can be controlled with the temperature set. An additional option is included to provide the maximum timeout

(in seconds) within which a process is expected to start. If the process is not started within this time, the machine shuts of automatically. Also, custom temperatures and time periods can be set.

Controls – The controls involve operations such as starting a process, halting a process and exiting the application.

Indicators – Temperature indicators indicate the temperature of the sample holder/plate and lid continuously. The information regarding the time lapse, phases and cycles are shown in the front panel. If a particular operation fails to occur within the pre-set time, the timeout indicator indicates it and the machine turns off automatically.

Visualization unit: Imaging of the sample of interest was carried out in the visualization unit. The visualization unit constituting a UV source (6W) with interchangeable light sources (for short, mid and long wavelength) and camera source enables to visualize, image the final products (through the luminescence of the synthesized Au NCs). The visualization unit is controlled through GUI 2 whose front panel is shown in **Figure 4.5**. The GUI 2 is divided into three sections.

Figure 4.5. Front panel of the GUI 2 to control the visualization unit with several options for image acquisition, analysis and generation of reports.

Acquisition – The acquisition tab in the GUI 2 enables to acquire images in auto or manual mode with flexibility to change camera and image related parameters for acquisition.

Analysis – The analysis tab allows to further process the image and analyse it over a region of interest (ROI) or along a line. ROIs in different geometrical shapes can be selected and information such as histogram data, X and Y averaged pixel profile, line profile can be obtained and exported.

Reports - The information obtained can be fit with linear regression techniques and can estimate the unknown points as per the fit.

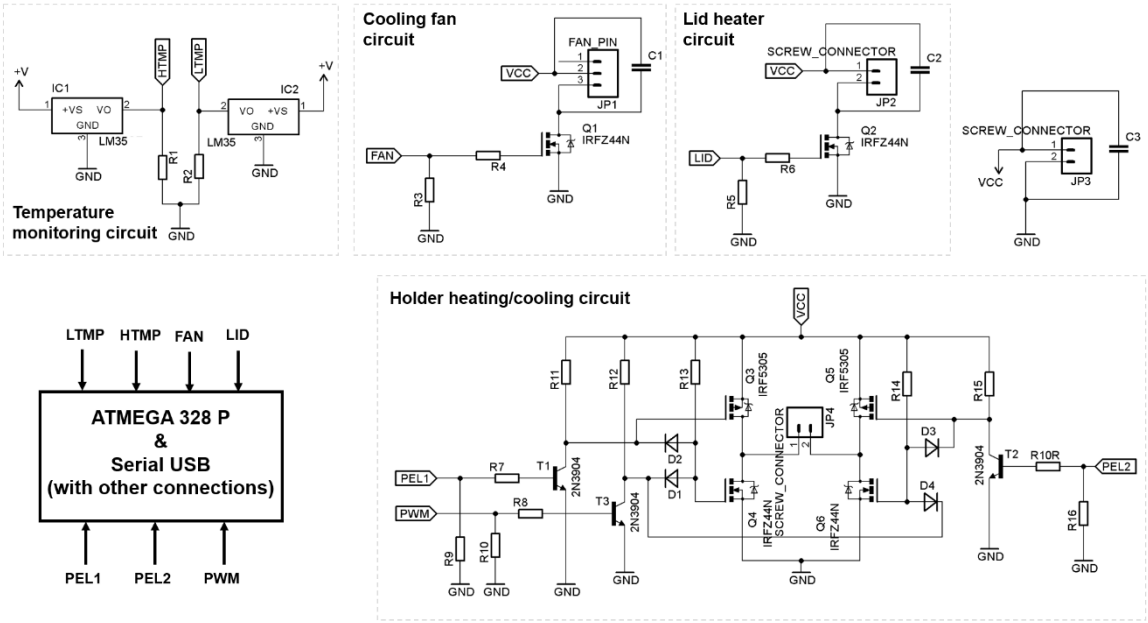

Figure 4.6. Schematic of the circuit used in the device.

Electronic circuit: The thermocycler unit in the device is programmatically controlled using an electronic circuit interfaced to a microcontroller (ATMEGA 328P) as shown in **Figure 4.6**. The microcontroller drives the sequence of operations as instructed by the user through the GUIs. The microcontroller sends/receives the data through serial communication. The holder temperature is controlled through the h-brige circuit connecting to the peltier unit and is driven by PID (proportional–integral–derivative) control. The lid heater circuit is connected to the catridge heating element and is controlled by using PWM (pulse width modulation) to heat the lid. An additional circuit to control the fan which aids in cooling the heat sink of the peltier is provided. The temperature of the holder and the lid are continuously obtained using the temperature monitoring circuit with temperature sensors and are displayed on the GUI. The whole circuit can be run from a 12V, 10A power supply.

Functional correlation: Since the device is built in a modular fashion, it is easy to access individual modules and even offers scope for upgradation. The switchable holders allow to carry out analysis in both liquid samples and on membrane for both PCR and array based analysis. The device is portable and can be accessed through user friendly GUIs. The protocols for PCR, array based techniques and synthesis of signal generating agents are embedded in the GUIs alongside tools for image acquisition, analysis and generating reports. The combination of the above mentioned various processes makes the GUI a useful feature which brings multiple processes in a common platform.

4.2 | Reverse Transcriptase Polymerase Chain Reaction

To evaluate the performance of the device, β-actin gene was amplified - using specific primers - for 35 cycles. A similar set was amplified in commercial PCR machine (Palm cycler), keeping the conditions of amplification same in both cases (**Appendix C, Experimental Procedures**). Standard gel electrophoresis with ethidium bromide (EtBr) staining methods were employed to analyze the

PCR amplicons. The gel images of the PCR amplicons as visualized in gel documentation system are shown in **Figure 4.7a**. Image analysis revealed that using the device a gene amplification efficacy of about 95 % could be obtained, in comparison to commercial PCR machine.

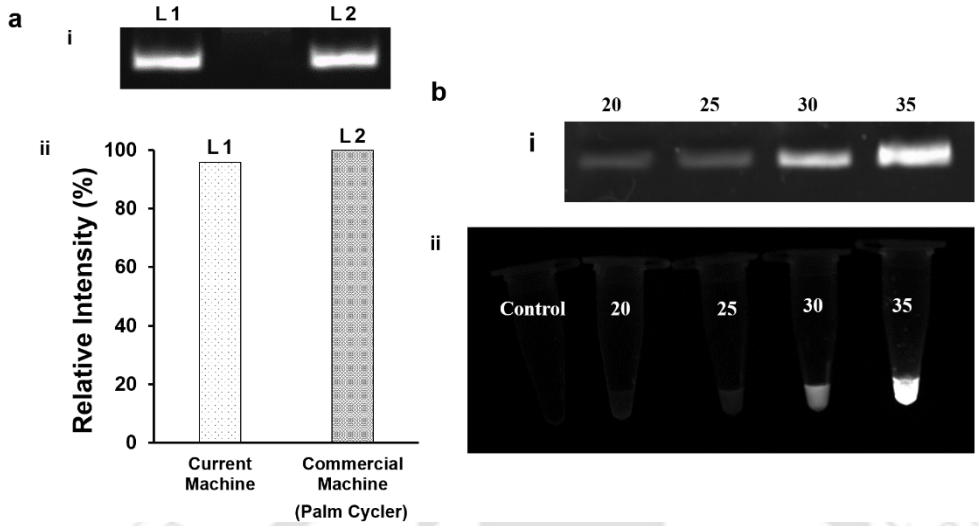

Figure 4.7. Amplification of DNA with the device and Au NCs as signal generating agent for PCR amplicon quantification. (a) β-actin gene was amplified using specific primers in the present device and commercial machine. Lane L1, L2 correspond to PCR amplicon from the present device and commercial device respectively. i) Visualization of the bands in agarose gel under UV illumination. ii) Relative luminescence intensities of the bands corresponding to PCR amplicon as analysed from image. **(b)** β-actin gene was amplified using specific primers - using the present device - for 20, 25, 30 and 35 cycles. i) Gel images corresponding to various cycles of EtBr stained PCR products under UV illumination. ii) Grayscale image of luminescence of Au NCs synthesized corresponding to different cycles of PCR amplicon under UV excitation (254 nm).

Instead of tedious gel electrophoresis and use of EtBr for quantifying PCR products, we devised a method to use luminescent Au NCs directly to visualize the PCR amplicons following amplification in the device. A temperature dependent facile and rapid synthesis of Au NCs for DNA quantification was developed with the flexibility to carry out the same in the PCR tube after gene amplification. The synthesis used the final PCR amplicon as the template with $HAuCl_4$ and MPA as the reagents and was subjected to a single heating and cooling cycle (between the temperatures 95 ºC and 15 ºC) in the thermocycler unit. This results in the synthesis of Au NCs in proportion to the amount of PCR amplicon present. The Au NCs emitted luminescence with a peak at 580 nm, when excited by 254 nm light. Further, the luminescence of the synthesized Au NCs provided a way for the semi-quantification of the PCR products.

In order to demonstrate quantification employing these Au NCs as signal generating agents, β - actin gene was amplified for different cycles (e.g., 20, 25, 30 and 35) using specific primers in the thermocycler unit of the device. Then, Au NCs were synthesized on the PCR amplicons by adding the reagents ($HAuCl_4$ and MPA) to the PCR tube, followed by heating to 95 ºC for 2 min and then cooling down to 15 ºC for 3 min. The PCR tubes were then directly imaged in the visualization unit under UV excitation of 254 nm and the image, shown in **Figure 4.7b**, was captured by a digital camera. It was observed that the luminescence intensity of these Au NCs increased with the

increasing number of cycles indicating increase in amplification of DNA. It was also observed that the lowest amount of DNA that the synthesized Au NCs could differentiate was for 20 cycles (starting with 0.5 μg of DNA). Another similar set was amplified for different cycles and validated by a standard process of agarose gel electrophoresis (with EtBr staining), which showed good agreement with the results obtained.

4.3 | Array based Gene Expression Studies

These results encouraged us to extend the application of the device for multiple gene expression studies in an array format, using these Au NCs as the signal generating agents. To achieve this, commercially obtained single stranded oligonucleotide (β-actin) probes, in increasing concentrations, were immobilized in two rows on a nitrocellulose membrane. Commercially obtained complementary target strands were then hybridized on the spots in the second row only as shown in **Appendix C, Figure C4.1**. Au NCs were then synthesized on all the spots in the membrane in the thermocycler unit as described above. Upon imaging in the visualization unit, the luminescence of the Au NCs was evident and it was observed that, for each concentration, the intensity in hybridized dsDNA spot was more in comparison to the control ssDNA spot.

To demonstrate the use of Au NCs for the study of relative gene expressions during apoptosis in cancer cells, commercially obtained sequences of common apoptotic genes (BCL - 2, BAX, Caspase - 3) were chosen. Au NCs were synthesized on different amounts of hybridized dsDNA for each set of genes. It was observed that, in each case, with the increase in the amount of hybridized product the luminescence increased proportionately, as shown in **Appendix C, Figure C4.2**. A set of experiments was also done with Au NCs synthesized on non-complementary pairs of commercially obtained sequences. The analysis showed that the luminescence intensity of non-complementary pairs was similar to ssDNA controls immobilized on membrane, as shown in **Appendix C, Figure C4.3**, possibly due to washing away of the non-complementary strands. Based on these results, it can be concluded that the luminescent Au NCs are viable alternative of commonly used organic dyes for studying gene expression.

In order to test further the above observations in vitro, relative gene expression studies were carried out in HeLa cells, which were subjected to apoptosis via anti-cancer drug DOX. The apoptosis specific genes in control and DOX treated cells (BCL - 2, BAX, Caspase - 3) were then amplified, in the device, using gene specific primers. Commercially obtained corresponding ssDNA apoptotic marker genes were immobilized on the nitrocellulose membrane in increasing amounts per spot. After this, PCR amplicons were heated and then snap - cooled in the thermocycler (to obtain single stranded products) and they were subsequently transferred to the above spots containing ssDNA. Following hybridization, Au NCs were synthesized on these spots and the gene regulation outputs were quantified in correlation to the luminescence profile (**Appendix C, Experimental Procedures**). As is evident from the relative intensities in **Figure 4.8**, the apoptotic genes BAX,

Caspase - 3 were upregulated and BCL - 2 was downregulated with respect to endogenous control β - actin, signifying apoptosis in case of DOX treated HeLa cells in comparison to the control HeLa cells. Conventional EtBr gel electrophoresis studies corroborated the aforementioned results obtained by the use of Au NCs. Hence Au NCs were successfully applied to probe the expressions of multiple genes governing the apoptosis pathway with the HeLa cells as a model system.

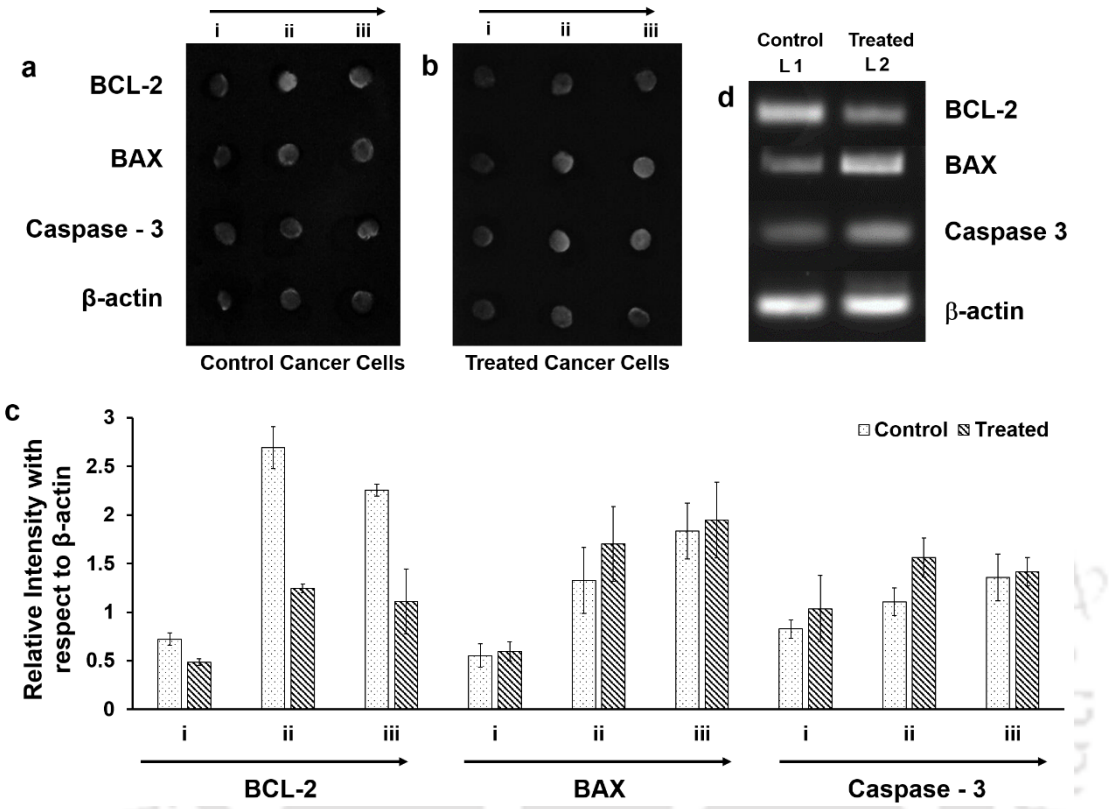

Figure 4.8. Study of expression of multiple genes in control HeLa cells and DOX-treated HeLa cells. (a) and **(b)** Grayscale images under UV illumination (254 nm) of Au NCs synthesized on various genes (spots) in control and treated HeLa cells (respectively). Firstly, commercially obtained ssDNA (as capture agent) of BCL - 2, BAX, Caspase - 3 in increasing amounts ((i) 0.18 µg, (ii) 0.37 µg and (iii) 0.74 µg; indicated by the arrow) were immobilized on the nitrocellulose membrane. Following this, increasing amounts of PCR amplicons of BCL - 2, BAX, Caspase - 3 ((i) 0.18 µg, (ii) 0.37 µg and (iii) 0.74 µg) obtained from control and DOX-treated cells were heated and snap-cooled to achieve single stranded products and were subsequently hybridized to above mentioned capture probes. Au NCs were then synthesized on all the spots of the membrane. **(c)** Relative luminescence intensity of Au NCs synthesized on BCL - 2, BAX, Caspase - 3 hybridized dsDNA in control and treated HeLa cells (obtained following image analysis). The data is represented as mean and standard deviation from three individual experimental sets. The graph depicts the averaged intensity of data from three separate experiments with their standard deviation. **(d)** Gel electrophoresis with EtBr staining of PCR amplicons of BCL - 2, BAX, Caspase - 3 from control and treated HeLa cells. L1 and L2 lanes correspond to control and treated samples.

4.4 | Concluding Remarks

Hence, the present invention introduced a new way of gene and protein assays, on a single platform based user-friendly device, with integrated methods to carry out both RT-PCR and array based techniques. The GUIs simplifies the operation by enhancing the user experience and lets to perform

tasks like inputting parameters, image acquisition and analysis. The modular approach in design of the device permits easy upgradation. The facile and rapid synthesis of signal generating agents (Au NCs) using the device itself on DNA allows semi-quantitative and qualitative analysis. Importantly, the techniques, methods and materials employed are bio and environmentally friendly. Further, membranes based approaches adopted in a view to avoid complicated fabrication steps provides opportunities to extend medical facilities to remote geographical locations. Taken in account all these sublime features, the device and the integrated methods may add a new dimension to the existing techniques with the amalgamation of nanotechnology. This may create motivation to converge various techniques and develop methods in a view to make point of care devices available to a majority of people across the globe.

4.5 | References

1) D. J. Lockhart, E. A. Winzeler, *Nature* **2000**, *405*, 827.
2) M. Tyers, M. Mann, *Nature* **2003**, *422*, 193.
3) S. Gaj, L. Eijssen, R. P. Mensink, et al., *Genes Nutr* **2008**, *3*, 153.
4) S. Brandt, S. Kloska, T. Altmann, et al., *Journal of Experimental Botany* **2002**, *53*, 2315.
5) L. Quijada, M. Soto, J. M. Requena, *Exp Parasitol* **2005**, *111*, 64.
6) J. B. Randolph, A. S. Waggoner, *Nucleic Acids Research* **1997**, *25*, 2923.
7) B. G. Moreira, Y. You, R. Owczarzy, *Biophys Chem* **2015**, *198*, 36.
8) A. Toutchkine, P. Nalbant, K. M. Hahn, *Bioconjugate Chemistry* **2002**, *13*, 387.
9) V. Espina, E. C. Woodhouse, J. Wulfkuhle, et al., *J Immunol Methods* **2004**, *290*, 121.
10) X. Lou, Y. Zhang, *ACS Appl Mater Interfaces* **2013**, *5*, 6276.
11) H. Li, J. Huang, J. Lv, et al., *Angew Chem Int Ed Engl* **2005**, *44*, 5100.
12) F. Sang, Y. Yang, H. Wang, et al., *Journal of Biomedical Science and Engineering* **2012**, *05*, 295.
13) Y. Bai, Y. Cui, G. C. Paoli, et al., *ACS Appl Mater Interfaces* **2015**, *7*, 13142.
14) M. Cai, F. Li, Y. Zhang, et al., *Nano Research* **2010**, *3*, 557.
15) D. Kim, W. L. Daniel, C. A. Mirkin, *Anal Chem* **2009**, *81*, 9183.
16) R. Q. Liang, W. Li, Y. Li, et al., *Nucleic Acids Res* **2005**, *33*, e17.
17) X. Yuan, Z. Luo, Q. Zhang, et al., *ACS Nano* **2011**, *5*, 8800.
18) M. N. Costa, B. Veigas, J. M. Jacob, et al., *Nanotechnology* **2014**, *25*, 094006.
19) D. D. Liana, B. Raguse, J. J. Gooding, et al., *Sensors (Basel)* **2012**, *12*, 11505.

Appendix C

C.1 | Figures

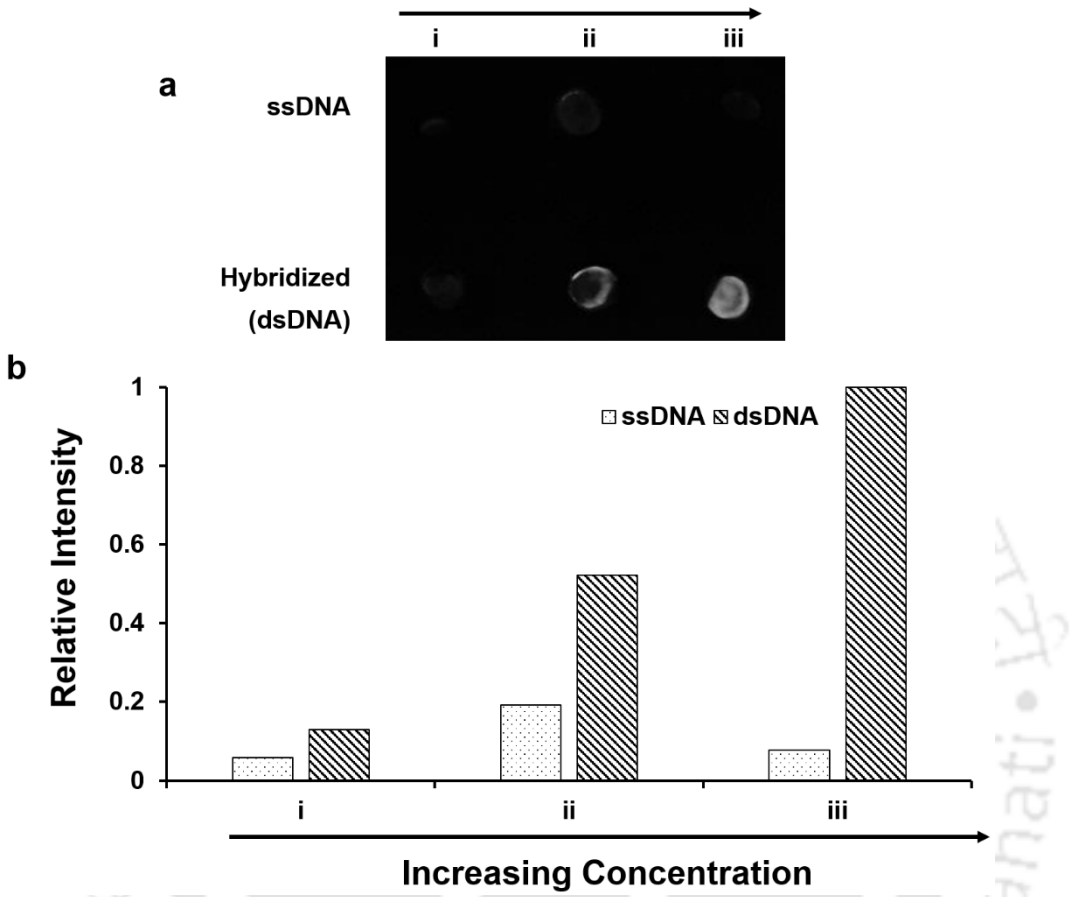

Figure C4.1. Luminescence profile of Au NCs synthesized on ssDNA and dsDNA on nitrocellulose membrane. (a) Grayscale image under UV illumination (254 nm) showing commercially obtained ssDNA (β-actin), hybridized dsDNA on the nitrocellulose membrane in increasing amounts (indicated by the arrow). (b) Relative luminescence intensities of the Au NCs synthesized on all spots (from image analysis).

Comments on Figure C4.1

Commercially obtained ssDNA (β - actin) was immobilized (spotted) on nitrocellulose membrane in increasing amounts ((i) 0.18 µg, (ii) 0.37 µg and (iii) 0.74 µg; indicated by arrow in **Figure C4.1a**) in two rows. Complementary target ssDNA (commercially obtained) were then hybridized only in the second row in increasing amounts ((i) 0.18 µg, (ii) 0.37 µg and (iii) 0.74 µg) from left to right. Following this, Au NCs were synthesized on all the spots using the thermocycler unit of the device. The membrane was then imaged using visualization unit (**Figure C4.1a**) and the spot intensities were analysed using the GUIs. From **Figure C4.1b**, it is clear that the intensity of the Au NCs increased with the increase in the concentration of hybridised product.

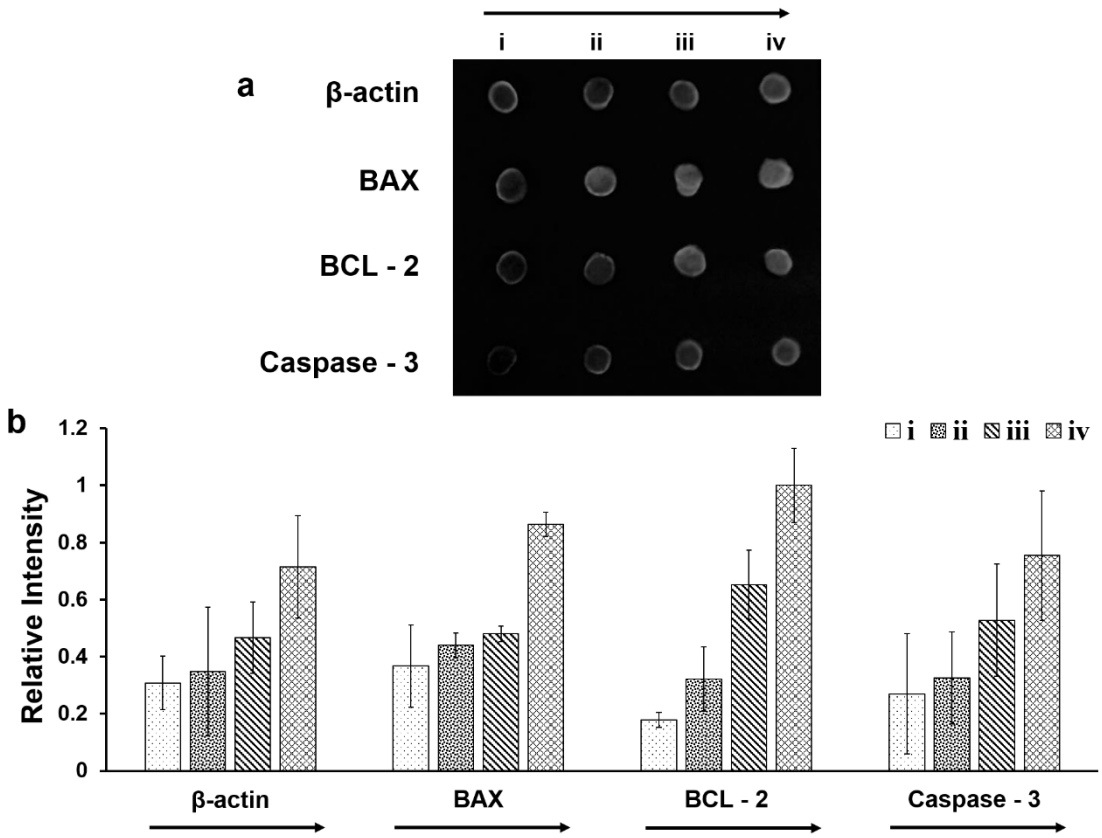

Figure C4.2. Luminescence intensities of Au NCs synthesized on commercially obtained apoptotic pathway gene sequences (hybridized dsDNA) on nitrocellulose membrane. (a) Grayscale image under UV illumination (254 nm) of Au NCs synthesized on commercially obtained hybridized dsDNA sequences of β-actin, BCL 2, BAX and Caspase 3 on nitrocellulose membrane in increasing amounts (indicated by the arrow). **(b)** Relative luminescence intensities of Au NCs synthesized on hybridized DNA spots (from image analysis).

Comments on Figure C4.2

ssDNA strands of commercially obtained apoptotic pathway genes BCL – 2, BAX, Caspase 3, β - actin was immobilized (spotted) on nitrocellulose membrane in increasing amounts ((i) 0.18 µg, (ii) 0.37 µg, (iii) 0.74 µg and (iv) 1.1 µg; indicated by arrow in **Figure C4.2a**) in two rows. Respective complementary target ssDNA (commercially obtained) were then hybridized on these spots in increasing amounts ((i) 0.18 µg, (ii) 0.37 µg, (iii) 0.74 µg and (iv) 1.1 µg). Au NCs were synthesized on all the spots using the thermocycler unit of the device and the membrane was imaged in visualization unit. The relative intensities of these spots as analysed from the image showed that the intensities of Au NCs increased with the concentration of the hybridised products in all these apoptotic genes suggesting their possibility of usage in studying multiple gene expression in cancer cells.

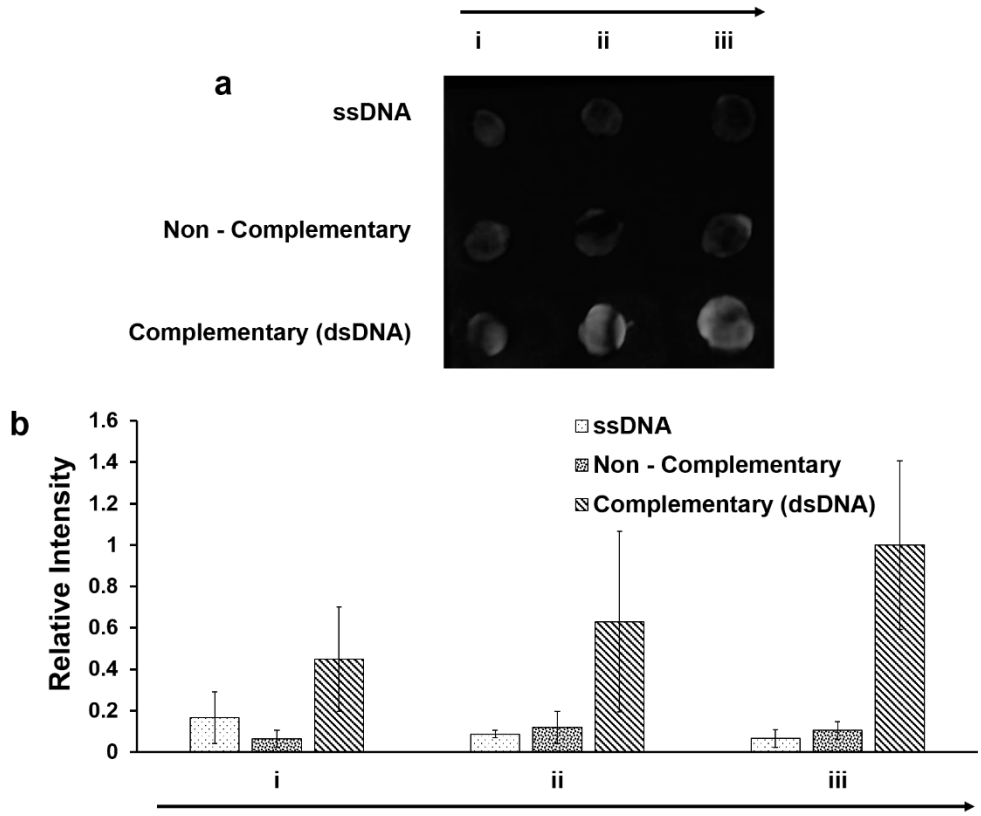

Figure C4.3. Luminescence profile of Au NCs synthesized on ssDNA, non-complementary and complementary strands on nitrocellulose membrane. (a) Grayscale image under UV illumination (254 nm) showing commercially obtained ssDNA, non-complementary and complementary strands on the nitrocellulose membrane in increasing amounts (indicated by the arrow). (b) Relative luminescence intensities of the Au NCs synthesized on all spots (from image analysis).

Comments on Figure C4.3

Commercially obtained ssDNA (β - actin) was immobilized (spotted) on nitrocellulose membrane in increasing amounts ((i) 0.18 µg, (ii) 0.37 µg and (iii) 0.74 µg; indicated by arrow in **Figure C4.3a**) in three rows. In the second row, commercial ssDNA of BCL-2 (non-complementary to β-actin) was interacted in increasing amounts ((i) 0.18 µg, (ii) 0.37 µg and (iii) 0.74 µg) from left to right. In the third row, commercially obtained complementary ssDNA of β - actin was hybridized in increasing amounts ((i) 0.18 µg, (ii) 0.37 µg and (iii) 0.74 µg). The first row is left as control for only ssDNA. Following this, Au NCs were synthesized on all the spots using the thermocycler unit of the device. The membrane was then imaged using visualization unit (**Figure C4.3a**) and the spot intensities were analysed using the GUIs. The intensity analysis (**Figure C4.3b**) showed that the luminescence didn't enhance in the case of non-complementary interactions as it did with increasing concentrations of complementary (hybridized) dsDNA possibly due to washing away of the nonspecific ssDNA.

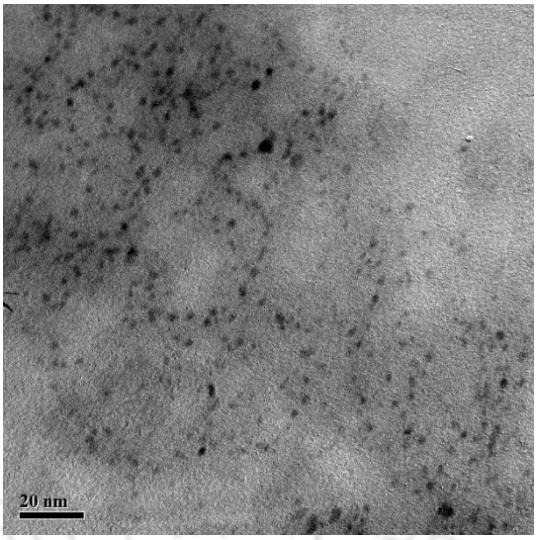

Figure C4.4. TEM image of Au NCs synthesized on DNA.

Comments on Figure C4.4

Au NCs were synthesized on DNA in liquid phase and were imaged with JEOL 2100 UHR-TEM operating at a maximum accelerating voltage of 200 kV). The formation of Au NCs on dsDNA is evident from the images.

C.2 | Experimental Procedures

Amplification of DNA with the device: β-actin gene was amplified for 35 cycles using specific primers in both the conventional PCR machine (Palm cycler) and the present device, keeping the conditions as initial denaturation at 95 ºC for 3 min followed by 35 cycles of three phases: 95 ºC for 30 sec, 55 ºC for 30 sec, 72 ºC for 1 min. After this, final extension was carried at 72 ºC for 10 min. The PCR amplicons obtained from both the devices were analysed using standard gel electrophoresis with EtBr staining. The stained gel was visualized under UV illumination as shown in **Figure 4.7a**. The amplification achieved by the present device was about 95 % compared to conventional PCR machine as analysed from the image.

Quantification of PCR products using Au NCs: Two sets of β - actin gene was amplified for 20, 25, 30, 35 cycles using specific primers by the thermocycler unit of the device with the conditions as initial denaturation at 95 ºC for 3 min followed by specific number of thermal cycles with each cycle as 95 ºC for 30 sec, 55 ºC for 30 sec, 72 ºC for 1 min and final extension for 10 min. In the first set, Au NCs were synthesized using the thermocycler with the following protocol. 1.0 mM $HAuCl_4$ and 0.01 M MPA were added in 3:1 (v/v) ratio to the end-point PCR product (inside the PCR tube itself) and was heated to 95 ºC for 2 min and then cooled to 15 ºC for 3 min. This resulted in the formation of Au NCs in proportion to the amplification. The final PCR tubes containing the PCR amplicons with synthesized Au NCs were then imaged and analysed using the visualization unit under UV excitation of 254 nm. Standard gel electrophoresis with Et Br staining is carried out for the second set of PCR amplicons. The gel was visualized under UV illumination.

Gene expression studies:

a) cDNA extraction from control HeLa cells and DOX treated HeLa cells

HeLa cancer cells were cultured in two 60 mm culture plates with cell density of 1 x 10^6 cells. Keeping one of the plates as control, the other plate was treated with anticancer drug DOX for 24 hr. Using standard RNA protocol, RNA was isolated from both the cells (control and treated). cDNA was obtained from mRNA using the thermocycler (42 ºC for 40 min, 95 ºC for 2 min) with Verso cDNA kit.

b) Amplification of specific genes using thermocycler unit of the device

BAX, BCL-2, Caspase 3 along with endogenous control β-actin were amplified using specific primers for 35 cycles (denaturation: 95 ºC for 3 min; 35 cycles with three phases: 95 ºC for 30 sec, 55 ºC for 30 sec, 72 ºC for 1 min and final extension for 10 min).

c) Immobilization of complementary oligonucleotide on nitrocellulose membrane

Nitrocellulose membrane (with maximum dimensions of 40mm x 40mm) was activated in 1X SSC (saline-sodium citrate) buffer and allowed to air dry. The commercial oligonucleotides were spotted and UV-cross linked in an array format by standard process.

d) Hybridisation of heat snap-cooled PCR products to the complementary oligonucleotides immobilized on nitrocellulose membrane

The PCR products were heated and snap cooled to obtain single stranded products and then were hybridized to their respective immobilized complementary nucleotides by the following process.

The membrane was blocked before hybridisation using blocking solution for 15 min to avoid unspecific binding. The hybridization was carried out in 5X SSC buffer, 10% polyethylene glycol (PEG) 6000 at 60 ºC for half an hour. The membrane was then washed with 1X SSC buffer.

e) Synthesis of Au NCs on hybridised membrane

After hybridisation, synthesis of Au NCs was carried out on the spots by adding 1.5 µL of 0.7 mM $HAuCl_4$ and 0.5 µL of 0.01 M MPA followed by heating the membrane using the thermocycler to 95 ºC for 2 min and then cooling it to 15 ºC for 3 min.

f) Image acquisition and analysis

The membrane with synthesized Au NCs was imaged and analysed using the visualization unit with GUIs under UV illumination (254 nm).

Primer sequences

Gene name	Sequence (5′ – 3′)
β-actin-F	5′CTGTCTGGCGGCACCACCAT3′
β-actin-R	5′GCAACTAAGTCATAGTCCGC3′
BCL2-F	5′AGATGTCCAGCCAGCTGCACCTGAC3′
BCL 2-R	5′AGATAGGCACCCAGGGTGATGCAAGCT3′
BAX-F	5′AAGCTGAGCGAGTGTCTCAAGCGC3′
BAX-R	5′TCCCGCCACAAAGATGGTCACG3′
Caspase3-F	5′TTTGTTTGTGTGCTTCTGAGCC3′
Caspase3-R	5′ATTCTGTTGCCACCTTTCGG3′

Table C4.1. Primers used for amplification of specific genes.

Gene sequences

Gene name	Sequence
β-actin-F	5′CACCATGGATGATGATATCGCCGCGCTCGTCGTCGACAACGGCTCC GGCATG TGCAAGGC3′
β-actin-FC	3′GTGGTACCTACTACTATAGCGGCGCGAGCAGCAGCTGTTGCCGAGGCCGTAC ACGTTCCG5′
BCL2-F	5′GCTTTTCCTCTGGGAAGGATGGCGCACGCTGGGAGAACAGGGTACGATAA3′
BCL2-FC	3′CGAAAAGGAGACCCTTCCTACCGCGTGCGACCCTCTTGTCCCATGCTATT5′
BAX-F	5′CGGCGGGAGCGGCGGTGATGGACGGGTCCGGGGAGCAGCCCAGA3′
BAX-FC	3′GCCGCCCTCGCCGCCACTACCTGCCCAGGCCCCTCGTCGGGTCT5′
Caspase3-F	5′AATAAAGGTATCCATGGAGAACACTGAAAACTCAGTGGATTCAAAAT3′
Caspase3-FC	3′TTATTTCCATAGGTACCTCTTGTGACTTTTGAGTCACCTAAGTTTTA5′

Table C4.2. Gene sequences used for array based analysis

Chapter 5

LED based Photodynamic Therapy and Colorimetric Assays on a Portable Device

ABSTRACT

A portable battery/AC powered device for carrying out photodynamic therapy (PDT) using silver nanorods (Ag NRs) as photosensitizers and for monitoring therapeutic success through optical detection is proposed. The device employs low power switchable LED (light emitting diode) arrays of specific wavelengths as light sources suitable for both PDT applications and detection purposes. Ag NRs were synthesized and their ability to act as photosensitizer to offer applications in PDT were explored. The effects of PDT on HeLa cells were studied using silver NRs only as photosensitizers and was also used in combination with doxorubicin for showcasing the potential for combinatorial photo-chemotherapy. The efficiency of the therapy was monitored through MTT (3-(4,5-dimethylthiazol-2-yl)-2,5-diphenyltetrazolium bromide) based cell viability and LDH based (lactate dehydrogenase) cell death monitoring assays using the device. The ability of the device to communicate wirelessly through a custom designed user application via android platform based smart devices makes it suitable for point-of-care diagnostics.

Cancer diagnosis, treatment and monitoring of its therapeutic success for a large populace has been limited due to several factors like inaccessibility of advanced facilities in remote locations, complex operation procedures, cost etc.[1] Besides these technical aspects, the failure rate of conventional chemotherapy based approaches due to relapse of cancer demands alternate routes of treatment. In recent times, combination therapy gained significant interest with promising developments to improve treatment efficiency.[2] In this respect, effective coupling of nascent techniques like photodynamic therapy (PDT) with prevailing chemotherapy could pave way for a proficient combinatorial therapy to combat cancer.[3] Herein, a multifunctional low cost portable device to achieve combinatorial cancer therapy and also to monitor its therapeutic efficacy through colorimetric assays is proposed for better management of cancer.

Amongst emerging techniques, PDT has shown huge potential and is a clinically approved technique which employs light in the biological window (600 nm to 900 nm) at specific irradiation/fluence rates in the presence of a photosensitizer and molecular oxygen to generate singlet oxygen responsible for killing cancer cells.[4-5] Traditionally used PDT photosensitizers suffers from issues like photo degradation, stability, solubility, low molar extinction coefficients, fixed wavelength excitation and in some cases inherent toxicity.[6] Nanomaterials, with unique photon dependent physical and chemical signatures, have proved to be significantly advantageous in PDT.

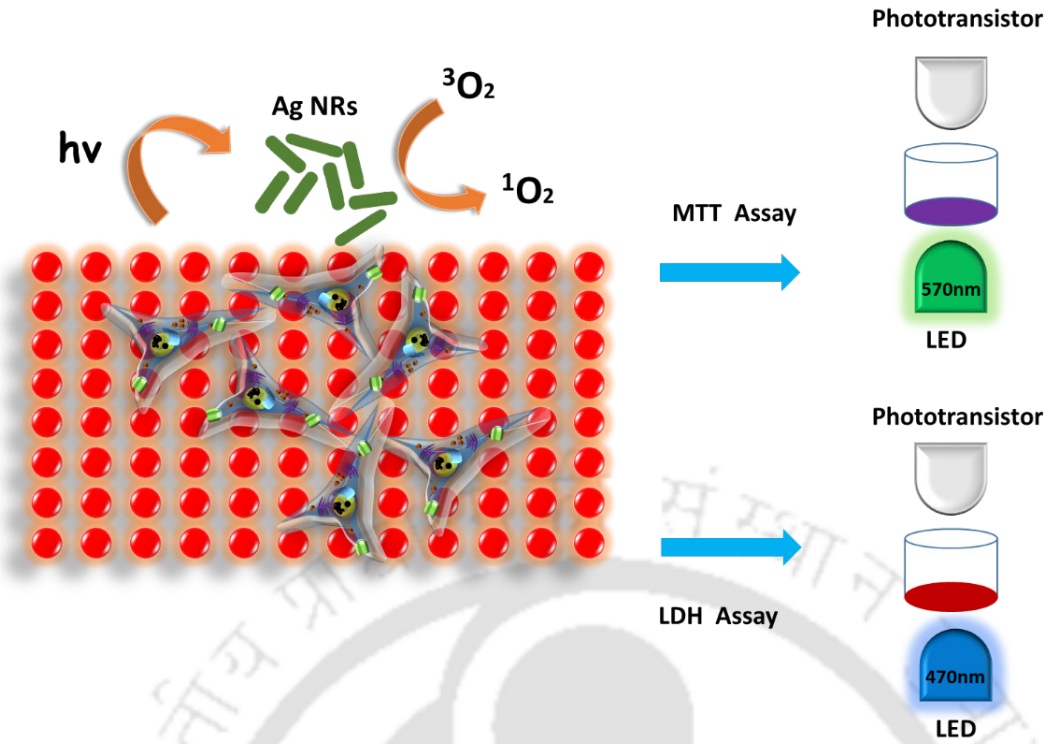

Figure 5.1. PDT therapy and colorimetric assay based detection using the device. The figure illustrates the generation of singlet oxygen using Ag NRs with low power LEDs. The therapeutic efficiency is monitored by using the transmission based assays with LEDs and phototransistors.

Several nanomaterials such as Au NRs, shells, nanocages, hexagons, QDs, carbon materials, Pd NPs etc., have been used in conjunction with commercial photosensitizers to enhance the efficacy of PDT.[7-8] Metal NPs in particular are promising in PDT due to their tunable optical extinction of light arising from localized surface plasmon resonance (LSPR). Also their high extinction coefficients are of immense significance when compared to organic photosensitizers. Although many nanomaterials were used in the past, they had been mostly operated in conjunction with photosensitizers to enhance the PDT. However, if the nanomaterial can itself generate the singlet oxygen for PDT, the need for separate photosensitizer can be avoided altogether. Recently, Au NPs, Ag NPs, Au NRs, Au nanoshells, Pt NPs etc., were shown to exhibit PDT potential by themselves without the need of any organic photosensitizers.[9-11] Very few works in this field have been reported and there lies enormous potential to develop novel materials which could act as photosensitizers to carry out PDT. Moreover, combinatorial therapy with PDT and chemotherapy can result in effective synergistic effects. The treatment can be more effective if the photosensitizer could also inherently generate toxicity for killing of cancer cells. This could result in significant reduction in doses of the individual therapeutic agents (including irradiation power) in comparison to their use when employed separately in the therapeutic regime. Ag nanomaterials have been of immense interest and are widely employed for antibacterial and cancer therapy. Among Ag nanomaterials, plasmonic Ag NRs with tunable LSPR is an interesting option for PDT alongside its inherent therapeutic properties. High power lasers and LEDs used for PDT would generally demand considerable amount of electrical power, heat sinks for long time operation. Sources like clinically relevant lower power LEDs are cost effective, easily

available, flexible, handy to use and would be well- suited for developing portable device.[12] Furthermore, these portable devices would be far more efficient if they could also monitor their success alongside therapy. Portable, low cost, microplate readers linked with smartphones have become a topic of research interest due to their extensive use in various biologically relevant clinical assays like ELISA, protein assays, bacterial OD measurements etc. This opened new avenues of using these plate readers as point of care diagnostic devices. In this respect, further integration of modules to also achieve therapy in these portable devices could result in significant multi-functional clinical health care devices.[13-14]

A portable battery/AC powered device capable of carrying out PDT and transmittance based detection is reported. The device employs low power switchable LED arrays of particular wavelength as the light source for PDT and detection purposes. The therapeutic effects of PDT on HeLa cells were studied using silver NRs only as photosensitizers and also in combination with drug doxorubicin (DOX). The efficiency of the therapy was monitored through MTT (3-(4,5-dimethylthiazol-2-yl)-2,5-diphenyltetrazolium bromide) and LDH (lactate dehydrogenase) assays using the device. The ability of the device to be operated wirelessly through a custom designed application via smartphone or PC/laptop makes it suitable for POC diagnostics. The theme of the work is schematically represented in **Figure 5.1**.

5.1 | Description of the Device

The design of the device allows the user to achieve both therapy and diagnosis of diseases on a single platform. The image of the device is shown in **Figure 5.2a**.

Modules of the device: The device has two major modules – illumination unit and the measuring unit as shown in **Figure 5.2b**.

Irradiation/Illumination unit: The bottom most level in the illumination unit constitutes the electronic circuitry and the switchable LED array. Above this level is the platform to support the 96 well plate (or) 6 well plate. The device is equipped with switchable LED arrays as those shown in **Figure 5.2c**. The modular design of the device adopts the provision for switching between LED arrays of different peak emission wavelength as per need. These LED arrays here serve two purposes – i.e., for irradiation (in PDT applications) and to provide specific wavelength of light for different assays in order to achieve transmission based detection. The device employs commercially available low power LEDs (rated 20 - 40 mA, 1.8 - 2.1V) as light sources for PDT. 96 no. of LEDs with same peak emission wavelength are patterned in an array format such that each LED irradiates a specific well in standard 96 well plate (or) cluster of LEDs irradiates 6 well plate. The LEDs illuminance can be tuned to fifteen different brightness levels. A plate holder is provided over the LEDs to support the 96 well plate or 6 well plate.

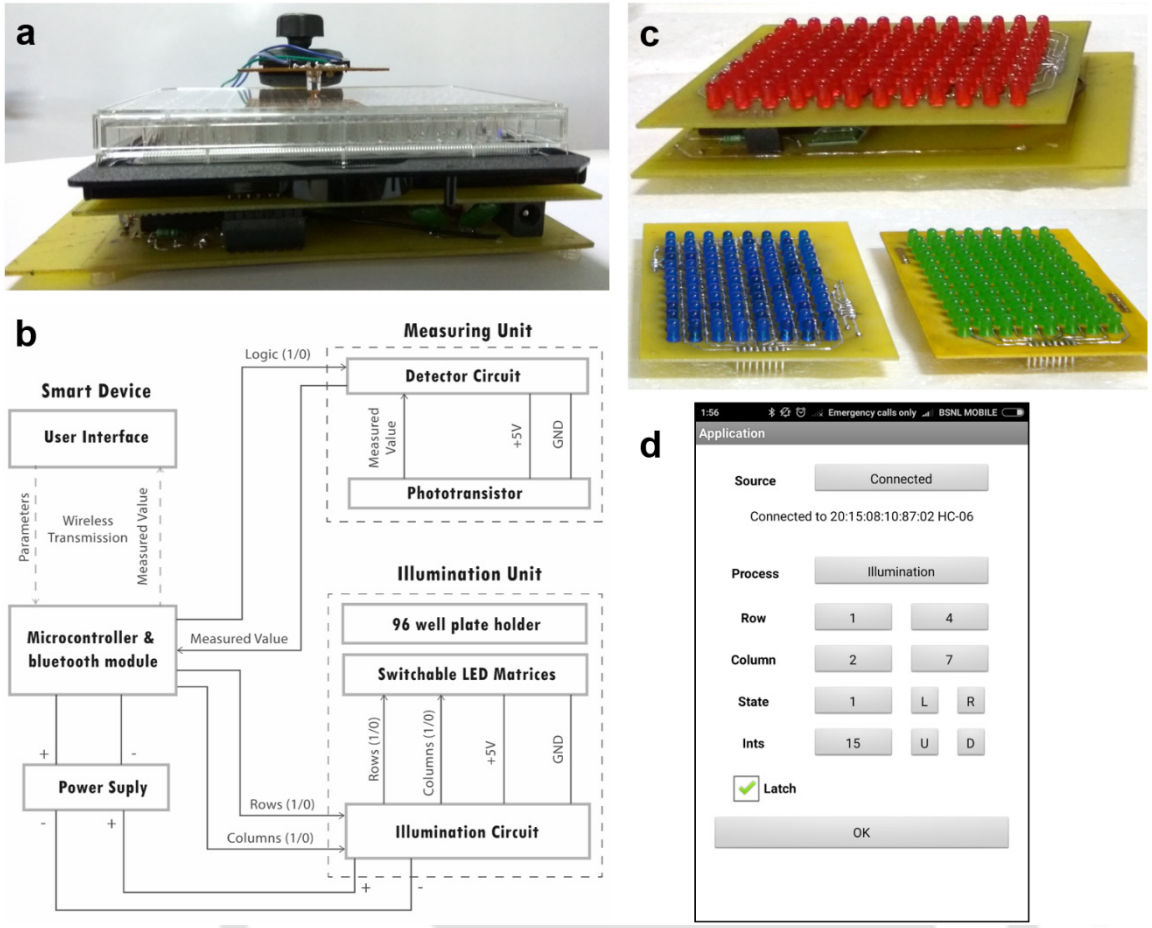

Figure 5.2. (a) Image of the device with electronic circuit at the bottom layer, 96 well plate in the middle and the phototransistor on the top. (b) Block diagram of the device with various interconnecting modules. (c) Switchable LEDs for PDT, MTT and LDH assays. (d) User interface to access the device wirelessly with smart devices.

Measuring unit: The measuring unit includes a phototransistor and the interfacing circuit. The LED from the array illuminates a single well (in a 96 well plate) at a given time. The phototransistor (inline and facing a particular LED in the array) measures the transmitted light from the underlying LED through the sample in the well plate. The circuit then converts this measured transmitted illuminance to corresponding voltage.

Electronic circuitry: The device is programmatically controlled using an electronic circuit interfaced to a microcontroller (ATMEGA 328P) as shown in **Figure 5.3**. The microcontroller drives the sequence of operations as instructed by the user through an application (Android based). The microcontroller receives/sends information to the user application wirelessly with the help of bluetooth module (HC-06). The LEDs in the device are arranged in rows and columns and are interfaced to the microcontroller using MAX7219 drivers. The MAX7219 ICs drive the LEDs (ON/OFF) as per the instructions from the microcontroller (which is instructed from the user application) and allows fast switching. The circuit in the measuring unit uses a phototransistor and the interfacing circuit to the microcontroller for electrical readout (in terms of voltage) of the

transmitted light. The whole circuit can be run from a 5V, 1A power supply (either battery or any other power source).

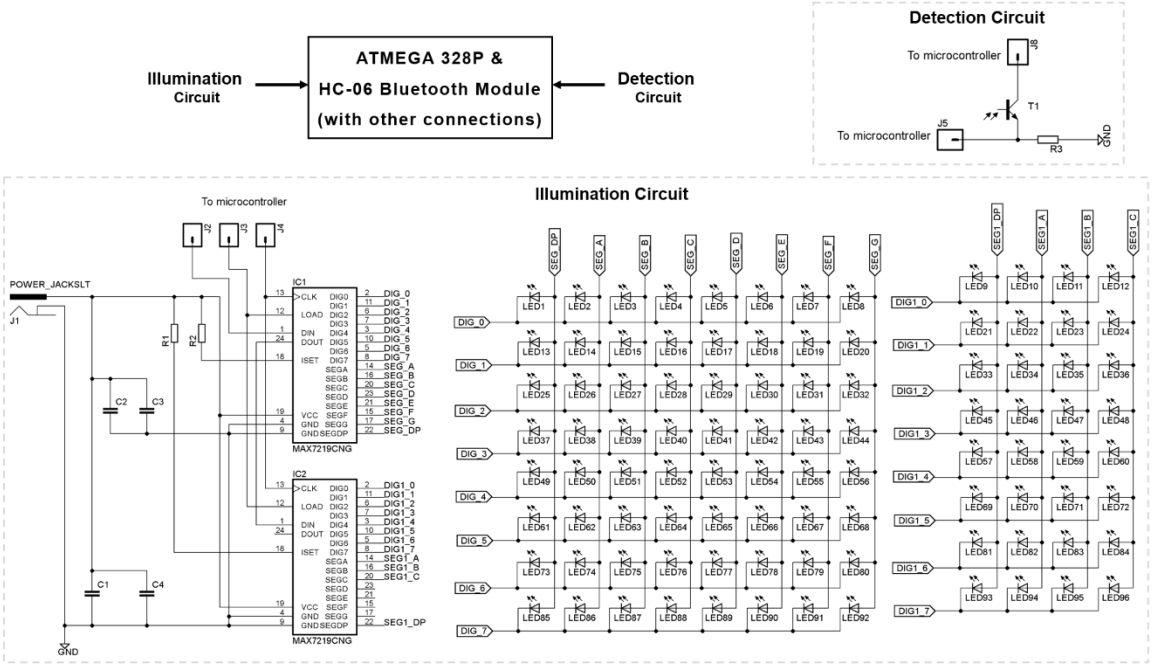

Figure 5.3. Schematic of the circuit used in the device.

Software application: A user application is developed as shown in **Figure 5.2d** to talk to the device wirelessly via android based smart devices without physically disturbing it. The application features the ability to select the process, i.e., either illumination for PDT or measure for transmission based detection. The application further allows selecting desired LEDs (single or multiple), their state (ON/OFF) and brightness levels. Easy access to subsequent rows and columns can be achieved using the L, R, U and D buttons for left, right, up and down directions. The application also allows to latch the previous state of LEDs when new parameters are selected.

Functional Correlation of the device: The simple design and construction, ease in carrying, low power operation (like portable battery) and ability to be accessed wirelessly make the device portable and be used even in remote locations. The modular approach adopted in device construction makes access to individual modules easy for repair and upgradation. With switchable LED arrays, the device allows achieving desired wavelength of illumination. This feature allowed the construction of the device to achieve both PDT and colorimetric based assays on a single platform. Multiple samples can be analyzed using the device. The user application simplifies the operation of the device allowing sending/receiving information wirelessly.

5.2 | Singlet Oxygen Generation with Ag NRs

For the application of Ag NRs as photosensitizers for PDT, their ability to generate singlet oxygen is to be determined. The as-synthesized Ag NRs (**see Appendix D, Synthesis and Characterization of Ag NRs**) exhibited strong absorbance at 630 nm (**Figure 5.4a**). To study singlet oxygen generation of Ag NRs, 1, 3 - diphenylizobenzofuran (DPBF) assay was performed.

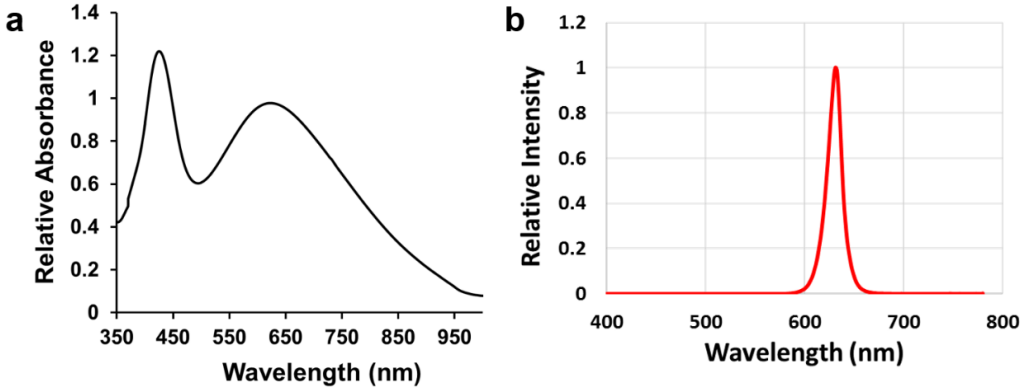

Figure 5.4. (a) Absorbance spectrum of the Ag NRs (relative to the absorbance at 630 nm). (b) Emission wavelength of the red LED used for PDT.

DPBF assay: The assay was performed on solution containing DPBF (in dimethyl sulfoxide, DMSO) along with Ag NRs which were kept in dark in a 96 well plate (**Appendix D, Experimental Procedures**). Another set containing only DPBF was kept as control. These solutions were irradiated for different intervals of time (0 to 6 min in steps of 1 min) using LED array of 632 nm (**Figure 5.4b**, 2000 lux). The luminescence of DPBF was recorded at 455 nm. It was observed that the luminescence quenched gradually with the progression of time in the presence of Ag NRs indication generation of singlet oxygen resulting in breakdown of DPBF as shown in **Figure 5.5**. However, noticeable decay in luminescence was not observed in the absence of Ag NRs.

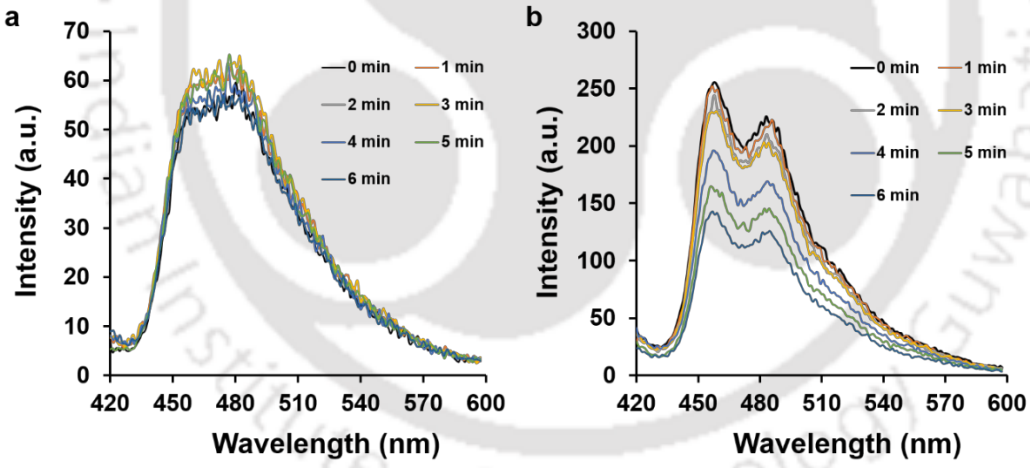

Figure 5.5. DPBF assay. Luminescence spectra of solution containing (a) only DPBF, (b) DPBF and Ag NRs irradiated with 630 nm light.

5.3 | Combinatorial Therapy with Ag NPs

The above results encouraged us to use Ag NRs for PDT in conjunction with chemotherapeutic drug DOX to achieve combinatorial therapy on HeLa cells. For this, HeLa cells were treated with the synthesized Ag NRs for 8 h and were irradiated with LED array of 632 nm wavelength (2000 lux, 30 min) to induce singlet oxygen generation. These cells were then treated sequentially with DOX after the irradiation and incubated for another 24 h. Other experimental sets for comparison of results include HeLa cells treated with only Ag NRs, only drug without irradiation (**Appendix D, Experimental Procedures**).

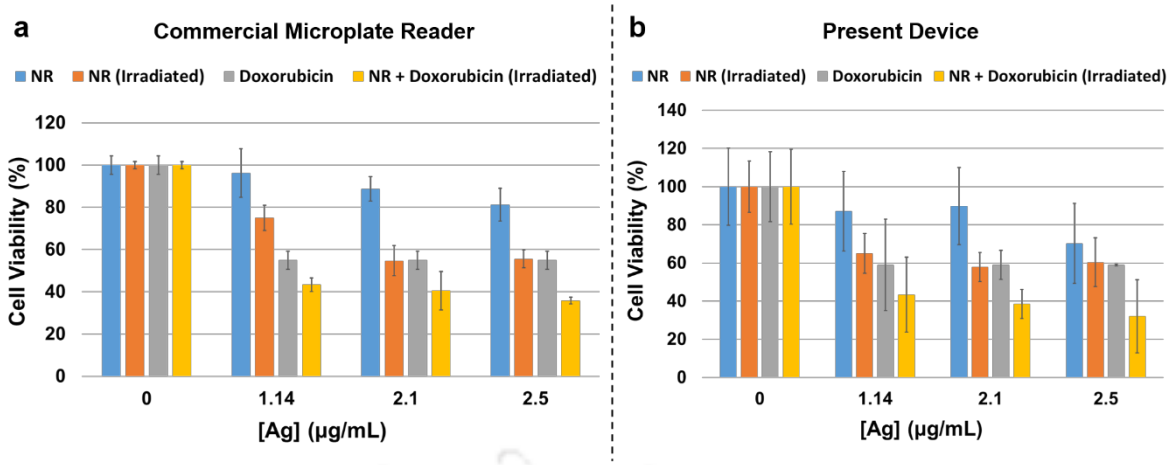

Figure 5.6. MTT assay. Cell viability studies of HeLa cells using (a) commercial microplate reader and (b) the present device. The MTT assay suggested that the combinatorial treatment with Ag NRs and DOX resulted in lower cell viability.

MTT assay for determining cell viability: MTT assay was performed to determine cell viability (**Appendix D, Experimental Procedures**). This was performed in the device by transmission based measurements of MTT assay by illuminating the samples with LED array of 570 nm peak wavelength and measuring with the photodetector. At a given time, a single well in the plate was illuminated with LED and the phototransistor perpendicular to the plane of well (and facing the LED) measured the transmitted light with and without the sample. The output voltage from the phototransistor corresponded to the illuminance. The absorbance value of the sample was calculated through programming in the microcontrollers using the following formula:

$$\textbf{Absorbance} = \log_{10}\left(\frac{\text{reading without sample in the well (blank)}}{\text{reading from sample in the well}}\right)$$

The cell viability was further calculated from the absorbance values using the below formula.

$$\textbf{\% of cell viability} = \left(\frac{\text{Absorbance}_{570\,\text{nm}} \text{ in treated sample}}{\text{Absorbance}_{570\,\text{nm}} \text{ in untreated sample}}\right) \times 100$$

The readings obtained from the machine were further validated by using a commercial microplate reader (TECAN infinite PRO) as shown in **Figure 5.6**, which indicated a good agreement with the values observed with the device. The cell viability assay revealed that around 80 % of the cells were viable at 2.5 µg/mL of Ag in case of the treatment with only Ag NRs without irradiation. However, the viability decreased to 55% in case of irradiated samples at the same dosage. The further decrease may be attributed to the singlet O_2 mediated cell death induced by Ag NRs under irradiation resulting in PDT. Thereafter, the viability of cells treated with DOX (8.3 µg/mL) and Ag NRs under irradiation showed about 43% viable cells at only 1.14 µg/mL of Ag. Whereas free DOX at same concentration marked a cell viability of 55%. The results from the MTT assay indicated that the cell viability in case of combinatorial therapy with Ag NRs and DOX was the least. The IC_{50} was achieved at lower

concentrations of Ag (1.14 µg/mL) and DOX (8.3 µg/mL) in comparison to the treatment with only Ag NRs or DOX at the same concentrations.

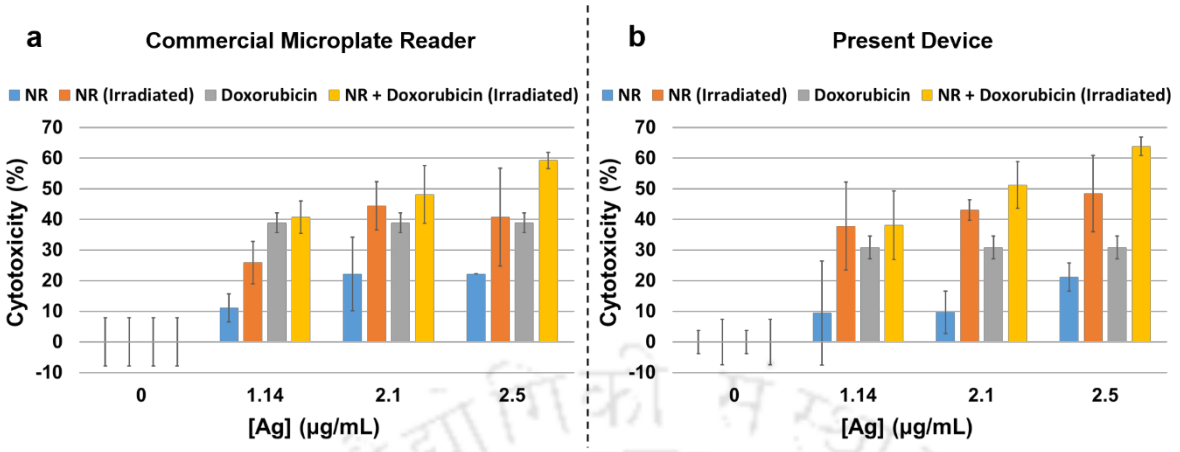

Figure 5.7. LDH assay. Cell death studies of HeLa cells using (a) commercial microplate reader and (b) the present device. The LDH assay suggested that the combinatorial treatment with Ag NRs and DOX resulted in increased cell death in comparison to treatment with Ag NR, DOX only.

LDH assay for determining cell death: Release of LDH enzyme in cell culture media was monitored to determine cytotoxicity using CytoTox 96 non-radioactive cytotoxicity assay kit (Roche Applied Science; **Appendix D, Experimental Procedures**). Transmission based measurements of LDH assay was performed as in MTT assay (mentioned above) by illuminating the samples with LED array of 470 nm peak wavelength and measured with phototransistor. The measured readings were validated by using a commercial microplate reader (TECAN infinite PRO) as shown in **Figure 5.7**. For positive control, cells were treated with 0.8 % (v/v) Triton x – 100 for 10 min whereas non treated cells formed the negative control. Only medium served as the background control.

$$\text{\% of cytotoxicity} = \left(\frac{\text{LDH release in treated cells} - \text{LDH release in negative control}}{\text{LDH release in positive control} - \text{LDH release in negative control}} \right) \times 100$$

The results from the device are in good agreement with the commercial reader. It was observed that the cell death was highest in the case of combinatorial therapy with Ag NRs and DOX (at same concentration of Ag and DOX). The LDH release from HeLa cells treated in combination with Ag NRs (irradiated) and DOX was significantly high in comparison to Ag NRs (dark) and DOX only, suggesting more effective cytotoxic nature of the combination therapy.

5.4 | Concluding Remarks

Ag NRs have been shown to act as photosensitizers and are capable of generating singlet oxygen under proper irradiation with low power LEDs. These Ag NRs in conjugation with chemotherapeutic drug DOX successfully induced combinatorial treatment resulting in cell death at very low doses of sample and irradiation in comparison to their individual contributions. The low power portable device was efficient in imparting PDT with Ag NRs and also in evaluating the therapeutic effects

through transmission based assays on a single platform. The present invention provides a scope for high throughput screening of multiple samples at a time. The switchable LED arrays makes the device more robust and use of desired array of particular wavelength for illumination at ease. Also, one could make custom LED matrices and embed into the device without affecting the underlying circuit. The custom designed software application that can be accessed on smartphones and laptops/PCs is simple in design and presents graphical information to execute the task. The ability of the device to be remotely accessed wirelessly enables to operate it from distant places and considering its portable nature and requirement of low power (such as portable battery) makes the device versatile and an important medical tool especially in remote geographical locations.

5.5 | References

1) J. Hempstead, D. P. Jones, A. Ziouche, et al., *Sci. Rep.* **2015**, *5*, 10093.
2) N. L. Komarova, C. R. Boland, *Nature* **2013**, *499*, 291.
3) M. Y. Nahabedian, R. A. Cohen, M. F. Contino, et al., *J. Natl. Cancer Inst.* **1988**, *80*, 739.
4) P. J. Muller, B. C. Wilson, *PMB* **1986**, *31*, 1295.
5) J.-L. Merlin, S. Azzi, D. Lignon, et al., *Eur. J. Cancer* **1992**, *28*, 1452.
6) T. Yogo, Y. Urano, Y. Ishitsuka, et al., *J. Am. Chem. Soc.* **2005**, *127*, 12162.
7) D. Hu, Z. Sheng, G. Gao, et al., *Biomaterials* **2016**, *93*, 10.
8) S. Wang, R. Gao, F. Zhou, et al., *J. Mater. Chem.* **2004**, *14*, 487.
9) G. Pasparakis, *Small* **2013**, *9*, 4130.
10) R. Vankayala, C. C. Lin, P. Kalluru, et al., *Biomaterials* **2014**, *35*, 5527.
11) R. Vankayala, Y. K. Huang, P. Kalluru, et al., *Small* **2014**, *10*, 1612.
12) A. Juzeniene, P. Juzenas, L. W. Ma, et al., *Lasers Med. Sci.* **2004**, *19*, 139.
13) L. Kwon, K. D. Long, Y. Wan, et al., *Biotechnol. Adv.* **2016**, *34*, 291.
14) B. Berg, B. Cortazar, D. Tseng, et al., *ACS Nano* **2015**, *9*, 7857.

Appendix D

D.1 | Synthesis and Characterization of Ag NRs

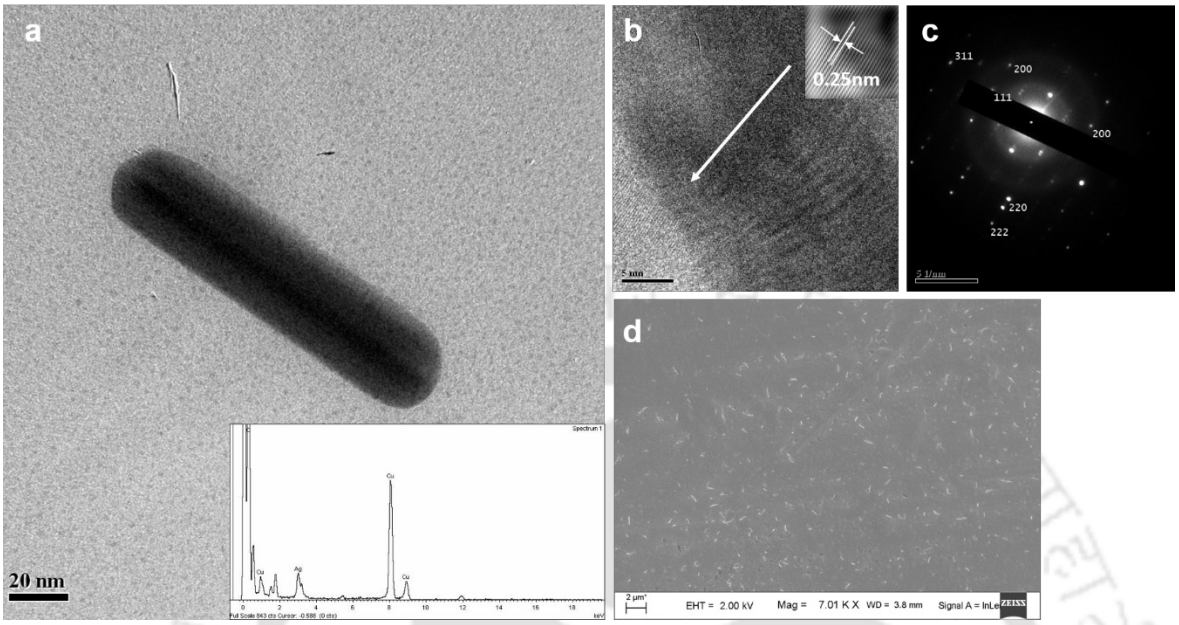

Figure D5.1. Electron microscopic analysis. **(a)** TEM images of Ag NRs. EDX analysis indicating the presence of Ag. **(b)** HRTEM images showing the lattice spacing of Ag NRs. **(c)** SAED analysis signifying the polycrystalline nature of Ag NRs with different lattice planes. **(d)** FESEM images showing the formation of Ag NRs.

Synthesis of Ag NRs: The synthesis of Ag NRs was achieved in two steps. The first step involved preparation of Ag seed solution. The was done by reducing 20 mL of 0.25 mM silver nitrate ($AgNO_3$) with ice cold 10 mM sodium borohydrate ($NaBH_4$) in the presence of 65 µL of tri-sodium citrate under vigorous stirring for 1 min. The resultant yellow coloured solution was left idle for 2 h before further use. The second step involved preparation of the growth solution. A mixture of 10 mL of 80 mM cetyl trimethylammonium bromide (CTAB), 500 µL of 100 mM ascorbic acid and 250 µL of 10 mM $AgNO_3$ was taken in a beaker and gentle mixed. To this, 60 µL of silver seed solution (as obtained from step 1), 100 µL of 1 M sodium hydroxide (NaOH) were added and gently shaken before leaving it undisturbed for the growth of Ag NRs. After 10 min, Ag NRs were formed as indicated by the initial visual appearance of green colour. Following this, excess amount of CTAB was removed by the following method. 3 mL of dichloromethane was added to 3 mL of hence prepared Ag NR solution and was shaken gently before it was left idle for a few minutes to achieve phase separation. The upper phase containing Ag NRs was transferred to fresh tubes and was then centrifuged at 6000 rpm for 30 min. Thereafter, the supernatant was removed and the pellet was washed, dissolved in water and centrifuged twice at 10000 rpm for 15 min. Finally, the pellet was dissolved in 1 mL of distilled water and was used for all further experiments.

Characterization of Ag NRs: Ag NRs exhibited strong absorbance at 630 nm due to LPSR which was evident from the UV - Vis spectroscopy measurements (performed using a JASCO V630

machine), as showed in **Figure D5.1**. TEM (JEOL 2100 UHR-TEM operating at a maximum accelerating voltage of 200 kV) analysis showed the formation of the Ag NR (**Figure D5.1a**). The aspect ratio of Ag NRs was found to be 4.3 ± 0.6 nm. The presence of silver was confirmed by EDX analysis as shown in **Figure D5.1a**. The HRTEM (**Figure D5.1b**) and the SAED (selected area electron diffraction, **Figure D5.1c**) analyses revealed the polycrystalline nature of the formed Ag NRs. FESEM (Zeiss - Sigma Advanced Analytical Microscopy) images (**Figure D5.1d**) also indicated the presence of Ag NRs with aspect ratio 4.67 ± 0.5 nm. The concentration of Ag was determined by atomic absorption spectroscopy (AAS) **(Figure D5.2).**

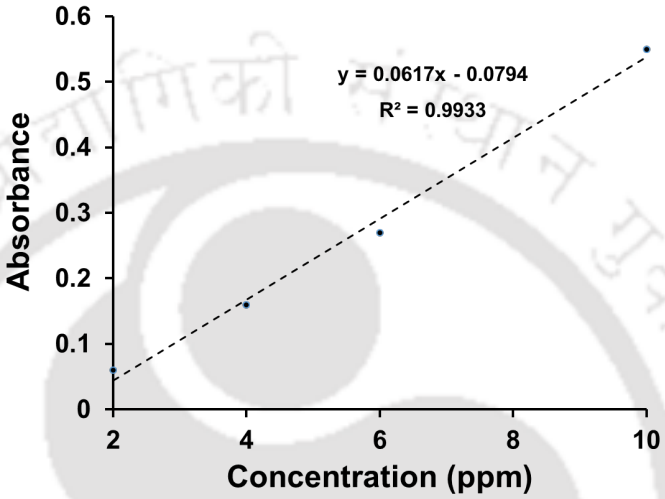

Figure D5.2. Standard calibration curve of Ag (standard) using AAS for measurement of Ag concentration.

D.2 | Experimental Procedures

DPBF singlet oxygen quenching experiment: A solution containing 100 µL of DPBF (0.08 mM) in DMSO and 100 µL of Ag NRs was prepared in dark in a 96 well plate. Another set containing only DPBF was kept as control. These solutions were irradiated for different intervals of time (0 to 7 min in steps of 1 min) using LED array of 630 nm (2000 lux). The luminescence of DPBF was recorded at 455 nm in Perkin-Elmer LS 55 fluorescence spectrometer.

Treatment of HeLa cells with Ag NRs and DOX: 5 x 10^3 cells (HeLa cells) were seeded in 96 well plate and was incubated for 24 h at 37 ºC in 5% CO_2. These cells were treated with the synthesized Ag NRs for 8 h and were then irradiated with LED array of 632 nm wavelength (for 30 min at 2000 lux) to induce singlet oxygen generation. For combination therapy, another set of cells were treated with the synthesized Ag NRs for 8 h and were irradiated with LED array of 632 nm wavelength. These cells were then treated with DOX and incubated for another 24 h. Control experiments without irradiation (in dark) were carried out by treating two individual set of cells with Ag NRs and DOX respectively.

MTT assay for determining cell viability: MTT assay was performed to determine cell viability. MTT, which is tetrazolium salt, was reduced into purple colored formazan by respiring mitochondria present in the live cells. In brief, 7.0 µL of MTT was added to each well of the microplate and was

left at 37 ºC for 1 h in 5% CO_2 incubator to form formazan. The medium was removed after 1 h of incubation and 70 µL of DMSO was added to each well for the development of purple color, which absorbs at 570 nm.

LDH assay for determining cell death: Release of LDH enzyme in cell culture media was monitored to determine cytotoxicity using CytoTox 96 non-radioactive cytotoxicity assay kit (Roche Applied Science). Aliquots of cell culture media were diluted with tetrazolium salt (INT) solution (substrate) in 1:1 ratio and incubated at 37 ºC for 30 min. As the reaction proceeded, INT was converted by released LDH to red formazan product.

D.3 | References

1) N. R. Jana, L. Gearheart, C. J. Murphy, *Chem. Commun.* **2001**, 617.

Chapter 6

Perspectives on the Future of Work

The dissertation presented a sect of device oriented approaches through utilization of the properties of nanoscale materials and technology. Particularly, surface and optical properties of nanomaterials were used to construct devices with on-board intelligence and with potential for healthcare.

Electrical energy was produced from autonomously moving composite bot. The periodicity, reproducibility of the motion and generation of electrical signal of sufficient magnitude for triggering applications indicate favourable prospects for the design of multifunctional autonomous microscopic bots. The idea further promotes the possible incorporation of low-voltage operating devices in autonomously moving electrically operative microbots. Synthetic autonomous bots could be developed with the ability to generate their own signal for running complex circuitry and communicate with each other through these electrical impulses.

The development of decision making systems in liquid media using biocompatible nanomaterials can be considered as important development in alternative computing. These systems could avoid many complications present in existing devices and are promising for contact-less and futuristic bionic devices. Intelligent synthetic static and mobile systems could be pursued. Further, systems responsive to various kinds of stimuli could be developed to offer application in diverse environments. One can conceive of light-induced or magnetic field induced local heating (in the presence of metal or magnetic NPs), introduction of acid/base and dissolved metal ions through microfluidic circuits for operation of logic structures.

Clinical devices for performing analytical techniques like RT-PCR, array based studies, colorimetric based assays and to achieve therapy like PDT were developed by employing optically active nanomaterials. Importantly, the techniques, methods and materials employed are bio and environmentally friendly, which may support efforts in incorporating such features in future devices. These devices inculcate the idea of developing new methods by modifying the conventional approach through amalgamation of emerging materials. This may lead to less complicated fabrication steps and provides opportunities to extend medical facilities to remote geographical locations. The modular approach in these devices gives way for easy upgradation. The software applications integrated to the device functionality may encourage to develop GUI based devices to make the experience user friendly alongside functionality. The ability of these devices to be remotely accessed enables to operate it in distant places and considering its portable nature and requirement of low power make them versatile and an important medical tool especially in remote places. This further encourages the motive to converge various techniques and develop methods in a view to make point-of-care devices available to a majority of people across the globe.

The inference from the current dissertation would be to highlight the importance of identifying the salient features of particular nanomaterials and to direct their utilization towards transforming technology. This may be through developing entirely new systems from the scratch or through effective alternations and modifications of existing techniques via conjugation of novel methods and materials. Finally, it is deemed that the works mentioned in this dissertation would encourage further efforts to engineer devices with low dimensional materials.

Publications and Patents

Publications

From Thesis Work:

1) S. K. Sailapu and A. Chattopadhyay. Induction of Electromotive Force by an Autonomously Moving Magnetic Bot. **Angew. Chem. Int. Ed. (2014)**, 53 (6), 1521-1524.
2) S. K. Sailapu, A. K. Sahoo, S. S. Ghosh and A. Chattopadhyay. Hierarchical Logic Structures Based on Responsive Fluorescent Gold Nanoclusters. **Small (2014)**, 10 (20), 4067-4071.
3) S. K. Sailapu, D. Dutta, A. K. Sahoo, S. S. Ghosh and A. Chattopadhyay. Luminescent Gold Nanocluster Probe based 'Bench Top Device (Methods)' for Gene and Protein Expression Analysis. (**Manuscript Under Preparation)**.
4) S. K. Sailapu, D. Dutta, A. T. Simon, S. S. Ghosh and A. Chattopadhyay. A Portable LED based Device for Photodynamic Therapy and Colorimetric Assay. (**Manuscript Under Preparation)**.

From Collaborations:

1) M. P. Sk,* S. K. Sailapu* and A. Chattopadhyay. Luminescent Carbon Dots for Logic Operations in Two Phases. **Chemphyschem (2015)**, 16 (4), 723-727. **(*Equal Contribution)**
2) A. K. Sahoo, S. K. Sailapu, S. Banerjee, S. S. Ghosh, A. Chattopadhyay. DNA-Templated Single Thermal Cycle Based Synthesis of Highly Luminescent Au Nanoclusters for Probing Gene Expression. **(Under revision).**

Patents

From Thesis Work:

1) Arun Chattopadhyay, Sunil Kumar Sailapu, Deepanjalee Dutta, Amaresh Kumar Sahoo, Siddhartha Sankar Ghosh. A device with integrated methods for reverse transcription polymerase chain reaction (RT-PCR) and/or dna/protein array based analyses. Indian Patent Application No.**1259/KOL/2015 A**
2) Arun Chattopadhyay, Sunil Kumar Sailapu, Deepanjalee Dutta, Amaresh Kumar Sahoo, Siddhartha Sankar Ghosh. A device with integrated methods for reverse transcription polymerase chain reaction (RT-PCR) and/or dna/protein array based analyses. International Patent Application No.**PCT/IN2016/000141**
3) Arun Chattopadhyay, Sunil Kumar Sailapu, Deepanjalee Dutta, Siddhartha Sankar Ghosh, Anitha T Simon. A portable device for LED based photodynamic therapy and colorimetric assay. **(Under preparation)**

Vitae

Sailapu Sunil Kumar received his Bachelor of engineering (B.E.) in Electronics and communication engineering (E.C.E) from Raghu Institute of Technology, Andhra University, Visakhapatnam. He started pursing research under the supervision of Prof. Arun Chattopadhyay at the Centre for Nanotechnology, IIT Guwahati – towards engineering devices with functional nanomaterials. His research interests include designing and development of devices with on-board intelligence and of clinical importance, by using the physical and chemical properties of nanomaterials.

Permissions

Figure 1.3

JOHN WILEY AND SONS LICENSE TERMS AND CONDITIONS

Sep 14, 2016

This Agreement between Sunil Kr Sailapu ("You") and John Wiley and Sons ("John Wiley and Sons") consists of your license details and the terms and conditions provided by John Wiley and Sons and Copyright Clearance Center.

License Number	3947800500391
License date	Sep 14, 2016
Licensed Content Publisher	John Wiley and Sons
Licensed Content Publication	Small
Licensed Content Title	Using Biological Inspiration to Engineer Functional Nanostructured Materials
Licensed Content Author	David W. Wendell,Jordan Patti,Carlo D. Montemagno
Licensed Content Date	Sep 15, 2006
Licensed Content Pages	6
Type of use	Dissertation/Thesis
Requestor type	University/Academic
Format	Print and electronic
Portion	Figure/table
Number of figures/tables	1
Original Wiley figure/table number(s)	Figure 4
Will you be translating?	No
Title of your thesis / dissertation	Engineering Devices with Functional Nanomaterials
Expected completion date	Sep 2016
Expected size (number of pages)	100
Requestor Location	Sunil Kr Sailapu Centre for Nanotechnology, IIT Guwahati, Assam, India Guwahati, Assam 781039 India Attn: Sunil Kr Sailapu
Publisher Tax ID	EU826007151
Billing Type	Invoice
Billing Address	Sunil Kr Sailapu Centre for Nanotechnology, IIT Guwahati, Assam, India Guwahati, India 781039 Attn: Sunil Kr Sailapu
Total	0.00 USD

ELSEVIER LICENSE TERMS AND CONDITIONS

Sep 14, 2016

This Agreement between Sunil Kr Sailapu ("You") and Elsevier ("Elsevier") consists of your license details and the terms and conditions provided by Elsevier and Copyright Clearance Center.

License Number	3947801128590
License date	Sep 14, 2016
Licensed Content Publisher	Elsevier
Licensed Content Publication	Cell
Licensed Content Title	The Molecular Motor Toolbox for Intracellular Transport
Licensed Content Author	Ronald D Vale
Licensed Content Date	21 February 2003
Licensed Content Volume Number	112
Licensed Content Issue Number	4
Licensed Content Pages	14
Start Page	467
End Page	480
Type of Use	reuse in a thesis/dissertation
Portion	figures/tables/illustrations
Number of figures/tables/illustrations	1
Format	both print and electronic
Are you the author of this Elsevier article?	No
Will you be translating?	No
Order reference number	
Original figure numbers	Figure 2
Title of your thesis/dissertation	Engineering Devices with Functional Nanomaterials
Expected completion date	Sep 2016
Estimated size (number of pages)	100
Elsevier VAT number	GB 494 6272 12
Requestor Location	Sunil Kr Sailapu Centre for Nanotechnology, IIT Guwahati, Assam, India Guwahati, Assam 781039 India Attn: Sunil Kr Sailapu
Total	0.00 USD

Figure 1.4

Copyright Clearance Center RightsLink® Home Create Account Help

ACS Publications Most Trusted. Most Cited. Most Read.

Title: Stretching and Transporting DNA Molecules Using Motor Proteins
Author: Stefan Diez, Cordula Reuther, Cerasela Dinu, et al
Publication: Nano Letters
Publisher: American Chemical Society
Date: Sep 1, 2003
Copyright © 2003, American Chemical Society

LOGIN
If you're a copyright.com user, you can login to RightsLink using your copyright.com credentials. Already a RightsLink user or want to learn more?

PERMISSION/LICENSE IS GRANTED FOR YOUR ORDER AT NO CHARGE

This type of permission/license, instead of the standard Terms & Conditions, is sent to you because no fee is being charged for your order. Please note the following:

- Permission is granted for your request in both print and electronic formats, and translations.
- If figures and/or tables were requested, they may be adapted or used in part.
- Please print this page for your records and send a copy of it to your publisher/graduate school.
- Appropriate credit for the requested material should be given as follows: "Reprinted (adapted) with permission from (COMPLETE REFERENCE CITATION). Copyright (YEAR) American Chemical Society." Insert appropriate information in place of the capitalized words.
- One-time permission is granted only for the use specified in your request. No additional uses are granted (such as derivative works or other editions). For any other uses, please submit a new request.

If credit is given to another source for the material you requested, permission must be obtained from that source.

BACK CLOSE WINDOW

Figure 1.5

RightsLink Printable License

JOHN WILEY AND SONS LICENSE TERMS AND CONDITIONS

Sep 17, 2016

This Agreement between Sunil Kr Sailapu ("You") and John Wiley and Sons ("John Wiley and Sons") consists of your license details and the terms and conditions provided by John Wiley and Sons and Copyright Clearance Center.

License Number	3951290178099
License date	Sep 17, 2016
Licensed Content Publisher	John Wiley and Sons
Licensed Content Publication	Angewandte Chemie International Edition
Licensed Content Title	Fantastic Voyage: Designing Self-Powered Nanorobots
Licensed Content Author	Samudra Sengupta,Michael E. Ibele,Ayusman Sen
Licensed Content Date	Aug 9, 2012
Licensed Content Pages	12
Type of use	Dissertation/Thesis
Requestor type	University/Academic
Format	Print and electronic
Portion	Figure/table
Number of figures/tables	1
Original Wiley figure/table number(s)	Figure 4
Will you be translating?	No
Title of your thesis / dissertation	Engineering Devices with Functional Nanomaterials
Expected completion date	Sep 2016
Expected size (number of pages)	100
Requestor Location	Sunil Kr Sailapu Centre for Nanotechnology, IIT Guwahati, Assam, India Guwahati, Assam 781039 India Attn: Sunil Kr Sailapu
Publisher Tax ID	EU826007151
Billing Type	Invoice
Billing Address	Sunil Kr Sailapu Centre for Nanotechnology, IIT Guwahati, Assam, India Guwahati, India 781039 Attn: Sunil Kr Sailapu
Total	0.00 USD

Copyright Clearance Center RightsLink® Home Create Account Help

ACS Publications Most Trusted. Most Cited. Most Read.

Title: Autonomous Nanomotor Based on Copper–Platinum Segmented Nanobattery
Author: Ran Liu, Ayusman Sen
Publication: Journal of the American Chemical Society
Publisher: American Chemical Society
Date: Dec 1, 2011
Copyright © 2011, American Chemical Society

LOGIN
If you're a copyright.com user, you can login to RightsLink using your copyright.com credentials. Already a RightsLink user or want to learn more?

PERMISSION/LICENSE IS GRANTED FOR YOUR ORDER AT NO CHARGE

This type of permission/license, instead of the standard Terms & Conditions, is sent to you because no fee is being charged for your order. Please note the following:

- Permission is granted for your request in both print and electronic formats, and translations.
- If figures and/or tables were requested, they may be adapted or used in part.
- Please print this page for your records and send a copy of it to your publisher/graduate school.
- Appropriate credit for the requested material should be given as follows: "Reprinted (adapted) with permission from (COMPLETE REFERENCE CITATION). Copyright (YEAR) American Chemical Society." Insert appropriate information in place of the capitalized words.
- One-time permission is granted only for the use specified in your request. No additional uses are granted (such as derivative works or other editions). For any other uses, please submit a new request.

If credit is given to another source for the material you requested, permission must be obtained from that source.

BACK CLOSE WINDOW

Copyright © 2016 Copyright Clearance Center, Inc. All Rights Reserved. Privacy statement. Terms and Conditions. Comments? We would like to hear from you. E-mail us at customercare@copyright.com

Copyright Clearance Center RightsLink® Home Create Account Help

ACS Publications Most Trusted. Most Cited. Most Read.

Title: Carbon-Nanotube-Induced Acceleration of Catalytic Nanomotors
Author: Rawiwan Laocharoensuk, Jared Burdick, Joseph Wang
Publication: ACS Nano
Publisher: American Chemical Society
Date: May 1, 2008
Copyright © 2008, American Chemical Society

LOGIN
If you're a copyright.com user, you can login to RightsLink using your copyright.com credentials. Already a RightsLink user or want to learn more?

PERMISSION/LICENSE IS GRANTED FOR YOUR ORDER AT NO CHARGE

This type of permission/license, instead of the standard Terms & Conditions, is sent to you because no fee is being charged for your order. Please note the following:

- Permission is granted for your request in both print and electronic formats, and translations.
- If figures and/or tables were requested, they may be adapted or used in part.
- Please print this page for your records and send a copy of it to your publisher/graduate school.
- Appropriate credit for the requested material should be given as follows: "Reprinted (adapted) with permission from (COMPLETE REFERENCE CITATION). Copyright (YEAR) American Chemical Society." Insert appropriate information in place of the capitalized words.
- One-time permission is granted only for the use specified in your request. No additional uses are granted (such as derivative works or other editions). For any other uses, please submit a new request.

If credit is given to another source for the material you requested, permission must be obtained from that source.

BACK CLOSE WINDOW

Copyright © 2016 Copyright Clearance Center, Inc. All Rights Reserved. Privacy statement. Terms and Conditions. Comments? We would like to hear from you. E-mail us at customercare@copyright.com

Copyright Clearance Center RightsLink® Home Create Account Help

ACS Publications Most Trusted. Most Cited. Most Read.

Title: Enhanced Transport into and out of Dead-End Pores
Author: Abhishek Kar, Tso-Yi Chiang, Isamar Ortiz Rivera, et al
Publication: ACS Nano
Publisher: American Chemical Society
Date: Jan 1, 2015
Copyright © 2015, American Chemical Society

LOGIN
If you're a copyright.com user, you can login to RightsLink using your copyright.com credentials. Already a RightsLink user or want to learn more?

PERMISSION/LICENSE IS GRANTED FOR YOUR ORDER AT NO CHARGE

This type of permission/license, instead of the standard Terms & Conditions, is sent to you because no fee is being charged for your order. Please note the following:

- Permission is granted for your request in both print and electronic formats, and translations.
- If figures and/or tables were requested, they may be adapted or used in part.
- Please print this page for your records and send a copy of it to your publisher/graduate school.
- Appropriate credit for the requested material should be given as follows: "Reprinted (adapted) with permission from (COMPLETE REFERENCE CITATION). Copyright (YEAR) American Chemical Society." Insert appropriate information in place of the capitalized words.
- One-time permission is granted only for the use specified in your request. No additional uses are granted (such as derivative works or other editions). For any other uses, please submit a new request.

If credit is given to another source for the material you requested, permission must be obtained from that source.

BACK CLOSE WINDOW

Copyright © 2016 Copyright Clearance Center, Inc. All Rights Reserved. Privacy statement. Terms and Conditions. Comments? We would like to hear from you. E-mail us at customercare@copyright.com

Figure 1.6

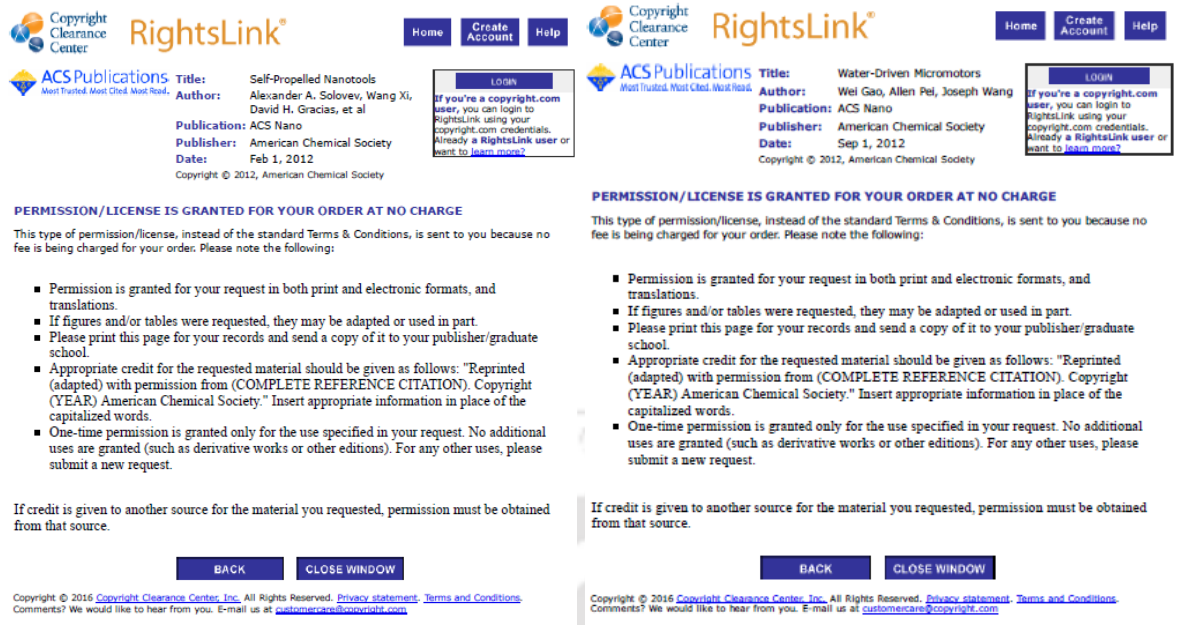

Copyright Clearance Center RightsLink®

Home | Create Account | Help

ACS Publications — Most Trusted. Most Cited. Most Read.

Title: Self-Propelled Nanotools
Author: Alexander A. Solovev, Wang Xi, David H. Gracias, et al
Publication: ACS Nano
Publisher: American Chemical Society
Date: Feb 1, 2012
Copyright © 2012, American Chemical Society

LOGIN
If you're a copyright.com user, you can login to RightsLink using your copyright.com credentials. Already a RightsLink user or want to learn more?

PERMISSION/LICENSE IS GRANTED FOR YOUR ORDER AT NO CHARGE

This type of permission/license, instead of the standard Terms & Conditions, is sent to you because no fee is being charged for your order. Please note the following:

- Permission is granted for your request in both print and electronic formats, and translations.
- If figures and/or tables were requested, they may be adapted or used in part.
- Please print this page for your records and send a copy of it to your publisher/graduate school.
- Appropriate credit for the requested material should be given as follows: "Reprinted (adapted) with permission from (COMPLETE REFERENCE CITATION). Copyright (YEAR) American Chemical Society." Insert appropriate information in place of the capitalized words.
- One-time permission is granted only for the use specified in your request. No additional uses are granted (such as derivative works or other editions). For any other uses, please submit a new request.

If credit is given to another source for the material you requested, permission must be obtained from that source.

BACK | CLOSE WINDOW

Copyright © 2016 Copyright Clearance Center, Inc. All Rights Reserved. Privacy statement. Terms and Conditions.
Comments? We would like to hear from you. E-mail us at customercare@copyright.com

Copyright Clearance Center RightsLink®

Home | Create Account | Help

ACS Publications — Most Trusted. Most Cited. Most Read.

Title: Water-Driven Micromotors
Author: Wei Gao, Allen Pei, Joseph Wang
Publication: ACS Nano
Publisher: American Chemical Society
Date: Sep 1, 2012
Copyright © 2012, American Chemical Society

LOGIN
If you're a copyright.com user, you can login to RightsLink using your copyright.com credentials. Already a RightsLink user or want to learn more?

PERMISSION/LICENSE IS GRANTED FOR YOUR ORDER AT NO CHARGE

This type of permission/license, instead of the standard Terms & Conditions, is sent to you because no fee is being charged for your order. Please note the following:

- Permission is granted for your request in both print and electronic formats, and translations.
- If figures and/or tables were requested, they may be adapted or used in part.
- Please print this page for your records and send a copy of it to your publisher/graduate school.
- Appropriate credit for the requested material should be given as follows: "Reprinted (adapted) with permission from (COMPLETE REFERENCE CITATION). Copyright (YEAR) American Chemical Society." Insert appropriate information in place of the capitalized words.
- One-time permission is granted only for the use specified in your request. No additional uses are granted (such as derivative works or other editions). For any other uses, please submit a new request.

If credit is given to another source for the material you requested, permission must be obtained from that source.

BACK | CLOSE WINDOW

Copyright © 2016 Copyright Clearance Center, Inc. All Rights Reserved. Privacy statement. Terms and Conditions.
Comments? We would like to hear from you. E-mail us at customercare@copyright.com

ROYAL SOCIETY OF CHEMISTRY LICENSE TERMS AND CONDITIONS

Sep 14, 2016

This Agreement between Sunil Kr Sailapu ("You") and Royal Society of Chemistry ("Royal Society of Chemistry") consists of your license details and the terms and conditions provided by Royal Society of Chemistry and Copyright Clearance Center.

License Number	3947811313512
License date	Sep 14, 2016
Licensed Content Publisher	Royal Society of Chemistry
Licensed Content Publication	Nanoscale
Licensed Content Title	Seawater-driven magnesium based Janus micromotors for environmental remediation
Licensed Content Author	Wei Gao,Xiaomiao Feng,Allen Pei,Yonge Gu,Jinxing Li,Joseph Wang
Licensed Content Date	Apr 26, 2013
Licensed Content Volume Number	5
Licensed Content Issue Number	11
Type of Use	Thesis/Dissertation
Requestor type	academic/educational
Portion	figures/tables/images
Number of figures/tables/images	1
Format	print and electronic
Distribution quantity	10
Will you be translating?	no
Order reference number	
Title of the thesis/dissertation	Engineering Devices with Functional Nanomaterials
Expected completion date	Sep 2016
Estimated size	100
Requestor Location	Sunil Kr Sailapu Centre for Nanotechnology, IIT Guwahati, Assam, India Guwahati, Assam 781039 India Attn: Sunil Kr Sailapu
Billing Type	Invoice
Billing Address	Sunil Kr Sailapu Centre for Nanotechnology, IIT Guwahati, Assam, India Guwahati, India 781039 Attn: Sunil Kr Sailapu
Total	0.00 USD

Figure 1.7

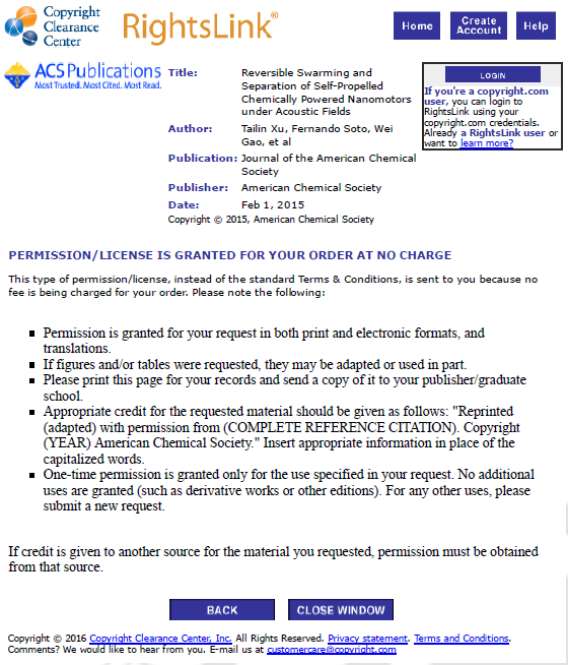

Copyright Clearance Center RightsLink®

Home | Create Account | Help

ACS Publications — Most Trusted. Most Cited. Most Read.

Title: Reversible Swarming and Separation of Self-Propelled Chemically Powered Nanomotors under Acoustic Fields

Author: Tailin Xu, Fernando Soto, Wei Gao, et al

Publication: Journal of the American Chemical Society

Publisher: American Chemical Society

Date: Feb 1, 2015

Copyright © 2015, American Chemical Society

LOGIN

If you're a copyright.com user, you can login to RightsLink using your copyright.com credentials. Already a RightsLink user or want to learn more?

PERMISSION/LICENSE IS GRANTED FOR YOUR ORDER AT NO CHARGE

This type of permission/license, instead of the standard Terms & Conditions, is sent to you because no fee is being charged for your order. Please note the following:

- Permission is granted for your request in both print and electronic formats, and translations.
- If figures and/or tables were requested, they may be adapted or used in part.
- Please print this page for your records and send a copy of it to your publisher/graduate school.
- Appropriate credit for the requested material should be given as follows: "Reprinted (adapted) with permission from (COMPLETE REFERENCE CITATION). Copyright (YEAR) American Chemical Society." Insert appropriate information in place of the capitalized words.
- One-time permission is granted only for the use specified in your request. No additional uses are granted (such as derivative works or other editions). For any other uses, please submit a new request.

If credit is given to another source for the material you requested, permission must be obtained from that source.

BACK | CLOSE WINDOW

Copyright © 2016 Copyright Clearance Center, Inc. All Rights Reserved. Privacy statement. Terms and Conditions. Comments? We would like to hear from you. E-mail us at customercare@copyright.com

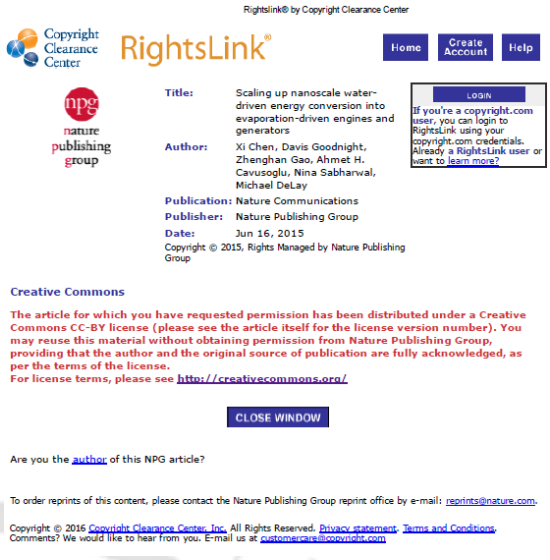

RightsLink® by Copyright Clearance Center

Copyright Clearance Center RightsLink®

Home | Create Account | Help

nature publishing group

Title: Scaling up nanoscale water-driven energy conversion into evaporation-driven engines and generators

Author: Xi Chen, Davis Goodnight, Zhenghan Gao, Ahmet H. Cavusoglu, Nina Sabharwal, Michael DeLay

Publication: Nature Communications

Publisher: Nature Publishing Group

Date: Jun 16, 2015

Copyright © 2015, Rights Managed by Nature Publishing Group

LOGIN

If you're a copyright.com user, you can login to RightsLink using your copyright.com credentials. Already a RightsLink user or want to learn more?

Creative Commons

The article for which you have requested permission has been distributed under a Creative Commons CC-BY license (please see the article itself for the license version number). You may reuse this material without obtaining permission from Nature Publishing Group, providing that the author and the original source of publication are fully acknowledged, as per the terms of the license.
For license terms, please see http://creativecommons.org/

CLOSE WINDOW

Are you the author of this NPG article?

To order reprints of this content, please contact the Nature Publishing Group reprint office by e-mail: reprints@nature.com.

Copyright © 2016 Copyright Clearance Center, Inc. All Rights Reserved. Privacy statement. Terms and Conditions. Comments? We would like to hear from you. E-mail us at customercare@copyright.com

RightsLink Printable License

JOHN WILEY AND SONS LICENSE TERMS AND CONDITIONS

Sep 17, 2016

This Agreement between Sunil Kr Sailapu ("You") and John Wiley and Sons ("John Wiley and Sons") consists of your license details and the terms and conditions provided by John Wiley and Sons and Copyright Clearance Center.

License Number	3951211246453
License date	Sep 17, 2016
Licensed Content Publisher	John Wiley and Sons
Licensed Content Publication	Angewandte Chemie International Edition
Licensed Content Title	Chemotactic Behavior of Catalytic Motors in Microfluidic Channels
Licensed Content Author	Larysa Baraban,Stefan M. Harazim,Samuel Sanchez,Oliver G. Schmidt
Licensed Content Date	Apr 24, 2013
Licensed Content Pages	5
Type of use	Dissertation/Thesis
Requestor type	University/Academic
Format	Print and electronic
Portion	Figure/table
Number of figures/tables	1
Original Wiley figure/table number(s)	Figure 1
Will you be translating?	No
Title of your thesis / dissertation	Engineering Devices with Functional Nanomaterials
Expected completion date	Sep 2016
Expected size (number of pages)	100
Requestor Location	Sunil Kr Sailapu Centre for Nanotechnology, IIT Guwahati, Assam, India Guwahati, Assam 781039 India Attn: Sunil Kr Sailapu
Publisher Tax ID	EU826007151
Billing Type	Invoice
Billing Address	Sunil Kr Sailapu Centre for Nanotechnology, IIT Guwahati, Assam, India Guwahati, India 781039 Attn: Sunil Kr Sailapu
Total	0.00 USD

Figure 1.8

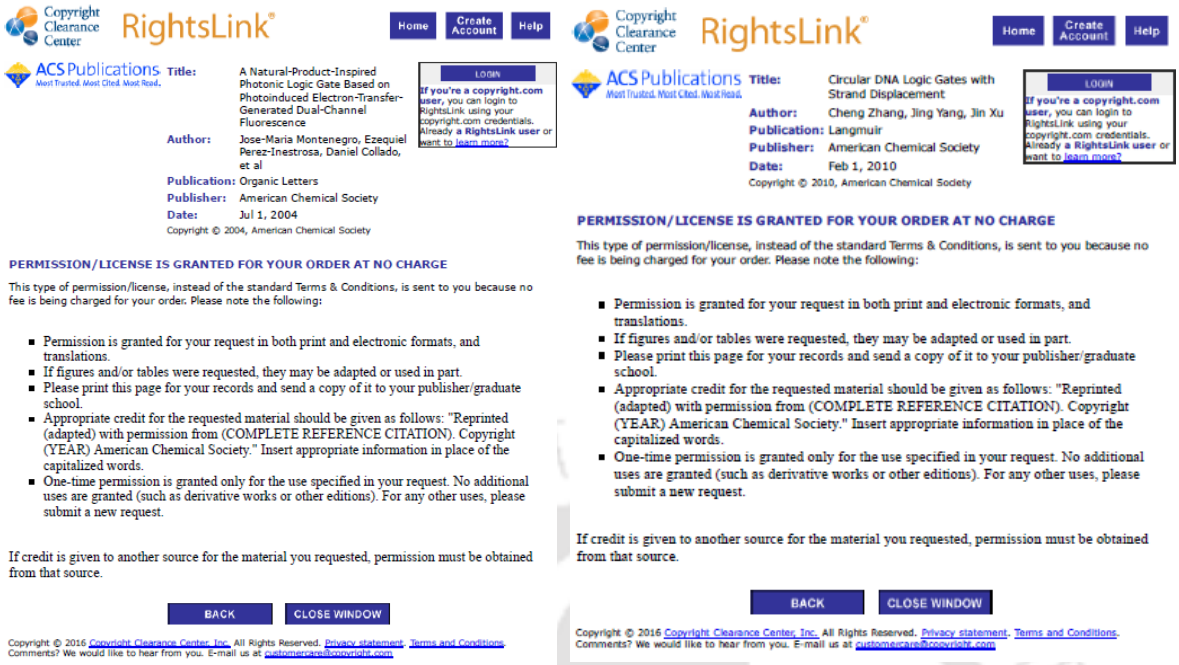

Copyright Clearance Center RightsLink®

Home | Create Account | Help

ACS Publications
Most Trusted. Most Cited. Most Read.

Title: A Natural-Product-Inspired Photonic Logic Gate Based on Photoinduced Electron-Transfer-Generated Dual-Channel Fluorescence
Author: Jose-Maria Montenegro, Ezequiel Perez-Inestrosa, Daniel Collado, et al
Publication: Organic Letters
Publisher: American Chemical Society
Date: Jul 1, 2004
Copyright © 2004, American Chemical Society

LOGIN
If you're a copyright.com user, you can login to RightsLink using your copyright.com credentials. Already a RightsLink user or want to learn more?

PERMISSION/LICENSE IS GRANTED FOR YOUR ORDER AT NO CHARGE

This type of permission/license, instead of the standard Terms & Conditions, is sent to you because no fee is being charged for your order. Please note the following:

- Permission is granted for your request in both print and electronic formats, and translations.
- If figures and/or tables were requested, they may be adapted or used in part.
- Please print this page for your records and send a copy of it to your publisher/graduate school.
- Appropriate credit for the requested material should be given as follows: "Reprinted (adapted) with permission from (COMPLETE REFERENCE CITATION). Copyright (YEAR) American Chemical Society." Insert appropriate information in place of the capitalized words.
- One-time permission is granted only for the use specified in your request. No additional uses are granted (such as derivative works or other editions). For any other uses, please submit a new request.

If credit is given to another source for the material you requested, permission must be obtained from that source.

BACK | CLOSE WINDOW

Copyright © 2016 Copyright Clearance Center, Inc. All Rights Reserved. Privacy statement. Terms and Conditions.
Comments? We would like to hear from you. E-mail us at customercare@copyright.com

Copyright Clearance Center RightsLink®

Home | Create Account | Help

ACS Publications
Most Trusted. Most Cited. Most Read.

Title: Circular DNA Logic Gates with Strand Displacement
Author: Cheng Zhang, Jing Yang, Jin Xu
Publication: Langmuir
Publisher: American Chemical Society
Date: Feb 1, 2010
Copyright © 2010, American Chemical Society

LOGIN
If you're a copyright.com user, you can login to RightsLink using your copyright.com credentials. Already a RightsLink user or want to learn more?

PERMISSION/LICENSE IS GRANTED FOR YOUR ORDER AT NO CHARGE

This type of permission/license, instead of the standard Terms & Conditions, is sent to you because no fee is being charged for your order. Please note the following:

- Permission is granted for your request in both print and electronic formats, and translations.
- If figures and/or tables were requested, they may be adapted or used in part.
- Please print this page for your records and send a copy of it to your publisher/graduate school.
- Appropriate credit for the requested material should be given as follows: "Reprinted (adapted) with permission from (COMPLETE REFERENCE CITATION). Copyright (YEAR) American Chemical Society." Insert appropriate information in place of the capitalized words.
- One-time permission is granted only for the use specified in your request. No additional uses are granted (such as derivative works or other editions). For any other uses, please submit a new request.

If credit is given to another source for the material you requested, permission must be obtained from that source.

BACK | CLOSE WINDOW

Copyright © 2016 Copyright Clearance Center, Inc. All Rights Reserved. Privacy statement. Terms and Conditions.
Comments? We would like to hear from you. E-mail us at customercare@copyright.com

Figure 1.9

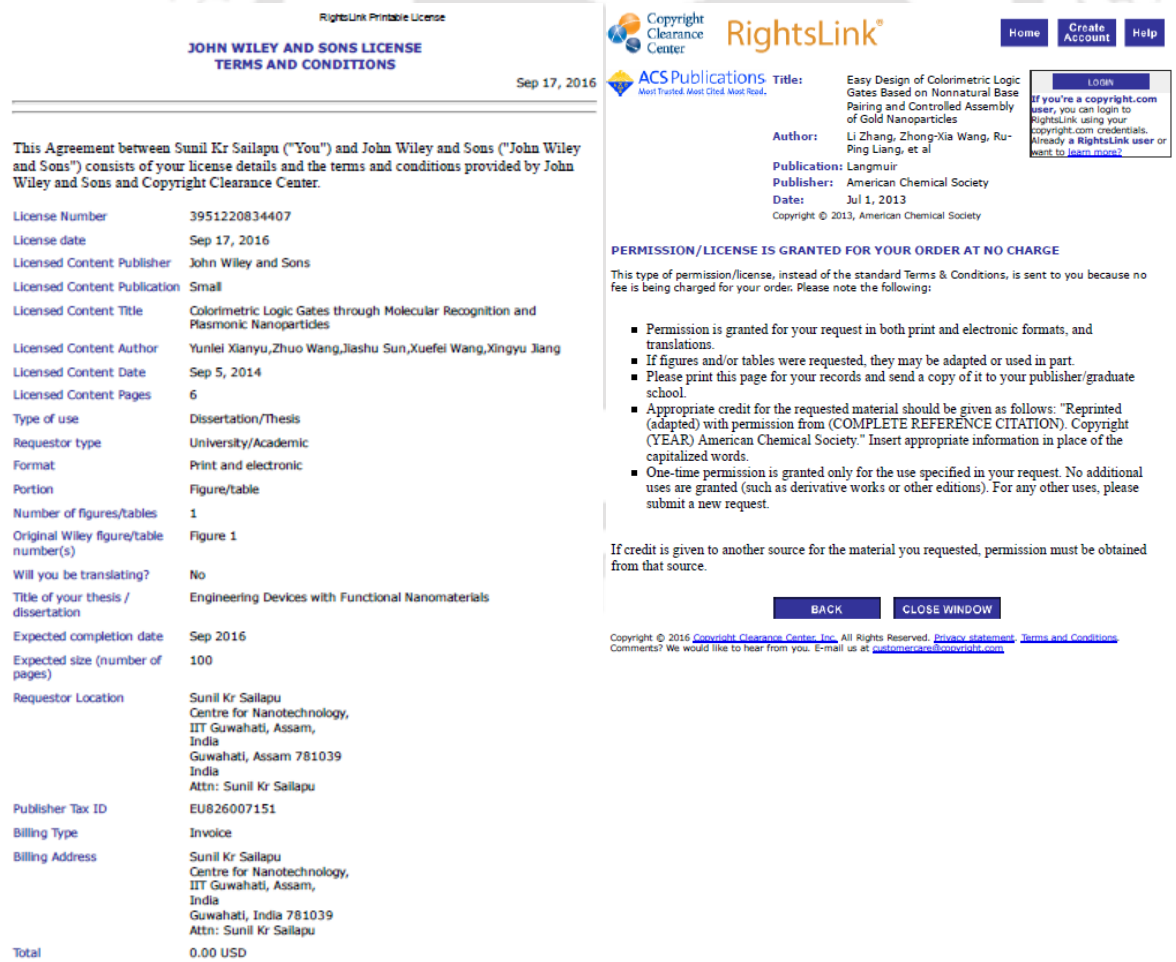

RightsLink Printable License

JOHN WILEY AND SONS LICENSE TERMS AND CONDITIONS

Sep 17, 2016

This Agreement between Sunil Kr Sailapu ("You") and John Wiley and Sons ("John Wiley and Sons") consists of your license details and the terms and conditions provided by John Wiley and Sons and Copyright Clearance Center.

License Number	3951220834407
License date	Sep 17, 2016
Licensed Content Publisher	John Wiley and Sons
Licensed Content Publication	Small
Licensed Content Title	Colorimetric Logic Gates through Molecular Recognition and Plasmonic Nanoparticles
Licensed Content Author	Yunlei Xianyu,Zhuo Wang,Jiashu Sun,Xuefei Wang,Xingyu Jiang
Licensed Content Date	Sep 5, 2014
Licensed Content Pages	6
Type of use	Dissertation/Thesis
Requestor type	University/Academic
Format	Print and electronic
Portion	Figure/table
Number of figures/tables	1
Original Wiley figure/table number(s)	Figure 1
Will you be translating?	No
Title of your thesis / dissertation	Engineering Devices with Functional Nanomaterials
Expected completion date	Sep 2016
Expected size (number of pages)	100
Requestor Location	Sunil Kr Sailapu Centre for Nanotechnology, IIT Guwahati, Assam, India Guwahati, Assam 781039 India Attn: Sunil Kr Sailapu
Publisher Tax ID	EU826007151
Billing Type	Invoice
Billing Address	Sunil Kr Sailapu Centre for Nanotechnology, IIT Guwahati, Assam, India Guwahati, India 781039 Attn: Sunil Kr Sailapu
Total	0.00 USD

Copyright Clearance Center RightsLink®

Home | Create Account | Help

ACS Publications
Most Trusted. Most Cited. Most Read.

Title: Easy Design of Colorimetric Logic Gates Based on Nonnatural Base Pairing and Controlled Assembly of Gold Nanoparticles
Author: Li Zhang, Zhong-Xia Wang, Ru-Ping Liang, et al
Publication: Langmuir
Publisher: American Chemical Society
Date: Jul 1, 2013
Copyright © 2013, American Chemical Society

LOGIN
If you're a copyright.com user, you can login to RightsLink using your copyright.com credentials. Already a RightsLink user or want to learn more?

PERMISSION/LICENSE IS GRANTED FOR YOUR ORDER AT NO CHARGE

This type of permission/license, instead of the standard Terms & Conditions, is sent to you because no fee is being charged for your order. Please note the following:

- Permission is granted for your request in both print and electronic formats, and translations.
- If figures and/or tables were requested, they may be adapted or used in part.
- Please print this page for your records and send a copy of it to your publisher/graduate school.
- Appropriate credit for the requested material should be given as follows: "Reprinted (adapted) with permission from (COMPLETE REFERENCE CITATION). Copyright (YEAR) American Chemical Society." Insert appropriate information in place of the capitalized words.
- One-time permission is granted only for the use specified in your request. No additional uses are granted (such as derivative works or other editions). For any other uses, please submit a new request.

If credit is given to another source for the material you requested, permission must be obtained from that source.

BACK | CLOSE WINDOW

Copyright © 2016 Copyright Clearance Center, Inc. All Rights Reserved. Privacy statement. Terms and Conditions.
Comments? We would like to hear from you. E-mail us at customercare@copyright.com

RightsLink Printable License

ROYAL SOCIETY OF CHEMISTRY LICENSE TERMS AND CONDITIONS

Sep 17, 2016

This Agreement between Sunil Kr Sailapu ("You") and Royal Society of Chemistry ("Royal Society of Chemistry") consists of your license details and the terms and conditions provided by Royal Society of Chemistry and Copyright Clearance Center.

License Number	3951221050586
License date	Sep 17, 2016
Licensed Content Publisher	Royal Society of Chemistry
Licensed Content Publication	Chemical Communications (Cambridge)
Licensed Content Title	Use of fluorescent gold nanoclusters for the construction of a NAND logic gate for nitrite
Licensed Content Author	Jia Zhang,Chuanxia Chen,Xiaowen Xu,Xiaolei Wang,Xiurong Yang
Licensed Content Date	Feb 15, 2013
Licensed Content Volume Number	49
Licensed Content Issue Number	26
Type of Use	Thesis/Dissertation
Requestor type	academic/educational
Portion	figures/tables/images
Number of figures/tables/images	1
Format	print and electronic
Distribution quantity	10
Will you be translating?	no
Order reference number	
Title of the thesis/dissertation	Engineering Devices with Functional Nanomaterials
Expected completion date	Sep 2016
Estimated size	100
Requestor Location	Sunil Kr Sailapu Centre for Nanotechnology, IIT Guwahati, Assam, India Guwahati, Assam 781039 India Attn: Sunil Kr Sailapu
Billing Type	Invoice
Billing Address	Sunil Kr Sailapu Centre for Nanotechnology, IIT Guwahati, Assam, India Guwahati, India 781039 Attn: Sunil Kr Sailapu
Total	0.00 USD

Copyright Clearance Center RightsLink® Home Create Account Help

ACS Publications Most Trusted. Most Cited. Most Read.

Title:	Ion-Tuned DNA/Ag Fluorescent Nanoclusters As Versatile Logic Device
Author:	Tao Li, Libing Zhang, Jun Ai, et al
Publication:	ACS Nano
Publisher:	American Chemical Society
Date:	Aug 1, 2011

Copyright © 2011, American Chemical Society

LOGIN

If you're a copyright.com user, you can login to RightsLink using your copyright.com credentials. Already a RightsLink user or want to learn more?

PERMISSION/LICENSE IS GRANTED FOR YOUR ORDER AT NO CHARGE

This type of permission/license, instead of the standard Terms & Conditions, is sent to you because no fee is being charged for your order. Please note the following:

- Permission is granted for your request in both print and electronic formats, and translations.
- If figures and/or tables were requested, they may be adapted or used in part.
- Please print this page for your records and send a copy of it to your publisher/graduate school.
- Appropriate credit for the requested material should be given as follows: "Reprinted (adapted) with permission from (COMPLETE REFERENCE CITATION). Copyright (YEAR) American Chemical Society." Insert appropriate information in place of the capitalized words.
- One-time permission is granted only for the use specified in your request. No additional uses are granted (such as derivative works or other editions). For any other uses, please submit a new request.

If credit is given to another source for the material you requested, permission must be obtained from that source.

BACK CLOSE WINDOW

Figure 1.10

Copyright Clearance Center RightsLink® Home Create Account Help

ACS Publications Most Trusted. Most Cited. Most Read.

Title:	Label-Free Protein Biosensor Based on Aptamer-Modified Carbon Nanotube Field-Effect Transistors
Author:	Kenzo Maehashi, Taiji Katsura, Kagan Kerman, et al
Publication:	Analytical Chemistry
Publisher:	American Chemical Society
Date:	Jan 1, 2007

Copyright © 2007, American Chemical Society

LOGIN

If you're a copyright.com user, you can login to RightsLink using your copyright.com credentials. Already a RightsLink user or want to learn more?

PERMISSION/LICENSE IS GRANTED FOR YOUR ORDER AT NO CHARGE

This type of permission/license, instead of the standard Terms & Conditions, is sent to you because no fee is being charged for your order. Please note the following:

- Permission is granted for your request in both print and electronic formats, and translations.
- If figures and/or tables were requested, they may be adapted or used in part.
- Please print this page for your records and send a copy of it to your publisher/graduate school.
- Appropriate credit for the requested material should be given as follows: "Reprinted (adapted) with permission from (COMPLETE REFERENCE CITATION). Copyright (YEAR) American Chemical Society." Insert appropriate information in place of the capitalized words.
- One-time permission is granted only for the use specified in your request. No additional uses are granted (such as derivative works or other editions). For any other uses, please submit a new request.

If credit is given to another source for the material you requested, permission must be obtained from that source.

BACK CLOSE WINDOW

Copyright Clearance Center RightsLink® Home Create Account Help

ACS Publications Most Trusted. Most Cited. Most Read.

Title:	DNA Biochip Using a Phototransistor Integrated Circuit
Author:	T. Vo-Dinh, J. P. Alarie, N. Isola, et al
Publication:	Analytical Chemistry
Publisher:	American Chemical Society
Date:	Jan 1, 1999

Copyright © 1999, American Chemical Society

LOGIN

If you're a copyright.com user, you can login to RightsLink using your copyright.com credentials. Already a RightsLink user or want to learn more?

PERMISSION/LICENSE IS GRANTED FOR YOUR ORDER AT NO CHARGE

This type of permission/license, instead of the standard Terms & Conditions, is sent to you because no fee is being charged for your order. Please note the following:

- Permission is granted for your request in both print and electronic formats, and translations.
- If figures and/or tables were requested, they may be adapted or used in part.
- Please print this page for your records and send a copy of it to your publisher/graduate school.
- Appropriate credit for the requested material should be given as follows: "Reprinted (adapted) with permission from (COMPLETE REFERENCE CITATION). Copyright (YEAR) American Chemical Society." Insert appropriate information in place of the capitalized words.
- One-time permission is granted only for the use specified in your request. No additional uses are granted (such as derivative works or other editions). For any other uses, please submit a new request.

If credit is given to another source for the material you requested, permission must be obtained from that source.

BACK CLOSE WINDOW

RightsLink Printable License

NATURE PUBLISHING GROUP LICENSE TERMS AND CONDITIONS

Sep 17, 2016

This Agreement between Sunil Kr Sailapu ("You") and Nature Publishing Group ("Nature Publishing Group") consists of your license details and the terms and conditions provided by Nature Publishing Group and Copyright Clearance Center.

License Number	3951221346213
License date	Sep 17, 2016
Licensed Content Publisher	Nature Publishing Group
Licensed Content Publication	Nature
Licensed Content Title	Weighing of biomolecules, single cells and single nanoparticles in fluid
Licensed Content Author	Thomas P. Burg, Michel Godin, Scott M. Knudsen, Wenjiang Shen, Greg Carlson et al.
Licensed Content Date	Apr 26, 2007
Licensed Content Volume Number	446
Licensed Content Issue Number	7139
Type of Use	reuse in a dissertation / thesis
Requestor type	academic/educational
Format	print and electronic
Portion	figures/tables/illustrations
Number of figures/tables/illustrations	1
High-res required	no
Figures	Figure 1
Author of this NPG article	no
Your reference number	
Title of your thesis / dissertation	Engineering Devices with Functional Nanomaterials
Expected completion date	Sep 2016
Estimated size (number of pages)	100
Requestor Location	Sunil Kr Sailapu Centre for Nanotechnology, IIT Guwahati, Assam, India Guwahati, Assam 781039 India Attn: Sunil Kr Sailapu
Billing Type	Invoice
Billing Address	Sunil Kr Sailapu Centre for Nanotechnology, IIT Guwahati, Assam, India Guwahati, India 781039 Attn: Sunil Kr Sailapu
Total	0.00 USD

Chapter 2

RightsLink Printable License

JOHN WILEY AND SONS LICENSE TERMS AND CONDITIONS

Sep 17, 2016

This Agreement between Sunil Kr Sailapu ("You") and John Wiley and Sons ("John Wiley and Sons") consists of your license details and the terms and conditions provided by John Wiley and Sons and Copyright Clearance Center.

License Number	3951271164832
License date	Sep 17, 2016
Licensed Content Publisher	John Wiley and Sons
Licensed Content Publication	Angewandte Chemie International Edition
Licensed Content Title	Induction of Electromotive Force by an Autonomously Moving Magnetic Bot
Licensed Content Author	Sunil Kumar Sailapu,Arun Chattopadhyay
Licensed Content Date	Jan 21, 2014
Licensed Content Pages	4
Type of use	Dissertation/Thesis
Requestor type	Author of this Wiley article
Format	Print and electronic
Portion	Full article
Will you be translating?	No
Title of your thesis / dissertation	Engineering Devices with Functional Nanomaterials
Expected completion date	Sep 2016
Expected size (number of pages)	100
Requestor Location	Sunil Kr Sailapu Centre for Nanotechnology, IIT Guwahati, Assam, India Guwahati, Assam 781039 India Attn: Sunil Kr Sailapu
Publisher Tax ID	EU826007151
Billing Type	Invoice
Billing Address	Sunil Kr Sailapu Centre for Nanotechnology, IIT Guwahati, Assam, India Guwahati, India 781039 Attn: Sunil Kr Sailapu
Total	0.00 USD

Chapter 3

RightsLink Printable License

JOHN WILEY AND SONS LICENSE TERMS AND CONDITIONS

Sep 18, 2016

This Agreement between Sunil Kr Sailapu ("You") and John Wiley and Sons ("John Wiley and Sons") consists of your license details and the terms and conditions provided by John Wiley and Sons and Copyright Clearance Center.

License Number	3951951140043
License date	Sep 18, 2016
Licensed Content Publisher	John Wiley and Sons
Licensed Content Publication	Small
Licensed Content Title	Hierarchical Logic Structures Based on Responsive Fluorescent Gold Nanoclusters
Licensed Content Author	Sunil Kumar Sailapu,Amaresh Kumar Sahoo,Siddhartha Sankar Ghosh,Arun Chattopadhyay
Licensed Content Date	Jul 19, 2014
Licensed Content Pages	5
Type of use	Dissertation/Thesis
Requestor type	Author of this Wiley article
Format	Print and electronic
Portion	Full article
Will you be translating?	No
Title of your thesis / dissertation	Engineering Devices with Functional Nanomaterials
Expected completion date	Sep 2016
Expected size (number of pages)	100
Requestor Location	Sunil Kr Sailapu Centre for Nanotechnology, IIT Guwahati, Assam, India Guwahati, Assam 781039 India Attn: Sunil Kr Sailapu
Publisher Tax ID	EU826007151
Billing Type	Invoice
Billing Address	Sunil Kr Sailapu Centre for Nanotechnology, IIT Guwahati, Assam, India Guwahati, India 781039 Attn: Sunil Kr Sailapu
Total	0.00 USD